2016

# The Mechanical Response and Parametric Optimization of Ankle-Foot Devices

Kevin Smith
*University of Central Florida*

# THE MECHANICAL RESPONSE AND PARAMETRIC OPTIMIZATION OF ANKLE-FOOT DEVICES

by

KEVIN CHRISTOPHER SMITH
B.S.M.E University of Central Florida, 2016

A thesis submitted in partial fulfillment of the requirements
for the degree of Master of Science
in the Department of Mechanical and Aerospace Engineering
in the College of Engineering and Computer Science
at the University of Central Florida
Orlando, Florida

Summer Term
2016

# ABSTRACT

To improve the mobility of lower limb amputees, many modern prosthetic ankle-foot devices utilize a so called energy storing and return (ESAR) design. This allows for elastically stored energy to be returned to the gait cycle as forward propulsion. While ESAR type feet have been well accepted by the prosthetic community, the design and selection of a prosthetic device for a specific individual is often based on clinical feedback rather than engineering design. This is due to an incomplete understanding of the role of prosthetic design characteristics (e.g. stiffness, roll-over shape, etc.) have on the gait pattern of an individual. Therefore, the focus of this work has been to establish a better understanding of the design characteristics of existing prosthetic devices through mechanical testing and the development of a prototype prosthetic foot that has been numerically optimized for a specific gait pattern. The component stiffness, viscous properties, and energy return of commonly prescribed carbon fiber ESAR type feet were evaluated through compression testing with digital image correlation at select loading angles following the idealized gait from the ISO 22675 standard for fatigue testing. A representative model was developed to predict the stress within each of the tested components during loading and to optimize the design for a target loading response through parametric finite element analysis. This design optimization approach, along with rapid prototyping technologies, will allow clinicians to better identify the role the design characteristics of the foot have on an amputee's biomechanics during future gait analysis.

# ACKNOWLEDGMENTS

I would like to thank my mentor and advisor Dr. Ali P. Gordon for his support and encouragement during my academic endeavors. I am additionally grateful for the support all of the academic faculty members and fellow researchers have offered me help during my time at the University of Central Florida. I would like to thank my defense committee members, Dr. Yuanli Bai, Dr. Alain Kassab, and Dr. Patrick Pabian for their time, guidance, and helpful insights. I would especially like to thank Dr. Bai and Dr. Seetha Raghavan for their support and use of their equipment.

I also wish to sincerely thank Dr. Les Kramer from TaiLor Made and Stan Patterson from the Prosthetics & Orthotics Associates for their time, expertise, and contributions that have made this research possible.

I would additionally like to thank the L.E.A.R.N program and the Research and Mentoring Program at the University of Central Florida for the academic opportunities and funding they have provided.

Finally, a special thanks to all of the members of the Mechanics of Materials Research Group who have helped me along the way.

# TABLE OF CONTENTS

# LIST OF FIGURES

# LIST OF TABLES

# CHAPTER 1: INTRODUCTION

In the United States there is currently an estimated 2 million people living with an amputation and this number expected to reach 3.6 million by 2050. Currently, the leading cause of amputation in the U.S are dysvascular diseases that originate from underlying conditions such as diabetes mellitus which account for 54% amputations and 97% of lower limb amputations (Dillingham et al., 2002; Ziegler-Graham et al., 2008). To improve rehabilitation techniques and assitive technologies for this growing population of lower limb amputees, a significant body of literature has been devoloped in the field of biomechanics and medical design with the goal of restoring function and independence to an amputee. To this end, investigations on lower limb prosthetic device have identified several key design parameters including, the roll-over shape (Hansen, Childress, et al., 2004), the viscous behavior (Geil, 2002), the component stiffness, and the elastic energy return during push-off (Hafner et al., 2002b). However, many gait analysis studies that examine the performance of existing prosthetic devices fail to report these response parameters making it difficult to interpt their influence on an specific amputee. This is largely due to the lack of standardization in reporting the mechanical respone of prosthetic devices. While several researchers have independently examined the effects of the roll-over shape (Klodd et al., 2010) and the stiffness (Fey et al., 2011) these prototype designs do not fully report all of the response parameters. To improve the mechanical characterization and design process of lower limb prosthetics this paper will consist of two parts. First mechanical testing will be conducted to evaluate the stiffness, energy return, and viscous properties of a used, but in good condition Freedom Innovations Renegade foot (Figure 1), as well as, a prototype foot called the TaiLor Made that was developed by TLM Prosthetics and allows for the clinicians to

independently select the stiffness of the toe, heel, and three internal compressive springs in base chamber shown in Figure 2 .

Figure 1: Freedom Innovations' Renegade prosthetic foot (Freedom-Innovations, 2015)

Figure 2: TLM Prosthetics' TaiLor Made foot (Prosthetics, 2015)

Finally this paper will offer an approach to parametrically generate prosthetic feet with a designed mechanical response using finite element simulations in ANSYS. This optimization process will allow for faster product development and potentially lead to additional insight on the influence the prosthetic device has on the biomechanics of amputee.

# CHAPTER 2: LITERATURE REVIEW

## 2.1 Prosthetic Design Criteria and Approaches

In the design of prosthetic devices, it is necessary to first develop an understanding of basic anatomical terms, gait dynamics, and the coupled relationship between the mechanical stresses on the device and the biomechanical forces on the amputee.

The gait cycle during walking consist of two main phases, the stance and swing phase as illustrated in Figure 3. The stance phase begins with a heel strike, or initial contact, and continues forward with the rollover of the ankle until the toe pushes off ground and the leg enters the swing phase of the gait cycle (Loudon et al., 2008). A gait analysis, which consist of the measurement the duration of the stance and swing phases, the stride lengths, walking velocity, and step cadence are commonly used in biomechanics to evaluate the functional performance of a prosthetic design and will be discussed in greater detail in Section 2.2.

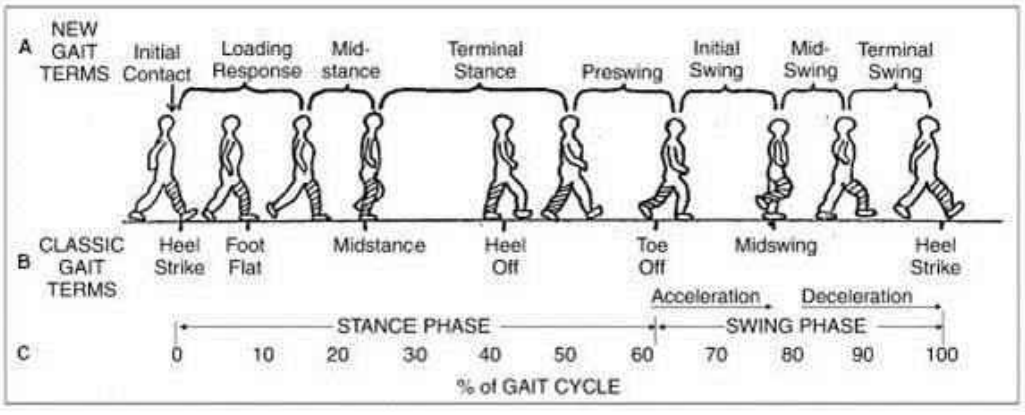


Figure 3: Gait Analysis (De Koster, 2004)

During the stance phase, many feet are designed to allow a degree of deflection when placed under the cyclic loads. This allows for the foot to simulate the dorsiflexion and plantarflexion motions (shown in Figure 4) of the ankle joint that the foot undergoes during perambulation.

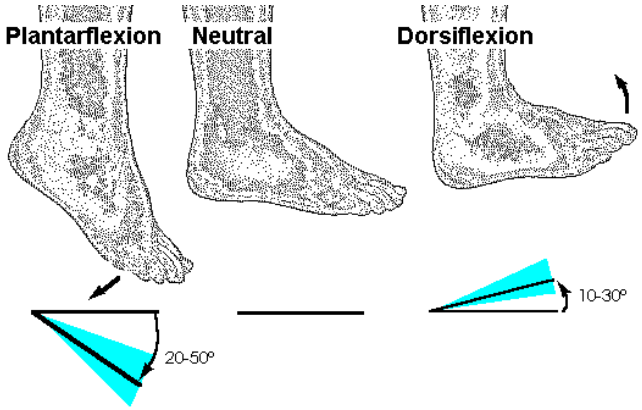


Figure 4: Movements of the ankle ("Dorsiflexion and Plantarflexion,")

The kinematic behavior of this deflection is often described by the roll-over shape of the foot (Hansen et al., 2014). This is the shape of a cam roller necessary to simulate the path of the ankle joint based on the mechanical deflections of the prosthesis. Studies by Hansen have suggested that increasing the roll-over radius can reduce the heel strike on the sound limb and increase the step length, however, it is important to remember that the roll-over shape is only one of several important variables in prosthetic design. As Hansen points out, the shape of the foot is independent from the mechanical behavior of the prosthetic. This is demonstrated in Figure 5 where Hansen has depicted two types of feet from his study with significantly different mechanical properties, but similar roll-over shapes. The shape of this rollover curve is generated by plotting the effective center of pressure acting on the foot into the shank axis as the foot rolls forward (Hansen et al., 2006).

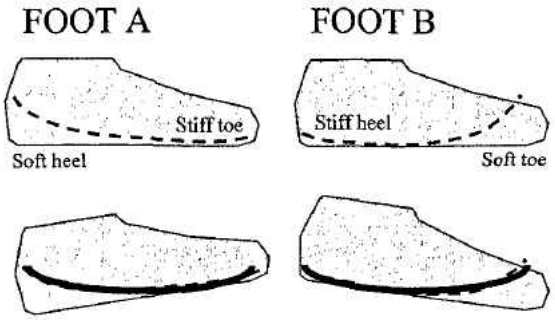


Figure 5: Roll-over shape of different designs prosthetic feet

Research in gait analysis (Winter, 2009) and bipedal dynamics (McGeer, 1990) has shown that in non-amputees the roll-over radius is typically about 15% of an individuals' height or 30% of their leg length; and that this radius is often invariant to changes in walking speeds (Hansen, Childress, et al., 2004) and heel height (Hansen & Dudley, 2004). Additionally, there is empirical evidence suggesting that there is an optimal roll-over radius and position of the center of curvature at which metabolic expenditure can be minimalized (Adamczyk et al., 2006).

The expected loads that the prosthetic foot will encounter are often approximated with reaction forces recorded with a load plate during a gait analysis study. The typically reaction forces during walking are shown in Figure 6 with respect to body mass. In these plots, the first peak in the vertical ground reaction force plot represents the heel strike which transfers into the maximal loading of the heel. The final peak in the vertical gait response represents the toe push-off. In the anterior-posterior reaction force plot, the first peak represents the breaking force provided during the loading response of the stance phase while the second peak represents push-off force opposite to the direction of walking. Finally, the medial-lateral reaction represents transverse force that occurs as the center of mass shifts side to side.

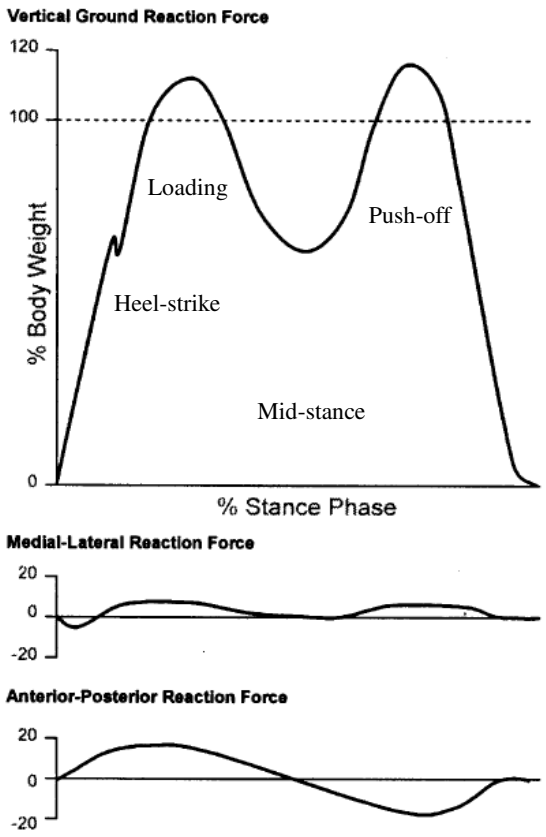


Figure 6: Walking reaction loads (Perry, 1992)

These loads are often further idealized as a symmetric waveform, shown in Figure 7, during fatigue testing with the ISO 22675 and 10328 standards for the testing of foot and ankle units using a load frame that supports dynamic roll-over of the ankle (International Organization for Standardization, 2006a, 2006b). In this plot, the vertical forces and tilt plate angle are represented as a function of time during the stance phase for the fatigue testing of a foot designed for a 60kg (P3), 80kg (P4), and 100kg (P5) individual.

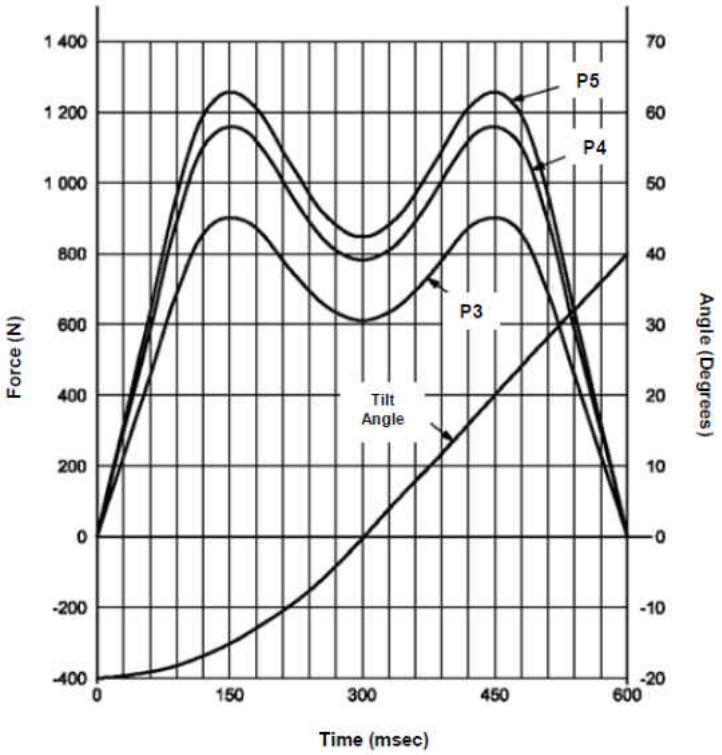


Figure 7: ISO 22675 cyclic loads and angle over time (International Organization for Standardization, 2006b)

## 2.2 Existing Designs

With the introduction of high performance composites and improved numerical design, the lower limb prosthetics industry has evolved over the past 30 years, expanding from designs focused only on functional recovery to performance based designs that allow for amputees to participate in sports in activities. This diversity among patient specific needs and recovery goals has led to the development of a wide variety of prosthetic technologies that can generally be categorized as fixed joint, passive joint, and active joint prosthetics.

The most traditional fixed joint prosthetic foot today is the solid ankle cushion heel (SACH) foot which consist of a rigid wooden keel with a foam heel (Figure 8) that simulates plantar flexion during compression (Nobbe Orthopedics). Because of the simplicity of the

design, the SACH foot is generally regarded as a light weight, inexpensive foot with low maintenance that is well suited to low level ambulators (Highsmith, 2009).

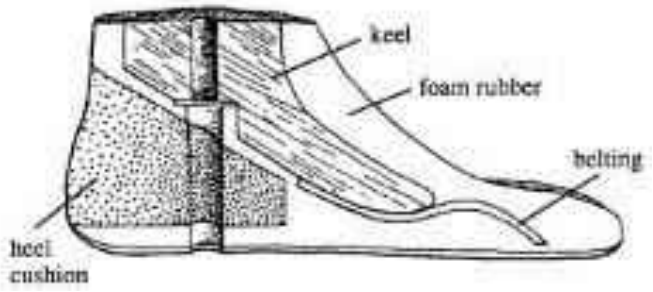


Figure 8: SACH foot design ("Postoperative SACH foot (cutaway),")

However, because of their rigid design, SACH feet offer a limited range of motion for dorsiflexion during the late stance phase of the gait. To increase this range of motion, a number of prosthetic designs have included a flexible keel made from lightweight high performance polymer matrix composites (PMCs), such as carbon fiber, aramid fibers, and fiber glass as shown in Figure 9.

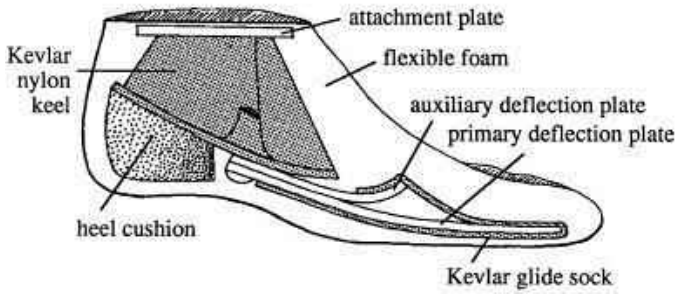


Figure 9: Flexible keel dynamic response foot (Kapp et al.)

Among the most successful of the flexible PMC fixed joint prosthetic designs are the energy storing and return (ESAR) prosthetic feet which consist of an elastic leaf spring (Figure 10) design that allows for a for a greater degree of ankle flexibility and dynamic energy return during push-off than traditional wood and foam prosthetics (Hafner et al., 2002a). Because of their flexibility, high energy return, and low maintenance, ESAR feet are particularly well suited to athletics sporting events and activities.

Figure 10: Carbon fiber Freedom Innovations Silhouette® (Innovations)

Feet with passive joints, such as single axis (Figure 11a) and multi-axis feet (Figure 11b) offer amputees a greater range of motion that leads to improved stability on uneven terrain as shown in (Nobbe Orthopedics). This is due to the frictionless bearing in the ankle joint allows foot to come into contact with ground quicker simulating flexion in single axis feet and eversion or inversion in multi-axis feet. While single axis feet are viable option for all amputees, this increase increased stability is particularly important to transfemoral amputees. However, as the designs become increasingly complex, the patient and prosthetist must balance the cost, the weight of the device, and the accommodation period to learn to walk again (Highsmith, 2009).

a) b)

Figure 11: a) Single Axis Truper College ("Truper," 2012) b) Multiaxial TruStep College Park (Thompson, 2006)

## 2.3 Biomechanics of Prosthetics

Since the introduction of the first carbon fiber ESAR foot in the early 1980s, there have been numerous studies on prosthetic feet to determine which types of designs work well and the design criteria that makes them successful. To accomplish this goal, research studies typically focus on either the patient-prosthetic interaction using a biomechanical analysis, or an unbiased structural analysis by applying static, dynamic and cyclic loads to the prosthetic device.

During a biomechanical analysis researchers often focus on at least one of the six areas of a gait analysis including: kinematics, kinetics, muscle activation, metabolic expenditure, and the stride and temporal characteristics (Hafner et al., 2002a). While each of these areas of study does provide insight into the performance of the prosthetic, these studies often provide results are often statistically insignificant and at times conflicting with both each other, and the perception of the patient.

Hafner summarized the results of a number of these studies which showed gait analysis with ESAR foot can have self-selected walking velocity anywhere from 0.00-13.11% higher than a traditional prosthetic foot (Barr et al., 1992; Lehmann, Price, Boswell-Bessette, Dralle, & Questad, 1993; Lehmann, Price, Boswell-Bessette, Dralle, Questad, et al., 1993; Macfarlane et al., 1991; Nielsen et al., 1988; Powers et al., 1994; Snyder et al., 1995; Torburn et al., 1990). While the increase in walking velocities in most studies are statistical insignificant ($P > 0.05$), all of the reviewed studies on ESAR feet have shown some increase in walking velocity with a mean value of 4.7% (Hafner et al., 2002a). This reflects the positive patient feedback received in surveys and polls performed Menard and others (Menard et al., 1989; Romo, 1999). However, the clinical significance of these results has often been questioned as the day-to-day self-selected walking velocity can vary in patients as much as 7.1% of the mean (Kadaba MP et al., 1989; Perry, 1992).

Further kinematic analysis has revealed that the cadence (steps / minute) remains relatively unchanged between SACH feet and ESAR feet (Powers et al., 1994; Snyder et al., 1995). Instead the increase in walking velocity is largely attributed to an increase in stride length due to the increase in the range of motion in the flexible ankle; where stride length consist of a forward step with each leg (Hafner et al., 2002a). Although not all authors go into detail, Barr and Macfarlane have suggested that the increased stride length is due to an increase in the step of the sound leg as there is a delay in the unloading of the bodyweight off of the prosthetic foot (Barr et al., 1992; Macfarlane et al., 1991).

In examining the effects of energy return on the kinetics during walking, researchers found that there was an increase in the posterior anterior force (Lehmann, Price, Boswell-Bessette, Dralle, Questad, et al., 1993; Powers et al., 1994). This was due to the plantarflexion of

the foot as elastic energy stored by the leaf spring design was released. Interestingly researchers also found that there was often a significant decrease in vertical heel reaction force on the sound side, but only minimal reduction in vertical forces on the affected side (Lehmann, Price, Boswell-Bessette, Dralle, Questad, et al., 1993; Powers et al., 1994; Snyder et al., 1995). These results support the previously mentioned conclusions from Barr and Macfarlane, the increased flexibility of the toe allows for a reduction in force during the two support phase of the subsequent step (Barr et al., 1992; Macfarlane et al., 1991).

Metabolic expenditure experiments have consistently shown that amputees demonstrate an elevated heart rate and 55% to 83% higher oxygen consumption when walking at similar speeds as non-amputees (Hoffman et al., 1997; Waters et al., 1999). The goal of many advance prosthetics is to minimize the additional exertion placed on the patient, however, only a few metabolic test have shown improvement using ESAR feet when compared to traditional feet. In a study by Nielsen that examined oxygen update and heart rate during walking, it was shown that the ESAR feet perform are less demanding at higher speeds, but the difference was less noticeable at speeds below 2.5mph (Nielsen et al., 1988). Nevertheless, there was no significant difference seen in muscle activation between ESAR feet and SACH feet (Torburn et al., 1990).

Despite the lack of statistically significant biomechanical data to support improvements during walking, there is an apparent trend that the energy that is returned by the ESAR toe during the push off phase of the gait cycle does assist the amputee.

## 2.4 Experimental Mechanics of Prosthetics

As previously discussed, biomechanical studies are subjected to a great deal of variance due small sample sizes and large variability between amputees. To provide a more repeatable

evaluation of the prosthetics, bench top testing is conducted to determine the mechanical strength and behavior of a prosthetic foot. These tests can include both fatigue and proof testing of the prosthesis often following the ISO 22523 and 22675 standards, as well as characterization of the mechanical properties such as stiffness, force relaxation, roll-over shape, and the energy return of dynamic feet.

### *2.4.1 Energy Return*

The energy return of an ESAR prosthetic foot is a measure of the elastic energy released by the foot relative to the potential energy stored during loading. During bench top testing, the cyclic work is measured through integration of the force displacement Eq.(2.4.1), which is represented by the hysteresis loop shown in Figure 12. Here the energy loss as a result of internal friction is represented by the area within the hysteresis loop (Hafner et al., 2002b).

$$W = \int_{x_0}^{x_1} F \cdot dx \tag{2.4.1}$$

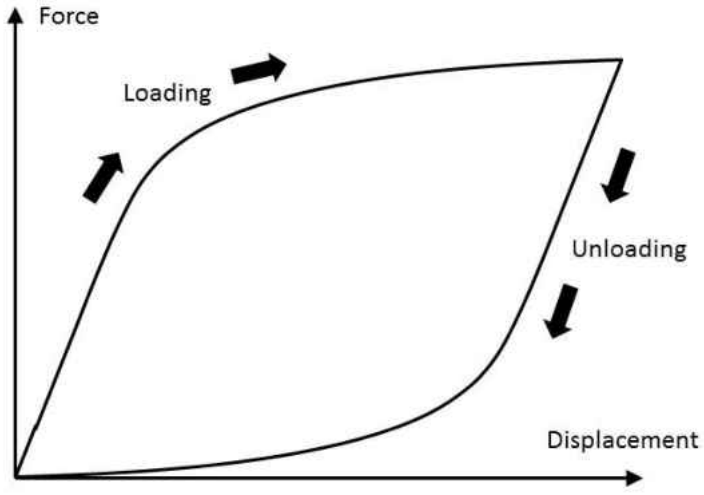


Figure 12: Generalized hysteresis loop

This energy loss is often expressed as a percentage shown in Eq.(2.4.2), with the energy returned during unloading relative to the work during loading.

$$\eta_{return} = \frac{\int_{x1}^{x0} F_{unload} \cdot dx}{\int_{x0}^{x1} F_{load} \cdot dx} \tag{2.4.2}$$

Although energy return testing has yet to be standardized in literature, the American Orthotic Prosthetic Association (AOPA) has provided guidelines on the energy testing of prosthetic feet to help classify prosthetic feet. According to the AOPA a dynamic response foot is classified as a foot that has an efficiency of at least 75% on the toe and 82% efficiency on the heel (American Orthotic Prosthetic Association, 2010). In review of a study conducted by the Rehabilitation Technology Research Unit at Monash University on 12 different model feet shown in Table 1, it is noted that in general feet made from high performance composites tend to perform with higher efficiency.

Table 1: Summary of RehabTech energy return results (Rihs et al., 2001)

| Foot Type | Keel Energy Return % | Keel Material |
|---|---|---|
| Human Foot | 119.6 | - |
| Seattle Foot M+IND, Natural SNF150 | 70.7 | Delrin |
| Flex Foot Modular II | 61.7 | Carbon Fiber |
| Quantum VESSA Truestep 25 type A N1562 | 59.5 | Fiber Glass |
| SAFE Cambell Childs | 58 | Urethane |
| Multi Axis Foot Blatchford Multiflex Foot 509153-67 | 56.7 | Carbon Fiber |
| Dynamic Foot - Otto Bock ID10 | 39.2 | Timber |
| Carbon Copy II | 35.2 | Kevlar / Nylon |
| SACH Foot Otto Bock IS70 | 32.1 | Timber |
| Greissinger Foot Otto Bock 1A13 | 31.7 | Timber |
| SACH Foot Kingsley Wayfarer (Post Op. Flatfoot) K10 | 19.1 | Timber |
| SACH Foot Otto Bock IS51 | 15.9 | Timber |
| STEN Kingsley | 15.8 | Timber |

While the energy return efficiency is the most commonly reported data statistic in literature, according to Geil the actual amount of energy return to the late stance phase is far more significant. It was observed in Geil's study on dynamic response model feet that the most compliant foot tested, the College Park's TruStep, may have had the lowest efficiency at 68.7%, but the prosthetic foot provided the greatest amount of energy return at 7.10 J during unloading (Geil, 2001).

### *2.4.2 Stiffness*

The mechanical stiffness and viscous properties of the prosthetic foot play a fundamental role in the absorption of energy and gait kinematics for amputees. This is due to the relatively large elastic deformations that the ESAR feet undergo during the stance phase of the gait. However, as Geil points out, the selection of optimal prosthetic device for the individual patient

often presents a challenge for prosthetists and clinicians as the mechanical behavior of the prosthetic foot is not standardized. When properties such as stiffness are reported they often use a subjective scale that varies between manufacturers. To help clinicians to make better-informed decisions regarding the selection of a prosthetic device, independent studies have helped to provide additional information on the mechanical behavior select devices and their performance during gait analysis (Geil, 2001).

Mechanical testing of the stiffness of prosthetic feet is typically conducted by placing a representative load on both the heel and toe of the foot and measuring the deflection of the foot. Two types of tests used to determine the mechanical behavior are uniaxial loading in a controlled load frame and impact testing with a weighted pendulum. In a study by Geil, a universal testing frame was used to determine that the stiffness of nine models of prosthetic feet which ranged from 28-76 N/mm when 800N compressive load was applied to the foot when it was 12° in plantarflexion (Geil, 2001). In a study by Klute, impact testing was conducted to determine the behavior of the heel of seven models of prosthetic feet when angled at 20° in dorsiflexion with kinetic energy similar to high load rates experienced during running; which can range from 151.9 - 213.9% of an individuals body weight per second in non-amputees (Logan, 2007). It was found that the heel stiffness of several types of prosthetic feet ranged from 27-68 N/mm (Klute et al., 2004).

While the individual testing of the heel and the toe provides characterization of the foot during the heel-strike and push-off, these test do not describe the behavior during the mid-stance phase of the gait. To characterize the behavior of the prosthetic device over the entire gait cycle, Haberman conducted uniaxial testing at fifteen data points over an idealize load curve that was adopted from the ISO 22675 standard. While Habermans' tests found similar toe stiffness as Geil

at 12°, Haberman also found that the stiffness of several prosthetic feet varied over the duration of the stance phase and exhibited a peak in stiffness when both the heel and the toe are providing support at 0° or 300ms based on the ISO 22675 loading curves. This change in compliance during roll-over is attributed to the contact mechanics and the non-uniform geometry (Haberman, 2008).

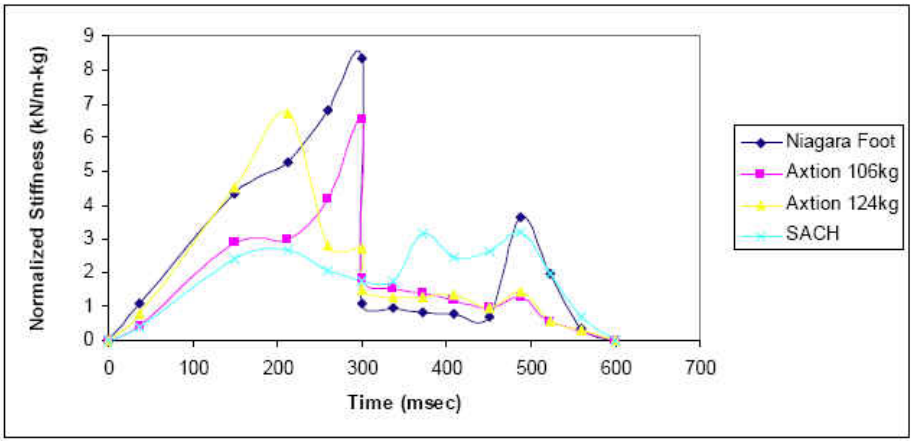


Figure 13: Normalized stiffness at critical load angles during stance phase (Haberman, 2008)

To better understand the role of the prosthetic foot stiffness on walking, Fey conducted a series of gait analysis using three variations of a 3D-printed thermoplastic prosthetic foot with levels of mechanical stiffness (Fey et al., 2011). The nominal level of the three feet was matched to a Freedom Innovations Highlander foot through mechanical testing and finite element modeling; the other two feet were designed to be 50% more compliant, and 50% stiffer than the nominal foot (South et al., 2009). Fey found that a more compliant foot allows for an increased ankle flexibility and prosthetic energy storage in the mid-to-late stance phase, however, a greater amount of muscle activity in the both residual limb and sound limb was also observed (Fey et al., 2011). This suggests that there is an apparent trade-off between energy return and stability.

### *2.4.3 Viscoelasticity*

While the influence of the viscous properties of an ankle-foot device on an amputee's gait pattern are poorly understood, Klute has suggested that increasing the energy dispersed by the viscoelastic behavior during heel loading could potentially reduce the risk of skin and soft tissue damage in an amputee's residual limb (Klute et al., 2004). To this end, several methods have been presented in literature including the use of impact and quasi-static loading to quantify the viscoelastic behavior of prosthetic feet. In Klute's approach, impact testing was conducted at a 20° angle on the heel of seven commonly prescribed prosthetic feet within their cosmetic foam covers and within walking shoes, running shoes, and orthotic shoes. The percentage of energy dissipation during impact was calculated by dividing the work energy from deformation during impact force by the kinetic energy of a weighted impactor pendulum, i.e.

$$D_s = \frac{\oint F dx}{\frac{1}{2} m v^2} \times 100\% \tag{2.4.3}$$

Where $x$ is the deformation of the heel, $F$ is the force during impact, $m$ is the mass of the pendulum, and $v$ is the velocity of the pendulum. It was observed that the energy dissipation percentage for the tested prosthetic feet ranged from 33.6% to 52.6%. Klute noted that wearing a shoes significantly increased the energy dissipation during impact. In the case of Trulifes' dynamic response Seattle foot, the dissipation energy was increased from 45.3% by itself, to 63.0% in walking shoes, 73.0% in running shoes, and 82.4% in orthotic shoes (Klute et al., 2004).

To quantify the viscous behavior, Klute developed a constitutive model of the force during impact with a nonlinear spring in parallel with a directionally-dependent damper as shown in Eq.(2.4.4),

$$F\left(x,\dot{x}\right)=ax^{b}+\text{sign}\left(\dot{x}\right)cx^{d}\left|\dot{x}\right|^{e} \tag{2.4.4}$$

Here the coefficients (*a*) and exponent (*b*) represent the nonlinear hardening behavior during elastic deformation and the coefficient (*c*), and exponents (*d*) and (*e*), represent the directionally dependent energy dissipation. The sign ($\dot{x}$) term goes to 1 when $\dot{x}$ is positive, -1 when $\dot{x}$ is negative, and 0 when $\dot{x}$ is equal to zero. The coefficients in this model are found through numerical regression, however, due to the non-linear behavior it is difficult to directly compare the coefficients values between different model feet. Klute points this out by examining the impact coefficients of a SACH foot and the VariFlex foot, one of several ESAR feet tested. It was found that the (*a*) coefficient VariFlex foot was higher than the SACH feet, suggesting that it would have a higher peak load. However, this is not the case due to a greater position dependent exponent (*b*) in the VariFlex foot, which instead led to a smaller peak load in the VariFlex than the SACH foot (Klute et al., 2004).

Other researchers have taken a more traditional approach to evaluating the viscous properties of ankle-foot devices by conducting stress relaxation, creep, and load rate testing. To adapt these mechanics of material experiments for the component level, Geil developed an angled fixture in a universal load frame to apply uniaxial loads to a prosthetic device with a 12 degree angle against a fixed flat surface (Geil, 2002). This allowed Geil to apply a constant load to the prosthetic device and measure the deformation over time during creep testing, to apply a

fixed displacement and measure the decay in force over time during stress relaxation testing, and measure the force response during tests conducted at a constant strain rate. To model the viscous behavior of nine different types of ESAR prosthetic feet under these loading conditions, Geil applied the three parameter standard linear viscoelasticity material model which consists of an elastic spring element ($k_1$) that is in series with an a Voigt element that is composed of elastic spring ($k_2$) that is parallel to a rate dependent viscous damper ($\eta$); the standard linear model can be expressed in its mechanical form shown in Figure 14.

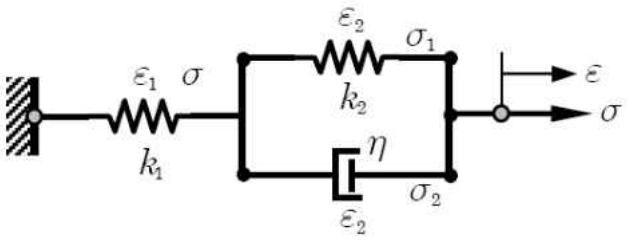


Figure 14: Standard Linear Model (Reddy, 2013)

This spring and dashpot representation can be converted to its equation form by applying compatibility conditions such that the stress ($\sigma$) and strain ($\epsilon$) components of the parallel elements must equal the total stress and strain in the system, i.e.

$$\sigma = \sigma_1 + \sigma_2 \tag{2.4.5}$$

$$\epsilon_1 = \epsilon_2 \tag{2.4.6}$$

Additionally, the stress-strain relations of the two spring elements can be determined by Hooke's law, the series spring and dashpot can be determined from the linear viscosity,

$$\sigma_1 = k_2 \epsilon_2 \tag{2.4.7}$$

$$\sigma_2 = \eta \dot{\epsilon_2} \tag{2.4.8}$$

$$\sigma = k_1 \epsilon_1 \tag{2.4.9}$$

Combining the compatibility conditions and the stress-strain relationships leads to a first order differential equation that is capable of modeling both stress relaxation and creep strain as follows,

$$\frac{\eta}{k_1}\frac{d\sigma}{dt} + \left(1 + \frac{k_2}{k_1}\right)\sigma = k_2 \epsilon + \eta \frac{d\epsilon}{dt} \tag{2.4.10}$$

When solving Eq.(2.4.10) for conditions of constant strain ($\epsilon_0$), it becomes apparent that the isolated spring $k_1$ element allows modeling of the long duration stiffness of the component, while the parallel spring $k_2$ and its dashpot $\eta$ capture the transient behavior of the material, i.e.

$$\sigma = \varepsilon_0 \left( k_1 + k_2 \exp\left( -\frac{\mathrm{t} k_2}{\eta} \right) \right) \tag{2.4.11}$$

Similarly, Eq. (2.4.10) can be solved for the creep response of a material with constant stress and $\dot{\sigma}$ equal to 0 as shown in Eq.(2.4.12),

$$\epsilon = \frac{1}{k_1}\left[ 1 - \left( \frac{k_2}{k_1 + k_2} \right) \exp\left( -\frac{t k_1 k_2}{\eta\left(k_1 + k_2\right)} \right) \right] \sigma_0 \tag{2.4.12}$$

As well as the constant strain rate ($\dot{\epsilon}$) response as shown in Eq.(2.4.13)

$$\sigma = \epsilon k_1 + \dot{\epsilon}\eta\left(1 - \exp\left(\frac{tk_2}{\eta}\right)\right) \tag{2.4.13}$$

While the standard linear model is typically used for engineering stress ($\sigma$), strain ($\epsilon$), and strain rate ($\dot{\epsilon}$) at the material level, these values could not be measured directly due to the geometry of the foot. Instead, Geil made an approximation of these values at the component level in order to quantify the viscoelastic behavior of the device. The component level stress response was estimated by dividing the force over the foots' plantar surface area, and the strain response was derived by dividing the deformation distance between the foot pylon and the loading surface by the original un-deformed distance. The viscoelasticity coefficients for the constitutive model for the three types of loading were determined from a quasi-Newton optimization routine of the experimental data for each foot. These experiments by Geil support previous findings by Lehmann that the Flex foot is more compliant than the Seattle foot, which is more compliant than a SACH foot (Lehmann, Price, Boswell-Bessette, Dralle, & Questad, 1993). While Geil admits there were some inaccuracies between the standard linear model and the experimental data, it was noted that the series spring constant ($k_2$) in the Flex foot was the highest out of all the feet tested, thus leading to a greater initial stiffness. This suggests that in the design and selection process of a prosthetic foot, there may be additional insight in examining viscoelastic behavior of the ankle-foot device rather than the device stiffness alone (Geil, 2002).

Due to the complex behavior between the ankle-foot devices, the cosmetic foam cover, and orthotic shoes the standard linear model may not be sufficiently robust to capture the viscous

response for prosthetic devices (Geil, 2002). To fill this gap in knowledge, this thesis will further examine the viscous response of prosthetic devices using the Norton-Bailey power law, the Maxwell-Wiechert model, and the Burgers model by replacing the stress parameter ($\sigma$) and strain parameter ($\epsilon$), respectively with force ($F$) vertical displacement ($\delta$). In the case of the Norton-Bailey power law it follows that,

$$\varepsilon = A\sigma^n t^m \rightarrow \delta = AF^n t^m \tag{2.4.14}$$

Where, by analogy the stress exponent ($n$) can referred to as the force exponent, and the strain hardening coefficient ($A$) can be referred to as the force coefficient. Additionally, $t$ represents time and $m$ represents the time exponent (Betten, 2008). During stress relaxation conditions Eq.(2.4.14) can be re-written as follows,

$$F = \left( \frac{\delta_0}{At^m} \right)^{1/n} \tag{2.4.15}$$

Here the force relaxation response is determined from the constant displacement ($\delta_0$) and the viscous parameters. An additional power law often used in the constitutive modeling of rubbers (Larson, 1985) is shown in Eq.(2.4.16),

$$F = F_0 t^m \tag{2.4.16}$$

It is noted that the Norton-Bailey law from Eq.(2.4.15) reduces to the form of Eq.(2.4.16), when the force exponent goes to -1. In such cases, the material could be considered to have a linear stress response.

Akin to the standard linear model, the Maxwell-Wiechart and Burgers model are derived from a spring and dashpot diagram shown in Figure 15. The Maxwell-Wiechert, or generalized Maxwell model, consists of a single elastic spring element ($k_e$) along with an arbitrary number ($J$) of Maxwell spring-dashpot elements to fully describe the stress relaxation behavior (Reddy, 2013).

a) b)

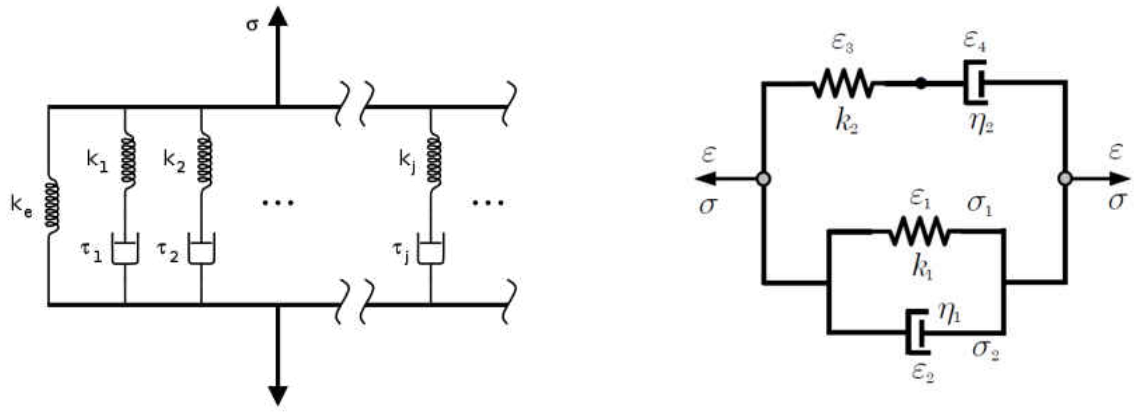


Figure 15: Mechanical diagram of Maxwell-Wiechert (a) and Burgers model (b) (Reddy, 2013)

Following a similar conversion of stress and strain as in Eq.(2.4.14), the Maxwell-Wiechert model is expressed as follows,

$$F = \delta\left( k_e + \sum_{j=1}^{J} k_1 \exp\left( -\frac{\mathrm{t}k_1}{\eta_1} \right) \right) \tag{2.4.17}$$

Where the viscoelastic spring ($k$) and dashpot ($\eta$) elements (Reddy, 2013). Due to the structure of Eq.(2.4.17), the Maxwell-Wiechert equation allows for a high degree of accuracy for stress relaxation with a sufficient number of Maxwell elements. On the other hand, the Burgers model shown in Eq.(2.4.18),

$$F = \delta\left[\frac{1}{k_1} + \frac{1}{k_2}\left(1 - \exp\left(-\frac{tk_2}{\eta_2}\right)\right) + \frac{t}{\eta_1}\right]^{-1} \tag{2.4.18}$$

consists of only four spring and dashpot element; however, because of the equation structure it is particularly well suited to complex creep flow (Reddy, 2013).

### *2.4.4 Fatigue and Proof Testing*

Prosthetic feet are regularly subjected to cyclic loading during the day-to-day perambulation of an amputee. Over time, this cyclic loading leads to void formation and crack growth through various failure mechanisms in composite laminate feet including de-bonding, delamination, and fatigue failure of the fiber reinforcement. To predict the lifespan of the device, many manufactures subject their lower limb prosthetic components to fatigue and proof testing at the peak loads and critical angles observed on the heel and toe of the foot during the stance phase of a gait analysis.

In literature, the fatigue testing of a prosthetic foot is often conducted by applying a load at a critical angle with one or more linear actuators (Figure 16a) or through the use of highly specialized testing equipment (Figure 16b) that allows for the dynamic rollover of the prosthetic

foot (Toh et al., 1993; Unnthorsson et al., 2008). While the inclusion of dynamic roll-over during of prosthetics is considered to a better representation of the service conditions for the device, relatively few publications have been made using fatigue testing with this full range of motion due cost and complexity (Daher, 1975; Wevers et al., 1987). Instead fatigue testing of lower limb prosthetics is typically conducted with the use of uniaxial testing frames which allows similar life cycle predictions as dynamic roll-over testing. This approach was used by Toh who observed that the foam heel is common site of failure in SACH feet often beginning to breaking down after 6 months of wear or 10,000 cycles of fatigue testing (Toh et al., 1993).

(a) (b)

Figure 16: (a) Wazau fixed angle test frame (2013) (b) prosthetic test frame with roll-over based on ISO 22675 (Western)

In recent years, many manufactures utilized the ISO 22675 and ISO 10328 standards for the structural testing of lower limb prosthetic devices and their components. As previously discussed in section 2.1, these two standards provide recommended test loads for fatigue and structural testing based on an idealized gait loads for a designed body mass. To comply with

these standards, prosthetic feet must endure the following fatigue and static loads without crack formation:

- Cyclic loading of the gait force shown in Figure 7 for $2 \times 10^6$ cycles, followed by a proof test at 175% of the peak gait load for 30 seconds
- Static ultimate test equal to 350% of the peak load in the gait cycle

However, a displacement criterion for permanent or loaded deformations has been also been used as a failure criterion (Toh et al., 1993; Unnthorsson et al., 2008). While components high performance composites, such as carbon fiber, tend to exhibit good fatigue resistance, this is not the case with lower cost polymer and foam prosthetic devices used in developing countries. Independent testing has shown that many SACH feet and thermoplastic monolimb prosthetic devices have a service life less than 100,000 cycles or approximately one year of use (Jensen et al., 2000; Jensen et al., 2007; Toh et al., 1993).

## 2.5 Numerical Approaches Used in Prosthetic Design

To help address the multivariable challenge in the design of lower limb prosthetics, the use of finite element analysis (FEA), optimization routines, and recent 3D printing techniques have been used to generate more robust designs, develop a better understanding of the patient-prosthesis adaptation, and improve the lifespan of the device.

In a study by Fey the influence of prosthetic foot stiffness on walking was examined through the use of three variations of a thermoplastic prototype prosthetic foot, generated through FEA modeling and selective laser sintering (SLS) (South et al., 2009). The initial findings from this biomechanical study showed that a more compliant foot leads to increased propulsive energy, it

also required greater muscle activation to compensate for decreased stability (Fey et al., 2011). To further verify these findings in a separate study, Fey was further able to use FE modeling to examine the muscle activation for walking with a 2D dynamics simulation of the lower body and prosthesis (Fey et al., 2013).

Finite element modeling has also been used in the optimization of the composite material of a prosthetic device. This approach has been used by Limmer who conducted experimental and finite element analysis of the elastically stored strain energy density for comparing the effects of the orientation of woven T300 carbon fiber ply-lay ups and 3D woven composites that utilize a designed elastic modulus (Limmer et al., 1996). In doing so, Limmer found that the localized control of the stiffness in the prosthetics' material allowed for increased elastically stored energy at both natural and fast walking speeds.

Due to the complex shape of a prosthetic device, finite element modeling has also allowed for the generation of life and reliability models without the need to conduct comprehensive component level fatigue testing. In a study by Chen the gait reaction forces from a 55 year old patient were used to identify the fatigue life and probability of failure of the patients polypropylene monolimb prosthetic over the service life of the device (Chen et al., 2006). This was accomplished by statistically modeling the material life, the uncertainty of the two peak loads during walking, and the cumulative damage on the device. According to Chen, the material life of thermoplastics is well represented by Wirschings S-N curve model in Eq.(2.5.1) where the cycles to failure ($N_f$) is determined from the fatigue stress ($S$), the fatigue strength exponent ($m$) and the fatigue strength coefficient ($K$).

$$N_f = K S^{-m} \tag{2.5.1}$$

The logarithmic uncertainty $(B)$ of the estimate peak loads $(S_i^e)$ during walking substituted into Miner's rule, as shown in Eq. (2.5.2), for linear cumulative damage where the median life of the material $(N_i)$ and number of cycles $(n)$ is used to predict the total damage $(\alpha)$ incurred on the material.

$$\alpha = \frac{n}{N_1} + \frac{n}{N_2} = \frac{B^m \left[ \left( S_1^e \right)^m + \left( S_2^e \right)^m \right] n}{K} \tag{2.5.2}$$

This cumulative damage expression was then integrated in the lognormal probability distribution function with experimentally determined uncertainty values for peak loads and the fatigue strength coefficient to determine the probability to failure over $n$ cycles during the service of the device.

# CHAPTER 3: EXPERIMENTAL APPROACHES

## 3.1 Load Platform Design and Fabrication

To characterize the mechanical behavior of commercially available prosthetic feet, a custom testing rig was designed and fabricated with the ability to interface with a both a 5kN MTS Insight and 50kN Instron unaxial load frame allowing for the uniaxial compression testing of prosthetic feet at the representative loads and angles of the stance phase of the gait cycle. The testing rig, shown in Figure 17, consisted of a rigid flat plate that was held at the target angle by a sine vise with stack blocks that were clamped to the 5kN MTS load frame that was used during the benchtop testing of the prosthetic feet.

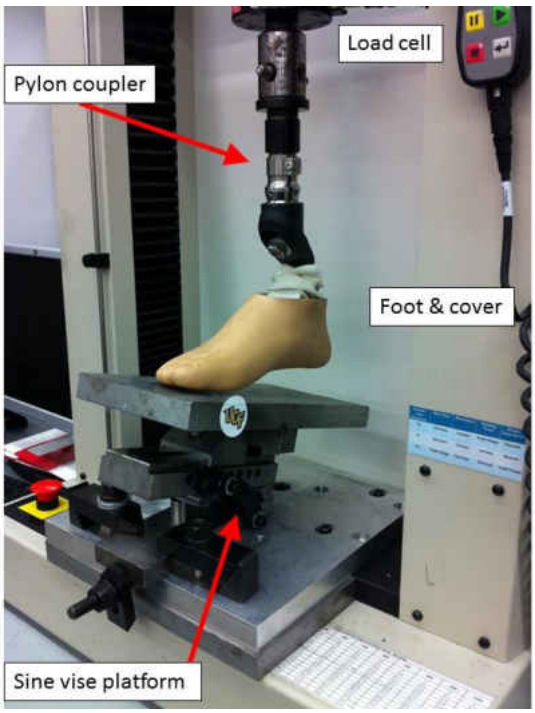


Figure 17: MTS 5kN Insight with custom testing platform

To mount the machine clamps to the load frame an aluminum interface plate was developed with its dimensions shown in the Appendix C. The rigid T-shaped load plate held by sine vise consisted of 1 x 12 x 6 in. steel that was welded to a 1 inch bar. This setup allowed for the examination of the force-displacement history during cyclic loading of the foot.

## 3.2 Preliminary Testing

Prior to the mechanical testing of the prosthetic feet, preliminary cyclic compressive tests were conducted to determine the effects of the loading rate, the load magnitude, and preconditioning effect on the stiffness and energy return efficiency. Additionally, preliminary force relaxation tests were conducted to determine the minimum test duration necessary to fully describe the viscous relaxation of the component. These preliminary tests were conducted on a size 28 Freedom Innovations Renegade prosthetic foot with a size 28 foam cover with a prescribed foot stiffness of seven, which is recommended for body mass up to 100 kg under high impact conditions, or a 130 kg individual under low impact applications (Freedom-Innovations, 2015). Following the ISO 22675 recommended loads and angles for a P5 category foot, the prosthetic was monotonically loaded to the target force using a 5kN MTS Insight and the custom testing rig.

Despite behaving elastically under the cyclic loads, the force displacement of the foot took on a nonlinear profile due to the foot geometry and contact mechanics. A typical force displacement response for the prosthetic foot with and without the foam cover is shown in Figure 18. The linear stiffness $(K)$ of the prosthetic foot during the preliminary testing was measured by calculating the tangential slope of the final 80% of the force displacement plot. The work energy lost during loading and unloading, shown by the area within each hysteresis loop, was calculated

by integration of the force ($F$) and displacement ($\delta$) with Eq.(2.4.1) using the trapezoidal integration method. It was noted that the Renegade foot was highly efficient in contrast to the other of the market prosthetic described in Table 1. At the 20° angle the Renegade foot returned 98% of the elastically stored energy during unloading and 92% of the stored energy with the cosmetic foam cover.

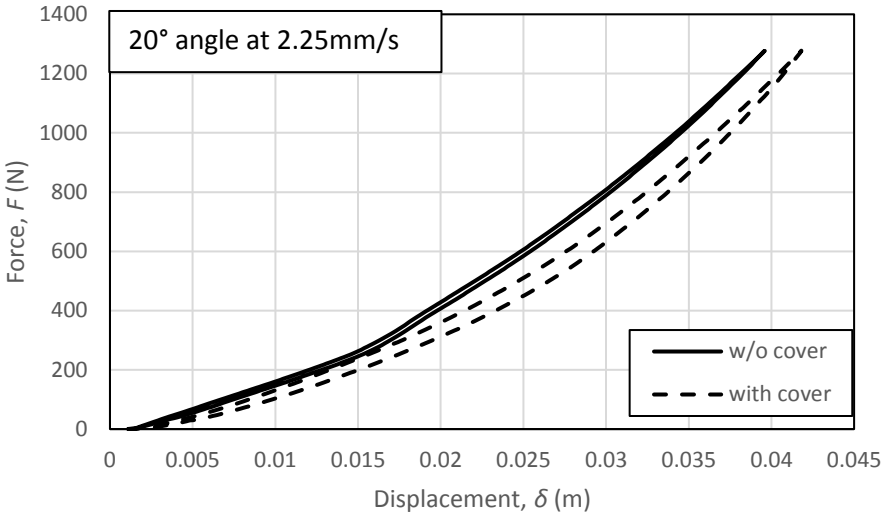


Figure 18: Hysteresis loop for 20° Renegade with and without foam cover

The preliminary displacement rate controlled test on the Renegade prosthetic foot was conducted at a 15 degree incline to a target load of 1271N with a controlled crosshead displacement speed between 0.2 mm/s and 10 mm/s as shown in Figure 19. It was noted that the displacement rate, and consequently the load rate, had minimal effect on the stiffness and energy return of the prosthetic foot during loading. On average, at the 15° angle the Renegade foot in its foam cover demonstrated a stiffness of 68.70 N/mm during compressive loading and returned 89.2% of the elastically stored work energy ($W$) during unloading. These results suggest that the

ISO 22675 standard's recommendations of a loading rate between 100-250 N/s for static proof testing is also an acceptable guideline for evaluating the energy return and the stiffness of prosthetic feet.

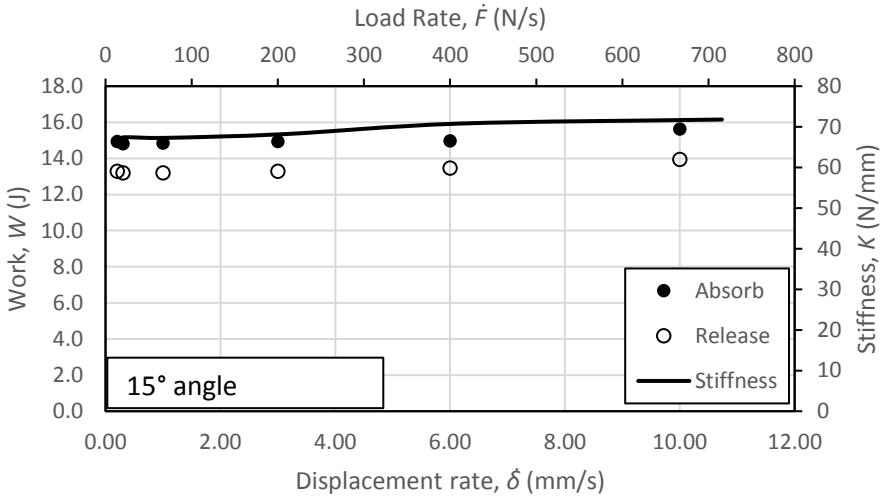


Figure 19: Displacement rate test on Renegade foot with cosmetic cover

The effect of the force magnitude on the stiffness and energy return of the Renegade prosthetic was examined with mechanical loading of the foot against a 15 degree incline load plate at a constant displacement rate of 2 mm/s. The results of these test are shown in Figure 20. As expected, the amount of work energy absorbed by the prosthetic foot is linearly proportional to the force placed on the foot. However, it was also observed that there was both an increase in the energy loss and an increase in the stiffness as the load was increased. These trends are attributed to the geometry of the foot during bending. This supports the assumption that evaluation of the stiffness and energy return must be conducted at the expected loads and angles during service.

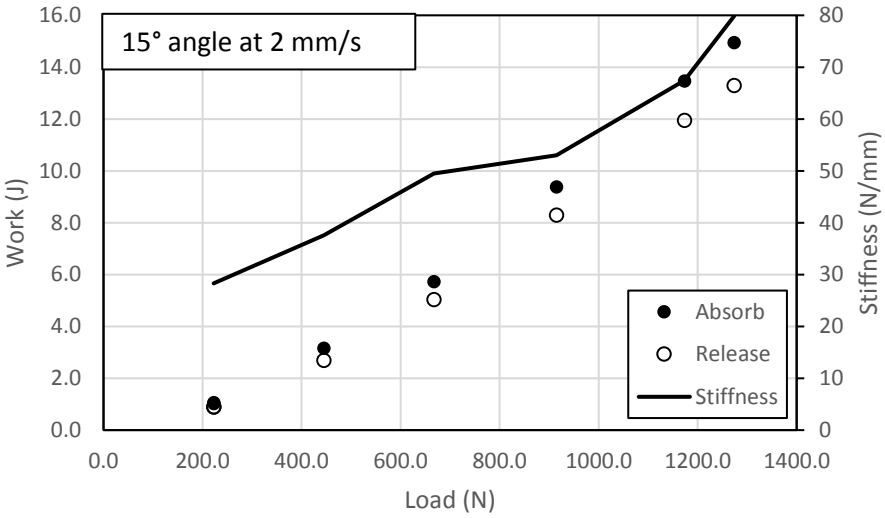


Figure 20: Load test on Renegade foot with cosmetic cover

To reflect the behavior during prolonged use, preliminary tests were conducted to determine the amount preconditioning necessary to remove any viscous effects that could be appear during the mechanical testing. This tests consisted of cyclically loading the Renegade prosthetic foot in its foam cover at a 15 degree angle to a load of 1271 N for ten cycles. It was determined that the energy return had stabilized by the third cycle. It was decided that a five cycle preload would be appropriate to eliminate any viscous effects present during the mechanical testing. The viscous effects of the prosthetic foot were examined by loading the Renegade foot with and without its foam cover at a rate of 0.2 mm/s to a load of 1276 N at an angle of 20 degrees and held at this load for a duration of 180s (Figure 21) based similar testing conducted by Haberman (Haberman, 2008). It was noted that there was only a 0.02% difference in load between 170s and 180s; therefore it is assumed that a 180s test duration provided sufficient time for the viscous effects to fully decay. During the preliminary relaxation test of the Renegade foot it was noted that the foot with its cover experienced 2.6% decay in force, whereas the foot without the cover experienced

1.25% decay in force. This indicates that the cosmetic foam cover does influence the viscous behavior of the prosthetic foot, however, the short term viscoelastic effects are relatively negligible. For a 100 kg individual during prolonged walking with the Renegade foot and its cover, the maximum viscoelastic deformations would be approximately 0.85 mm.

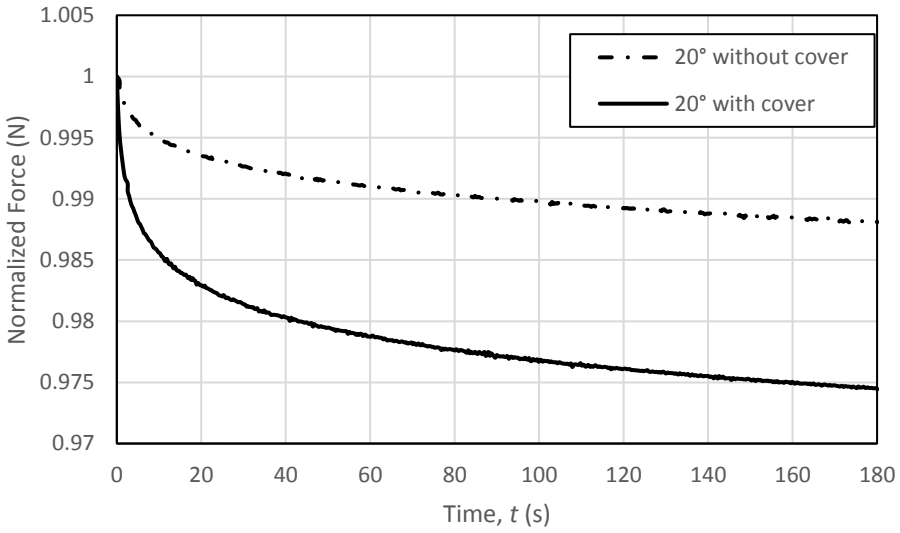


Figure 21: Force Relaxation of Renegade foot with cover at 20 degrees

To characterize the force relaxation data, the standard linear viscoelasticity model, the Norton-Bailey, the Burgers model, and the generalized Maxwell-Wiechert model, that were previously discussed in Section 2.4.3 , were fitted to the experimental data using numerical regression software. For convince, these models are reproduced as follows,

Power Law: $$F = F_0 t^m \tag{3.2.1}$$

Norton-Bailey: $$F = \left( \frac{\delta}{A t^m} \right)^{1/n} \tag{3.2.2}$$

Standard linear:
$$F = \delta\left( k_1 + k_2 \exp\left( -\frac{\mathrm{t}k_2}{\eta} \right) \right) \tag{3.2.3}$$

Burgers:
$$F = \delta\left[ \frac{1}{k_1} + \frac{t}{\tau_1} + \frac{1}{k_2}\left( 1 - \exp\left( -\frac{tk_2}{\tau_2} \right) \right) \right]^{-1} \tag{3.2.4}$$

Maxwell-Wiechert:
$$F = \delta\left( k_1 + \sum_{n=2}^{N} k_2 \exp\left( -\frac{\mathrm{t}k_2}{\eta_1} \right) \right) \tag{3.2.5}$$

To adapt the viscoelasticity models in Eq.(3.2.3) through Eq. (3.2.5) for the force relaxation testing, the $k_1$ stiffness, which represents the long duration elastic properties, was set equal to the experimental force $F(t)$, at time ($t$) equals $180$ seconds, over the constant displacement ($\delta_0$) as shown in Eq.(3.2.6).

$$k_1 = \frac{F\left(t = 180\right)}{\delta_0} \tag{3.2.6}$$

The long duration stiffness $k_1$ represents the force behavior after force has completely decayed and viscosity has become negligible. A comparison of these three models of these models with the preliminary force relaxation data shown in Figure 22.

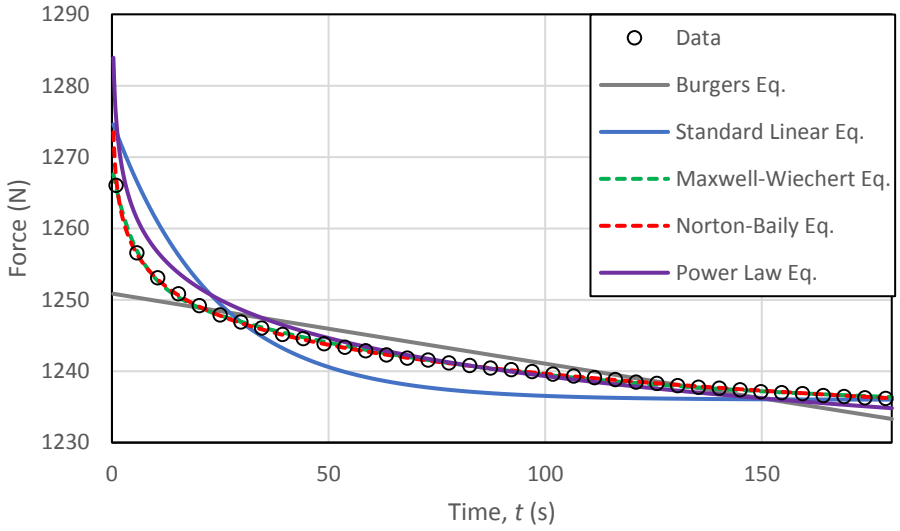


Figure 22: Force-relaxation models for 20° Renegade foot and foam cover

While the Norton-Baily model goes to infinity at time equal to zero, it was observed that for all other time increments the 3-term Norton- Bailey model produced the best fit of the force relaxation data coefficient of determination ($R^2$) of 0.999. Both the power law and Maxwell-Wiechert model were also able to produce a similarly accurate model with $R^2$ equal to 0.999 and 0.998 respectively, however, in both cases, the residual error was greater than the Norton-Bailey model. In contrast, the standard linear and Burgers model did not fit as well with a correlation coefficient of 0.92 and 0.78, respectively. It was also noted than the time exponent ($m$) in the power law (-0.0062) and the Norton-Bailey equation (-0.0068) were similarly valued. This is a result of the force exponent ($n$) having a value of -1.45; as $n$ goes towards -1, both the power law and the Norton-Baily equation would have an identical time exponent.

## 3.3 Compressive Testing

The forces and angles used in the mechanical characterization of the Renegade foot and the TaylorMade prototype foot were based on the idealized gait load curve from the ISO 22675 standard shown in Figure 7. The tabulated values of this loading curve, shown in Table 2, was used to develop an analytical model of the idealized gait response for the normalized vertical loads and the angle of the tibia with respect to the vertical. Fifteen data points over this idealize loading pattern were then selected for mechanical testing in the testing rig.

Table 2: ISO 22675 cyclic load points

| **Time, *t* (ms)** | **Angle (deg.)** | **P5 Load (N)** | **P4 Load (N)** | **P3 Load (N)** |
|---:|---:|---:|---:|---:|
| 0 | -20 | 0 | 0 | 0 |
| 30 | -19.5 | 331 | 306 | 238 |
| 60 | -19 | 663 | 612 | 477 |
| 90 | -18 | 996 | 919 | 716 |
| 120 | -16.5 | 1221 | 1126 | 878 |
| 150 | -15 | 1273 | 1173 | 915 |
| 180 | -13 | 1215 | 1120 | 873 |
| 210 | -10.5 | 1092 | 1007 | 785 |
| 240 | -7.5 | 969 | 893 | 697 |
| 270 | -4 | 880 | 811 | 632 |
| 300 | 0 | 850 | 783 | 611 |
| 330 | 4 | 879 | 810 | 632 |
| 360 | 8 | 966 | 891 | 694 |
| 390 | 12 | 1086 | 1003 | 781 |
| 420 | 16 | 1204 | 1110 | 866 |
| 450 | 20 | 1256 | 1158 | 903 |
| 480 | 24 | 1198 | 1105 | 861 |
| 510 | 28 | 971 | 895 | 698 |
| 540 | 32 | 643 | 593 | 463 |
| 570 | 36 | 321 | 296 | 231 |
| 600 | 40 | 0 | 0 | 0 |

The idealized vertical loads $L(t)$ and loading angles $D(t)$ were developed using a three-term sinusoidal equation.

$$L(t) = \cos(7.1308 \cdot \cos(\sin(5.2553 + 0.003431 \cdot t))) \tag{3.3.1}$$

$$D(t) = 6.4034 \cdot t^2 - 19.9878 \cdot \cos(-0.004274 \cdot t) \tag{3.3.2}$$

The constants in Eq.(3.3.1) and Eq.(3.3.2) were developed through numerical regression of the normalized loads from the tabular data in Table 2. During mechanical testing at the P3, P4, and P5 load levels, the force over time was determined by multiplying Eq.(3.3.1) by the peak load in each respective category. Fifteen data points over this load pattern were selected at every five degrees from -20 to 40 degrees, with an additional two data points at -19.25 and -17.5 degrees to capture the slower initial roll-over during heel loading. The tabulated ISO 22675 data, the data points for mechanical testing, and the analytical models of vertical force and angle are shown in Figure 23.

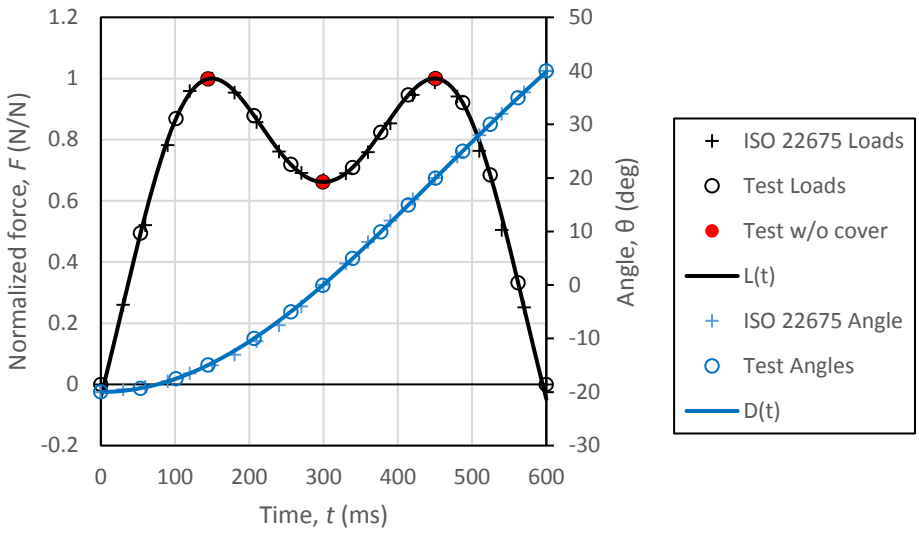


Figure 23: Test loads with regression of idealized gait from ISO 22675

The test points are reasonably distributed to capture the behavior of the foot over the entire loading pattern. Alternatively the six-term polynomial provided in the ISO standard could also have been used to generate the idealized loading pattern. To examine the influence of the foam cover on the stiffness and energy return of the prosthetic feet, mechanical testing was additionally conducted on the feet at the three critical angles of -15, 0, and 20 degrees shown in red on Figure 23. A test matrix for the appropriate load and the desired testing angles for each foot was generated based on the recommended body mass and ISO 22675 testing standard. This matrix is listed in Appendix D.

During the preliminary compressive testing, the stiffness ($K$) was measured from the tangential slope of the linear region of the force displacement plot. This is a typical approach used to evaluate the elastic modulus during material testing. However it was noted in

Figure 18 that the force-displacement response of the prosthetic foot has a nonlinear elastic behavior. For this reason, it was determined that the overall component stiffness ($K_c$) should also be evaluated at each angle during the compressive testing.

$$K_c = \frac{F_{max}}{\delta_{max}} \tag{3.3.3}$$

Where the component stiffness is equal to the peak force ($F_{max}$) over the maximum deflection ($\delta_{max}$)of the prosthetic foot. While the linear stiffness provides a well understood analogy to the elastic modulus of a material, the overall component stiffness may be more beneficial for clinicians.

Additionally, the energy return at each of the fifteen test angles was calculated from the force-displacement plots following a similar procedure as the preliminary testing. The work energy during loading and unloading of at each test angle was calculated through the integration of Eq.(2.4.1) via the trapezoidal method. Following Eq.(2.4.2), this allowed for the calculation of the work energy efficiency of the foot at each test angle.

## 3.4 Force Relaxation Testing

During the relaxation testing of the Renegade and TaiLor Made prosthetic feet, each foot was subjected to a cyclic preconditioning followed by force relaxation testing at fifteen angles with the cover and three critical angles without the foam cover. Based on the preliminary testing in section 3.3, the preconditioning consisted of loading prosthetic foot from rest to the target force five times. The force relaxation testing of the prosthetic feet consisted of loading the prosthetic foot to the target load and then holding the MTS crosshead in a fixed position for a

duration of 180s while recording the decay of force on the load cell. The fifteen angles used for testing with the foam cover and foot consisted of the data points shown in Figure 23, while the relaxation testing without the foam cover was conducted three critical angles of -15, 0, and 20 degrees.

Based on the preliminary testing in section 3.2, the force relaxation of each angle was characterized through the use of the Norton-Bailey creep model shown in Eq.(3.4.1).

$$F = \left( \frac{\delta_0}{At^m} \right)^{1/n} \tag{3.4.1}$$

By fitting the force coefficient $(A)$, the force exponent $(n)$, and the time exponent $(m)$ to the decay in force $(F)$ over time $(t)$ through numerical regression.

## 3.5 Digital Image Correlation

During the structural testing of the prosthetic feet the crosshead displacement was used to measure the vertical deflection of the foot; however, because of the complex geometry of the component, this displacement provides little insight into the localized stress and strain acting on the component. To identify these localized values, digital image correlation (DIC) was performed during mechanical testing to optically measure the surface strain on the carbon fiber layers during the structural loading of the Renegade and TaiLor Made prosthetic feet. While optical strain measurement techniques, such as digital image correlation, are primarily used to develop a displacement map of 2D and 3D specimen surfaces during material testing, it has previously been shown by Parnell that these techniques can also be used to evaluate prosthetic feet at the component level during mechanical proof testing (Parnell, 2014).

The digital image correlation technique is an expansion of the laser speckle interferometry method that determines the displacement field of a speckle painted surface as a specimen is subjected to mechanical loads. In contrast to traditional laser interferometry methods that require highly specialized equipment, DIC can be conducted with an ordinary monotone light source, a computer, and the charge-coupled device (CCD) array found in a high resolution digital video camera as depicted in Figure 24 (Pan et al., 2014). Following a similar approach as Parnell, the DIC analysis was conducted during by painting the side of each foot with white paint flecks to provide to provide a sufficient contrast to allow optical measurements of the strain through the ply thickness.

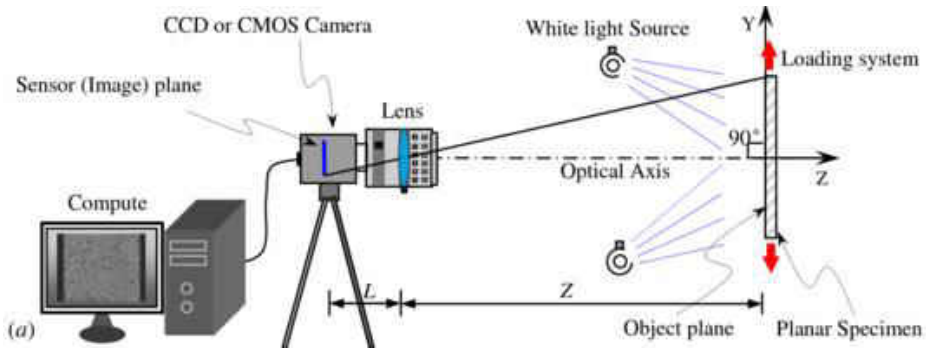


Figure 24: Diagram of experimental setup used for Digital Image Correlation (Pan et al., 2014)

As the prosthetic foot was subjected to mechanical loads, the speckles of the painted surface experience relative motion due to the surface deformations of the foot. This movement is recorded in a series of images showing a progression of the surface from its original state, to its final deformed state. These images are digitally converted to an intensity map by the CCD-array allowing for the displacement mapping of target features between successive images. The target point $P(x, y)$ in a reference state was mapped to the point $P^*(\tilde{x}, \tilde{y})$ in the image of the deformed

state using the displacement components *u* and *v* as shown in Eq.(3.5.1) and Eq. (3.5.2) (Dally et al., 2005).

$$\tilde{x} = x + u(x, y) \tag{3.5.1}$$

$$\tilde{y} = x + v(x, y) \tag{3.5.2}$$

The displacement mapping parameters of components *u* and *v* are expressed as a 12 parameter second order Taylor series expansion of an arbitrary point $S_p = P(x_0, y_0)$ that exists in a subset of points *S* in the image, as follows:

$$\tilde{x} = x_0 + u_0 + \frac{\partial u}{\partial x}\Delta x + \frac{\partial u}{\partial y}\Delta y + \frac{1}{2}\frac{\partial^2 u}{\partial x^2}\Delta x^2 + \frac{1}{2}\frac{\partial^2 u}{\partial y^2}\Delta y^2 + \frac{\partial^2 u}{\partial x \partial y}\Delta x \Delta y \tag{3.5.3}$$

$$\tilde{y} = x_0 + u_0 + \frac{\partial u}{\partial x}\Delta x + \frac{\partial u}{\partial y}\Delta y + \frac{1}{2}\frac{\partial^2 u}{\partial x^2}\Delta x^2 + \frac{1}{2}\frac{\partial^2 u}{\partial y^2}\Delta y^2 + \frac{\partial^2 u}{\partial x \partial y}\Delta x \Delta y \tag{3.5.4}$$

These mapping parameters are determined by minimizing a correlation coefficient *C*, shown in Eq.(3.5.5), between the target point locations in reference state and its location in the deformed state. In this equation, the gray scale pixel intensity of the reference state and the deformed state are represented using continuous bi-cubic spline functions respectively shown in Eq.(3.5.6) and Eq.(3.5.7). The pixel intensity function $g(x, y)$ of the reference state depends only on the pixel location in the reference image and its spline coefficients $a_{mn}$, whereas the intensity function $h(\tilde{x}, \tilde{y}, P)$ of the deformed state depends on the new pixel location, the coefficients $b_{mn}$, and the

mapping parameters $P$ which represents both the displacement vector as well as the coefficient $\alpha$ to adjust any changes in the brightness between the two images (Dally & Riley, 2005).

$$C = \frac{\sum_{S_p \in S} \left\{ g\left(S_p\right) - h\left(S_p, P\right) \right\}^2}{\sum_{S_p \in S} g\left(S_p\right)^2} \tag{3.5.5}$$

$$g\left(x, y\right) = \sum_{m=0}^{3} \sum_{n=0}^{3} a_{mn} x^m y^n \tag{3.5.6}$$

$$h\left(\tilde{x}, \tilde{y}, P\right) = \sum_{m=0}^{3} \sum_{n=0}^{3} b_{mn} \tilde{x}^m \tilde{y}^n + \alpha \tag{3.5.7}$$

To record the surface strain of the prosthetic feet during loading a CCD camera with a 2448x2048 resolution and Tokina AT-X Pro D M100 F2.8 lens was centered on the ankle joint of the prosthetic foot. Due to space limitations, it was necessary to conduct the DIC compressive testing on a 50 kN MTS Insight Wide load frame with a as shown in Figure 25. The DIC analysis of the recorded images was conducted using Vic – 2D version 2009 software.


Figure 25: Camera setup with prosthetic foot in load frame

# CHAPTER 4: EXPERIMENTAL RESULTS

## 4.1 Compressive Test Results

Uniaxial compression test were conducted on the Freedom Innovations Renegade foot and the TaiLor Made foot to determine the deflection, the stiffness, and energy return during quasi-static loading at select fifteen selected angles over the idealized loading pattern with and without their cosmetic covers as depicted in Figure 23. The magnitude of the loading pattern for each respective foot was determined by the manufactures body mass recommendations. The Renegade foot examined in this study was size 28 foot with a stiffness of 7 and recommended for body between 100kg and 130kg, which corresponds to P5 loading conditions by the ISO 22675 standard (Freedom-Innovations, 2015). The size 23 TaiLor Made foot that was examined was recommended for a 60kg individual under the P3 loading conditions. The TaiLor Made prosthetic foot was also equipped with three blue internal tibial springs. The cosmetic covers used in this test were both Freedom Innovations covers as the TaiLor Made covers were not yet commercially available. A direct comparison of the displacement for each foot over the loading curve is shown in Figure 26. The normalized vertical loads are also plotted as a reference for heel strike and toe push-off.

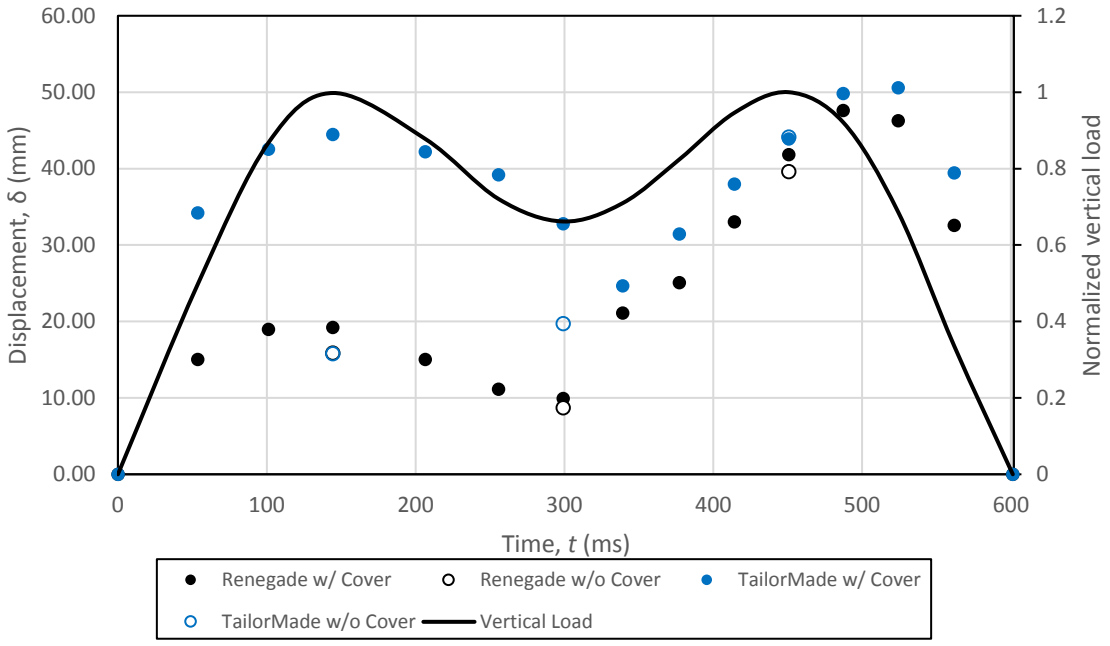


Figure 26: Displacement profile of Renegade and TaiLor Made prosthetic foot with and without foam

Interestingly, both feet exhibited an identical amount of deflection during heel strike without their foam covers and at their respective loads. However, as roll-over progressed the TaiLor Made foot was subjected to greater deflections than the Renegade foot. It was additionally noted there was relatively large amount of the heel deflection in the TaiLor Made foot with its cosmetic cover. This is attributed to an imperfect fit between the cosmetic cover and the TaiLor Made foot.

Both the linear stiffness and the component stiffness of each test angle were calculated following the procedures described in Section 3.3. The slope of the linear region of the force displacement plot is shown in Figure 27 and the component stiffness from Eq.(3.3.3) is examined

in Figure 28. By comparing these two plots it becomes apparent that linear stiffness may overestimate the behavior of the device. This is due to the nonlinear hardening behavior that compressive loading. For this reason, it is assumed that the overall component stiffness may be more useful to clinicians.

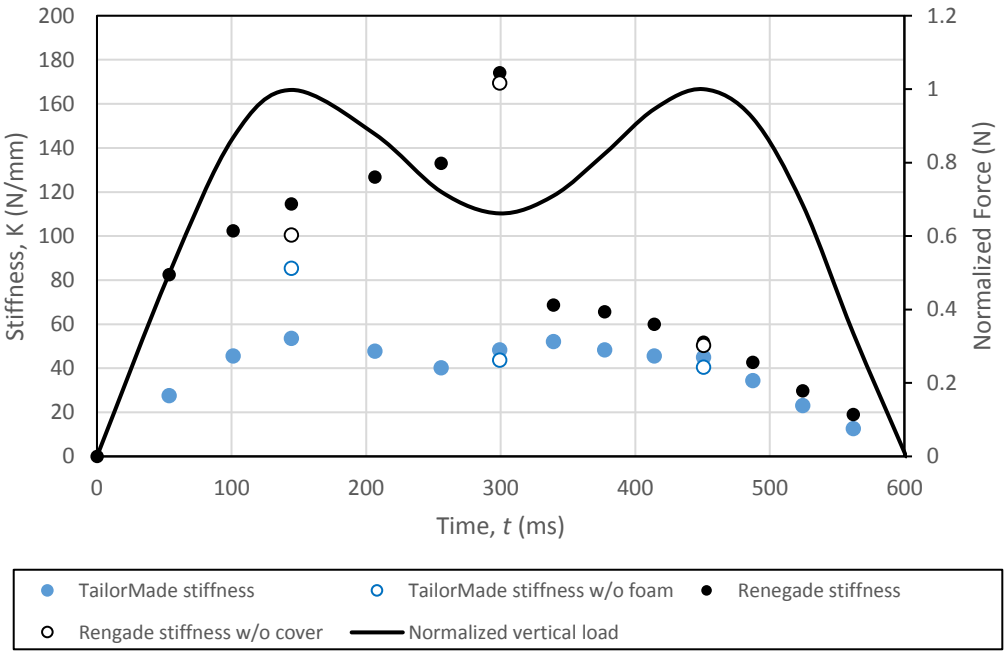


Figure 27: Tangential stiffness profile of Renegade and TaiLor Made foot with and without foam

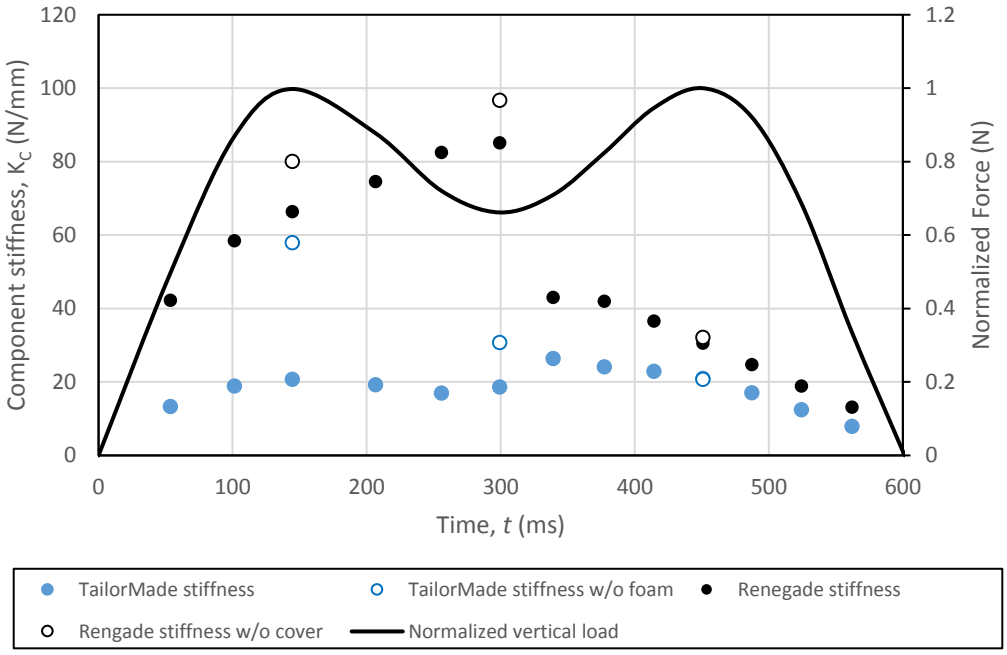


Figure 28: Component stiffness profile of Renegade and TaiLor Made foot with and without foam

Further examination of Figure 28 shows that the cosmetic cover can reduce stiffness behavior of the prosthetic foot assembly. However, this effect was observed to a much greater extent on the heel of the TaiLor Made foot. It was also noted at 0° the stiffness of the TaiLor Made was significantly lower than that of the Renegade foot; a potential result of the tibial springs in the TaiLor Made foots' design.

Using the cyclic force displacement data from each of these tests the strain energy density during loading and unloading was calculated through integration of the work with Eq.(2.4.1) and the trapezoidal method. The energy return efficiency $(\eta)$ was calculated as a ratio of the work energy during loading to the energy during unloading following in Eq.(2.4.2) at each angle over the load pattern. The energy return profile for the Renegade and TaiLor Made foot are plotted in Figure 29 and Figure 30 respectively.

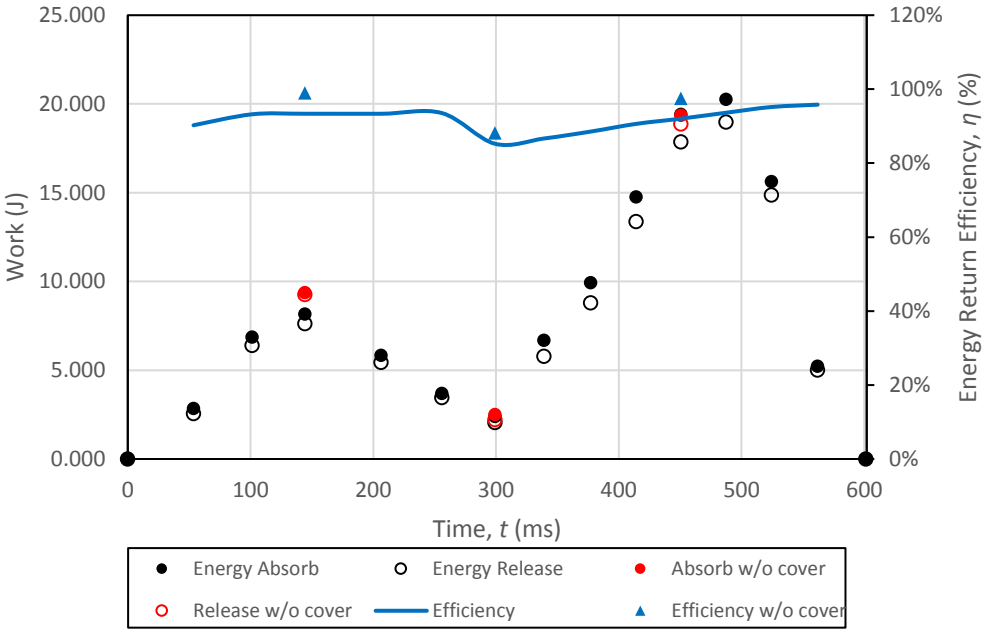


Figure 29: Energy return profile for Renegade prosthetic foot with and without foam

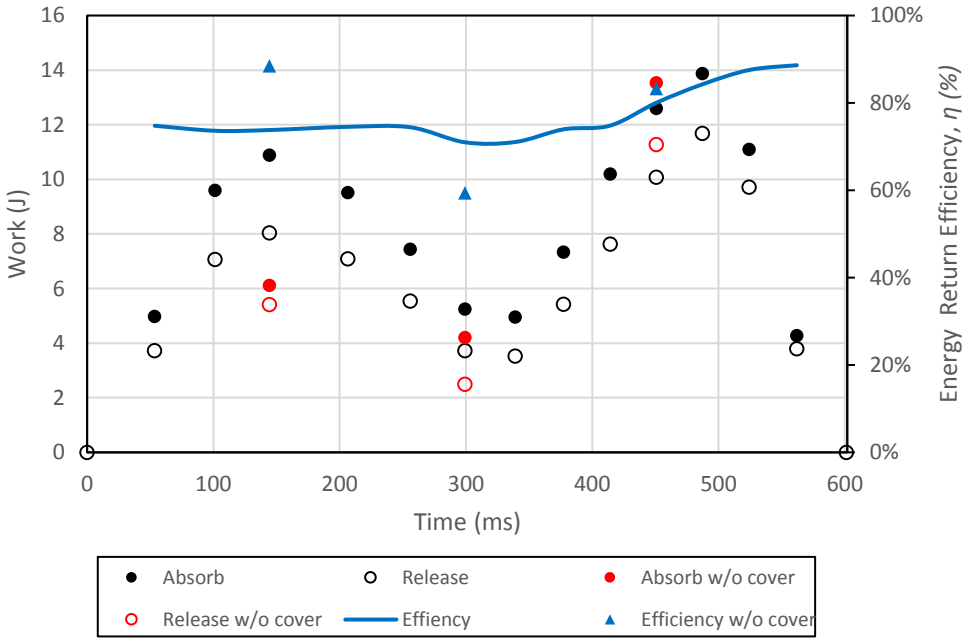


Figure 30: Energy return profile for TaiLor Made prosthetic foot with and without foam

Here it is observed that the both the Renegade and the TaiLor Made foot exhibit a much higher energy return efficiency in comparison to various other prosthetic feet that were listed in Table 1. Interestingly, the peak energy capacity on the toe of both the Renegade and TaiLor Made foot did not occur at the at the peak load at 20 degrees, instead it occurred 25 degrees. It was additionally noted that the return energy efficiency ($\eta_c$) in the cosmetic cover decreased by 5% and 6% in comparison to the efficiency ($\eta$) without a cover on the heel and toe of the Renegade foot. In contrast, the TaiLor Made prosthetic foot experienced a 15% and 3% decrease in efficiency on its heel and toe, however, the energy return efficiency of the TaiLor Made actually increased by 12% with its cosmetic cover at vertical loading as listed in Table 3.

Table 3: Energy return efficiency with and without a cosmetic cover

| | **Time (ms)** | **Angle** | **Efficiency w/o cover ($\eta$)** | **Efficiency with cover ($\eta_c$)** |
|---|---|---|---|---|
| **Renegade** | 144 | -15 | 99% | 93% |
| | 299 | 0 | 88% | 85% |
| | 451 | 20 | 98% | 92% |
| **TaiLor Made** | 144 | -15 | 88% | 74% |
| | 299 | 0 | 59% | 71% |
| | 451 | 20 | 83% | 80% |

This unexpected behavior is likely due to the internal tibial springs of the TailorMade foot falling into proper alignment when the cosmetic cover is present to help distribute the force of the load plate.

## 4.2 Force Relaxation Results

Following the force relaxation procedure developed in preliminary testing section 3.2 and the experimental outline in section 3.4 force relaxation testing was conducted on the Renegade and TaiLor Made foot at fifteen different angles with its cosmetic cover and an additional three

angles without its cosmetic cover. The force relaxation over time was fitted to the Norton-Bailey power law to determine the time exponent, the force exponent, and the force coefficient. When the time exponent $(m)$ of the Renegade foot is plotted against over the duration of roll over as shown in Figure 31, it is observed that without the foam cover the value of $m$ remains relatively constant, however, with the foam cover the value of $m$ varies as the foot progresses through the roll-over.

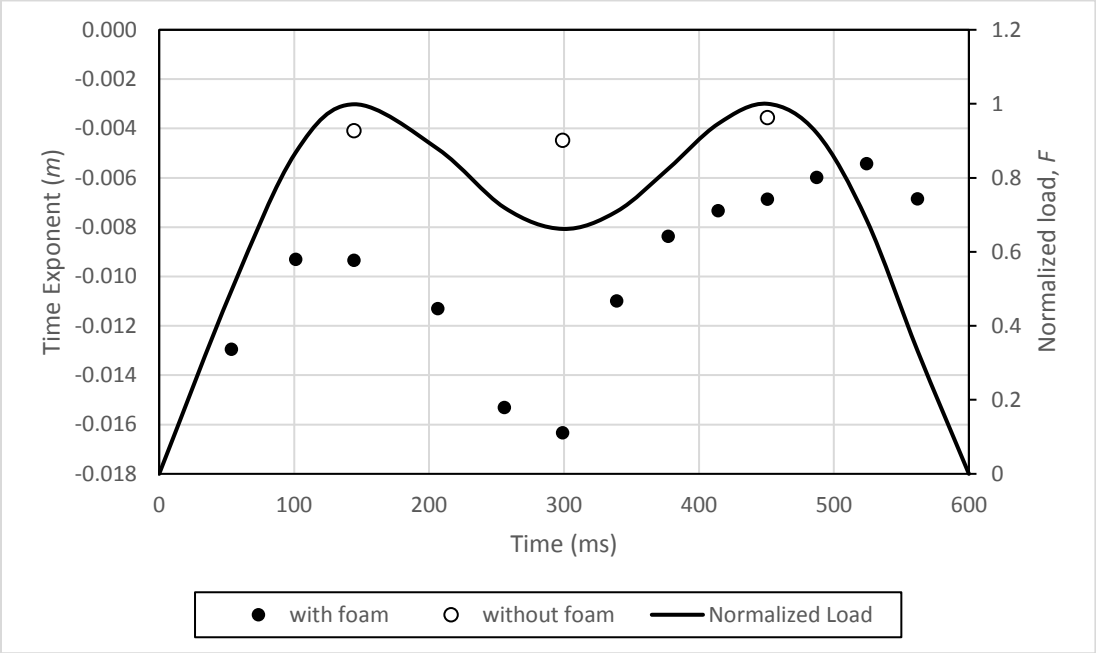


Figure 31: Renegade foot time exponent $(m)$ with and without the foam cover

This behavior is due to the time dependent behavior of the cosmetic cover. As the foot progresses through the roll-over, the foam experiences different levels of localized stress leading to variations in the viscous behavior of the overall component. Conversely, when the carbon fiber prosthetic is tested without the cosmetic cover, the prosthetic device is less dependent on time with $m$ closer to the value of zero. Similarly, when plotting $m$ values of the TaiLor Made

prosthetic foot, in Figure 32, it is noted that the heel region of the prosthetic foot exhibited a much more negative time exponent. This indicates that a greater amount of energy is dissipated by the heel of the TaiLor Made foot within its cosmetic cover.

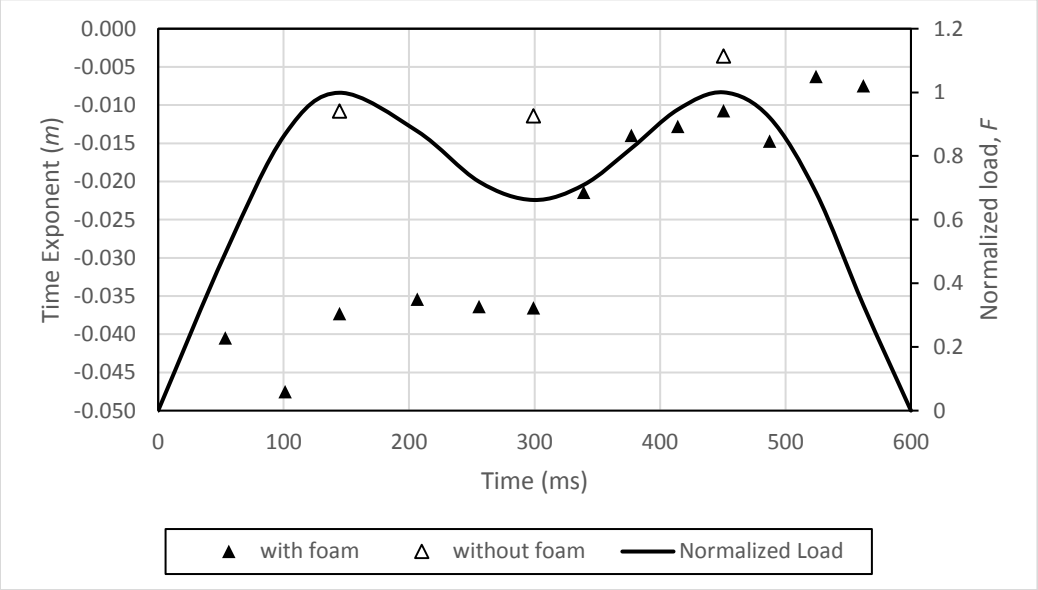


Figure 32: TaiLor Made time exponent $(m)$ with and without the foam cover

When the force exponent $(n)$ of Norton-Bailey equation was plotted over the idealized load cycle as shown in Figure 33, it was noted that the values of $n$ were similar in both the TaiLor Made and Renegade foot, and that over the load cycle $n$ shows a similar trend as the normalized load. This is because the $n$ exponent characterizes the loading function while the force coefficient $(A)$ has a greater correlation with the stiffness of the component.

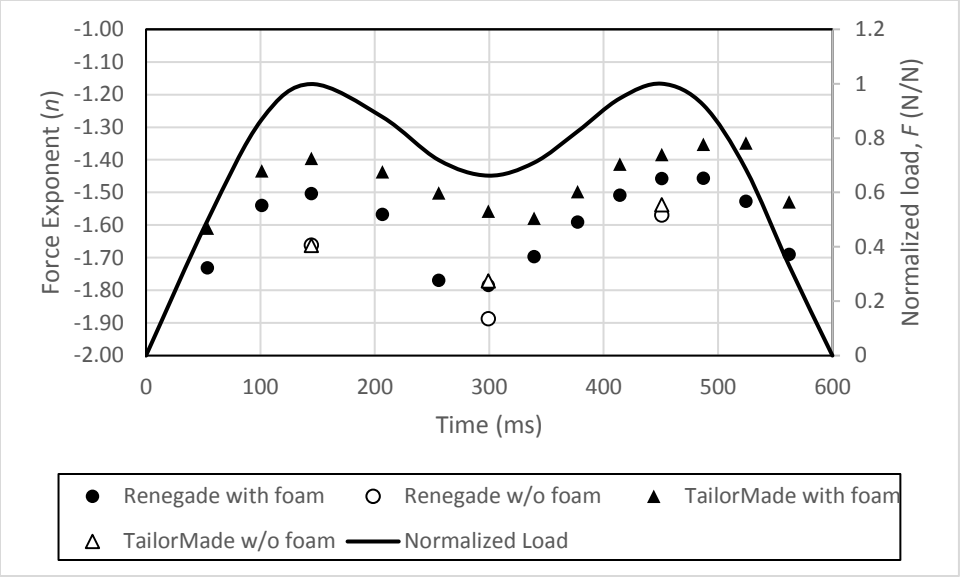


Figure 33: Renegade and TaiLor Made foot force exponent $(n)$ with and without the foam cover

When the force coefficient $(A)$ is plotted by itself in Figure 34 it was observed that the coefficients of the TaiLor Made foot are relatively constant, while the Renegade foot coefficients peak near the 0° loads. This is likely a result of the both the heel and the toe coming in to contact with the load plate and the additional compliance of the tibial springs in the TaiLor Made foot.

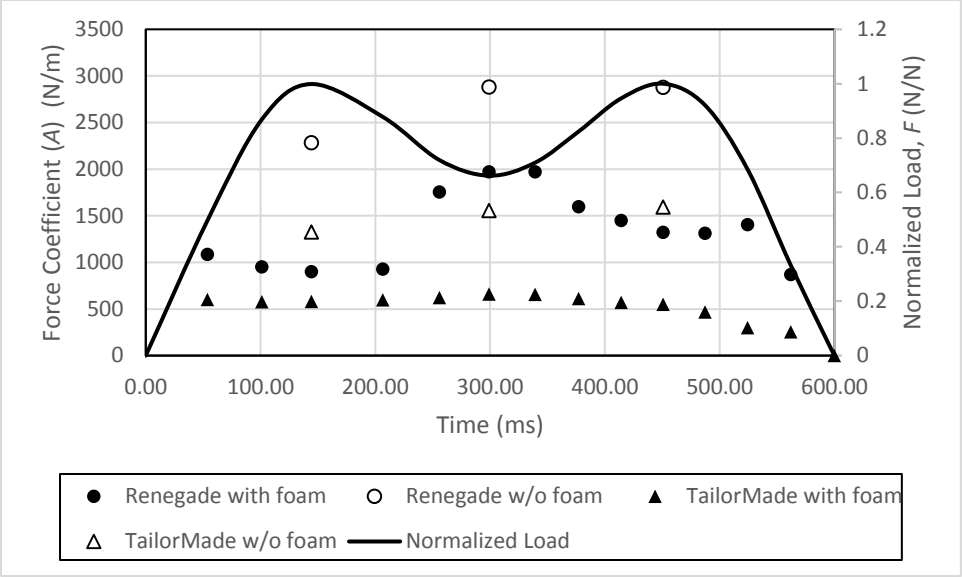


Figure 34: Renegade foot force relaxation coefficient $(A)$ with and without the foam cover

The Norton-Bailey power law from Eq.(2.4.15) can also be rewritten as shown in Eq.(4.2.1) where $A^{-1/n}$ can be considered a load parameter and *m/n* can be considered a viscous time parameter for decay in force over time $(t)$ at fixed displacement $(\delta_0)$.

$$F = \delta_0 A^{-1/n} t^{-m/n} \tag{4.2.1}$$

Interestingly, when this load parameter is plotted over the load cycle, as shown in Figure 35, it is observed that there both the TaiLor Made and Renegade prosthetic foot behavior similarly in the heel region, despite testing the TaiLor Made and Renegade foot at different force values.

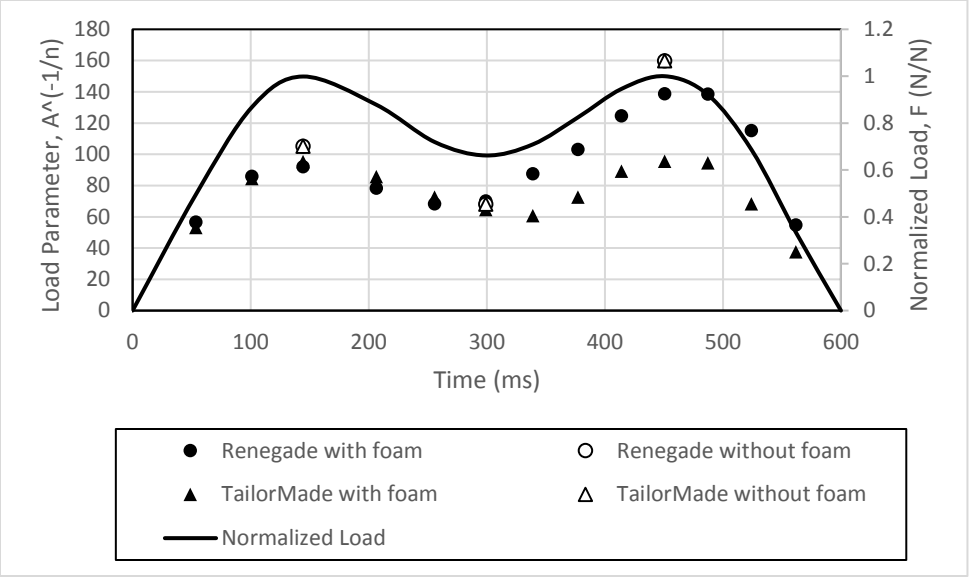


Figure 35: Viscoelasticity parameter of the Renegade and TaiLor Made foot

This would suggest that the load parameter $A^{-1/n}$ is representative of the loading function and that it is likely influenced by the compliance of the cover. Similarly, the stress exponent and time exponent can be plotted together as a time parameter *m/n* shown in Figure 36.

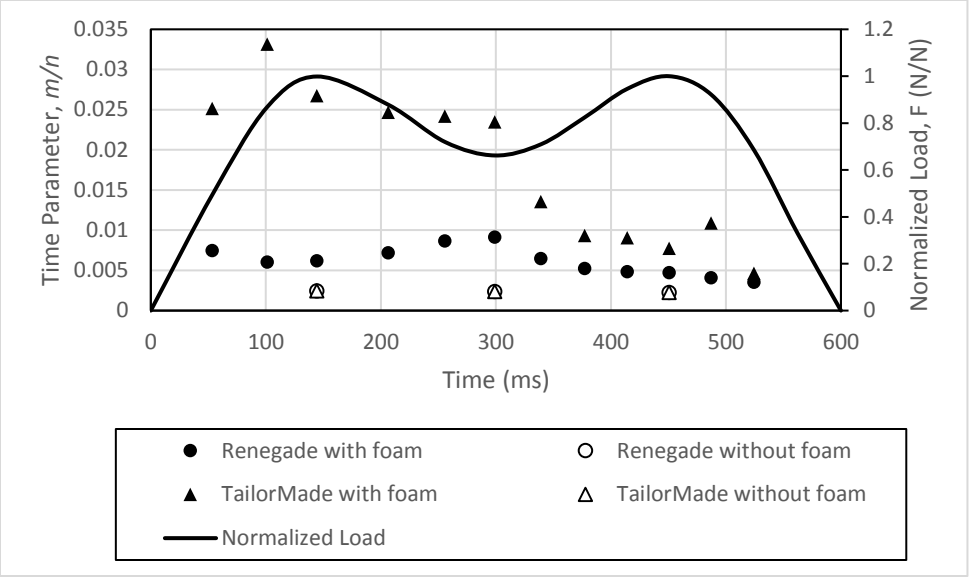


Figure 36: Time parameter of the Renegade and TaiLor Made foot

In doing so, it becomes easier to see that that the foam cover contributes significantly greater viscosity to the heel of the TaiLor Made foot. Again, this increased viscoelasticity is likely the result of the geometry of the heel and the fit of the cover. This is further demonstrated by Figure 37, in which the energy dissipated over the duration of the relaxation test is plotted for the TaiLor Made and Renegade foot.

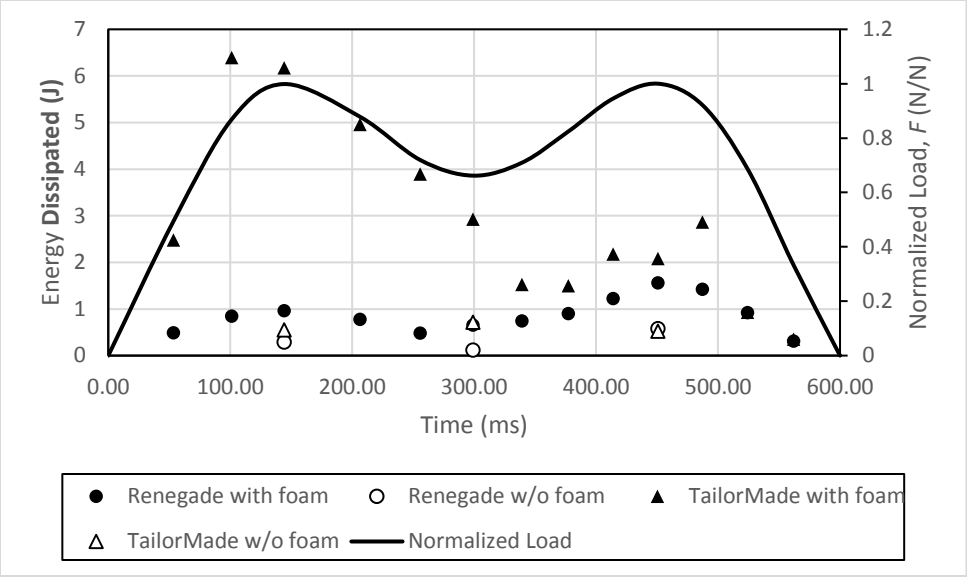


Figure 37: Energy dissipation during force relaxation

While Klute (Klute et al., 2004) had previously suggested that analysis of the viscous properties of a prosthetic foot may provide additional insight in to their ability to dissipate energy, the findings in Figure 37 suggest this capacity is predominately caused by foot covers and shoes; and that by themselves the carbon fiber prosthetics may dissipate energy similarly.

## 4.3 Digital Image Correlation

Optical strain measurements were taken on the prosthetic feet during loading at 20 degrees using the digital image correlation (DIC) technique with a CCD camera and the Vic 2D imaging software as described in Section 3.5. During this process a contour map was generated of the surface Von Mises strain in the Renegade foot during loading at 20 degrees as shown in Figure 38. Here it is observed that the maximum Von Mises strain in the geometry occurs at the inner and outer radius of the toe similar to curved beam in bending.

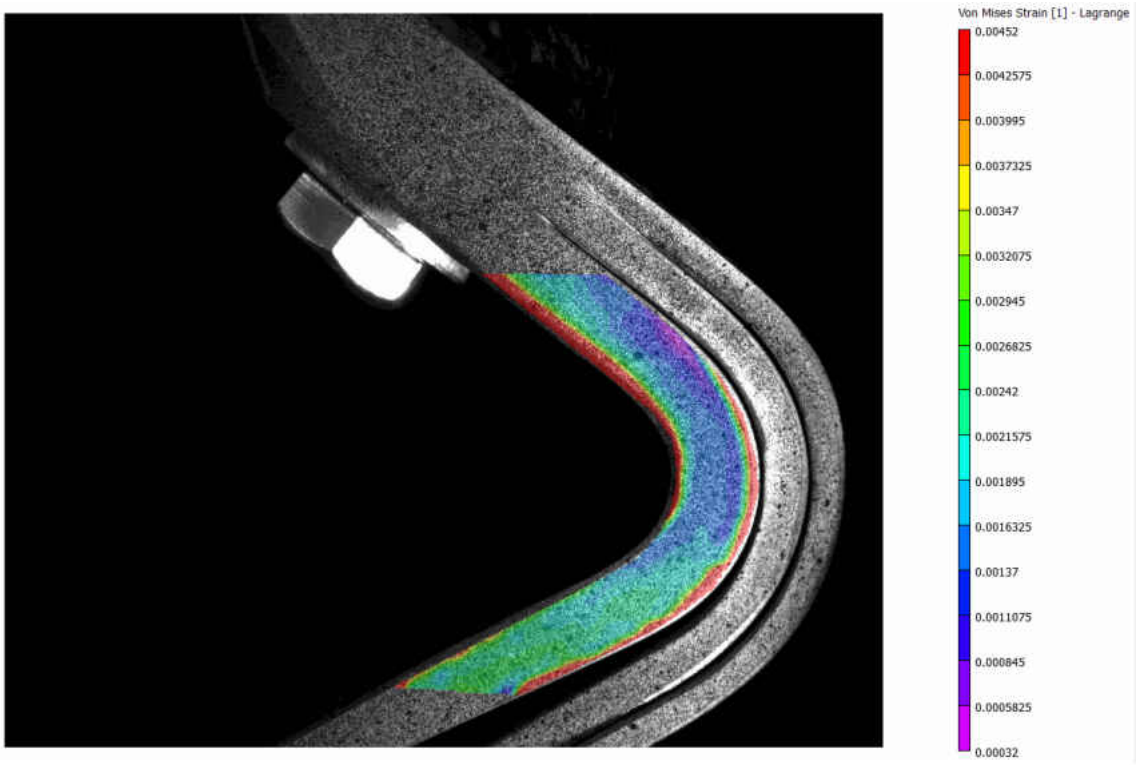


Figure 38: DIC Von Mises strain in Renegade toe during 20° loading

It was also noted that the software could not pick up on the all of the surface points of the toe cross-section, however, it can be inferred that the component experiences a surface strain near the maximum recorded strain value of 0.00452 along the inner and outer radius. Due to time constraints the optical strain of the TaiLor Made foot will be explored in a future paper.

# CHAPTER 5: FINITE ELEMENT ANALYSIS

The finite element method (FEM) has been utilized in this study for the evaluation of a prosthetic foot designs by examining the loading response, the strain energy, the maximum stress, the reaction moment, and the kinematic profile during roll over. This approach allows for the development of a conceptual device that meets set performance criteria under the gait response for a specific individual. For the purpose of this study, the gait response has been idealized with the forces and angles from the ISO 22675 standard during cyclic loading. To verify this approach, a Computer-Aided-Design (CAD) prosthetic foot model was developed in SolidWorks based on the geometry of the Freedom Innovations Renegade prosthetic foot and subjected to the ISO 22675 loading pattern in the ANSYS Workbench Mechanical FEA software. An approximation of the material properties for the FEA model were developed by comparing the experimental response of the Renegade foot in Section 4.1 with the FEA model through a parametric analysis. To optimize this FEM model for target performance criteria, such as the strain energy capacity, roll over shape, mass, reaction moment, and factor of safety, additional parametric analyses were conducted through topographic optimization.

## 5.1 Renegade Foot Model

The material of the Renegade foot in the FEM analysis was assumed to behave isotropically and to be fully described by only the elastic modulus and Poisson's ratio. A series of parametric static analysis were conducted on the FEA model to determine the approximate values of these properties by comparing the vertical deflection of the pylon with the experimental

data for the Renegade foot during quasi-static loading at -15, 0, and 20 degrees. Additionally, it was noted during the compressive testing of the Renegade foot that the over load spring did not come into contact with the heel spring of the foot during loading. For this reason, the inclusion of the overload spring in the initial model was omitted as shown in Figure 39.

a) b)


Figure 39: Representative CAD model (a) and Renegade foot (b) (Freedom-Innovations, 2015)

To simulate the behavior of the foot during bending a 20-node hexahedral element was used to mesh the CAD. While shell elements are often used during the modeling of composites, brick element were selected for this model to ensure the accurate modeling of the geometry thickness and the contact behavior. To reduce the computational cost of the model a symmetric boundary condition was applied in the sagittal plane (*XY*) of the foot as shown in Figure 40. Additionally, constraints were added to the model to prevent movement of the pylon in the X-direction and the separation of the foot's contact elements with the plate.

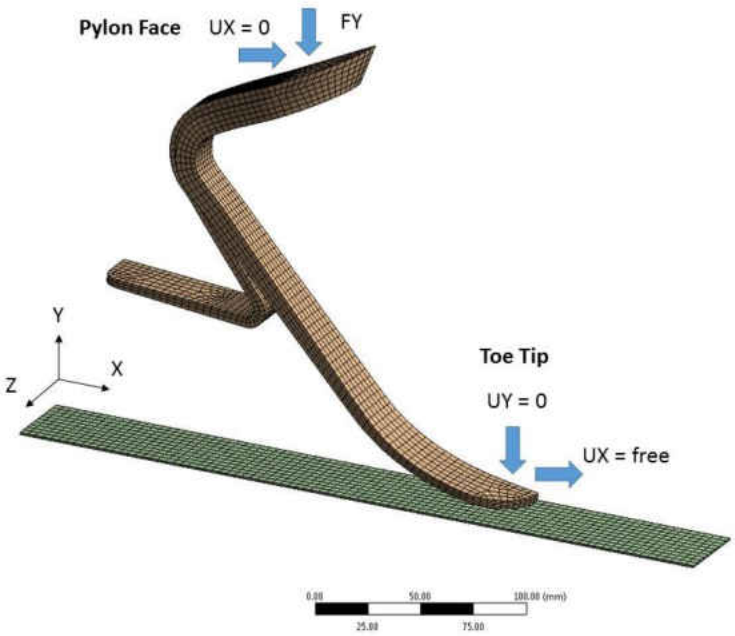


Figure 40: Renegade foot mesh and boundary conditions

During the parametric analysis, a range of potential composite material properties from literature were examined (ACP Composites, 2014; Corum, 2001). The Poisson's ratio ($\nu$) was set to range between 0.1-0.4 and the Young's Modulus ($E$) was set to range between 40-100 GPa. A twenty-five data point parametric analysis was developed using the central composite method within Ansys' Design Exploration. To match the behavior of the Renegade foot observed in Section 4.1, a genetic aggregation response surface optimization was used to determine the material properties necessary to produce a vertical displacement ($UY$) of -39.60 mm at 20°, a displacement of -8.71 mm at 0°, and -15.88 mm at -15° in the FEM model. The response plot of the vertical displacement at 20° with various values of the Young's modulus and Poisson's ratio is shown in Figure 41.

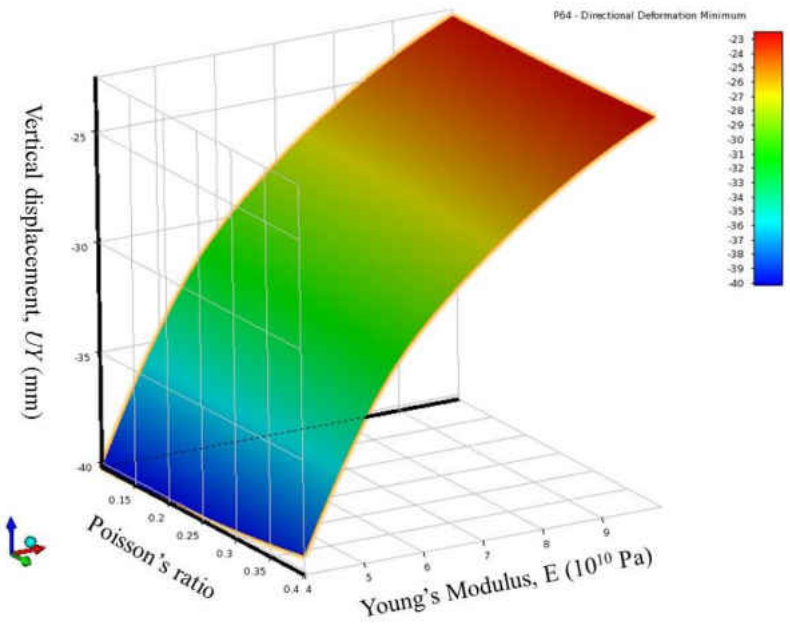


Figure 41: Response plot of vertical displacement, Young's modulus, and Poisson's ratio

After adding additional verification points to the response surface, it was determined that the FEM model would require a Young's modulus of approximately 67 GPa and a Poisson's ratio of 0.34 in the heel, and modulus of 42.7 GPa and Poisson's ratio of 0.14 in the toe, as summarized in Table 4.

Table 4: Comparison of finite element model deflection and Renegade experimental data

| **Angle, $\theta$ (degrees)** | **FEA Deflection, *UY* (mm)** | **Actual Deflection, *UY* (mm)** |
|---|---|---|
| -15.00 | -14.80 | -15.88 |
| 0.00 | -11.94 | -8.71 |
| 20.00 | -38.53 | -39.6 |

These results suggest that the stiffness of carbon fiber used in the Renegade foot is between 42.7 and 67 GPa, which is consistent with 0/90° woven carbon fiber fabric found in literature and the

aerospace industry. However, it was noted that the Poisson's ratio of carbon fiber typically falls between 0.05 and 0.1 for 0/90° woven composites, depending on the manufacture and fiber type (ACP Composites, 2014; Corum, 2001). This discrepancy is likely the result of the simplification of the material model and not including the overload spring of the Renegade foot.

Further examination of the FEA model reveals the maximum equivalent stress in the foot geometry appears along the inner surface of the fillets in both the heel and the toe as shown in Figure 42 and Figure 43 respectively at the -15° and 20° loading. In the plot of the 20° loading it was noted that a singularity occurred at the tip of the toe due the sharp edges of the geometry in contact with the plate; these unrealistic stress values have been omitted. It was shown that with the estimated material properties that the foot geometry would experience peak equivalent stress of 582.6 MPa during heel loading and 357.48 MPa during toe push-off.

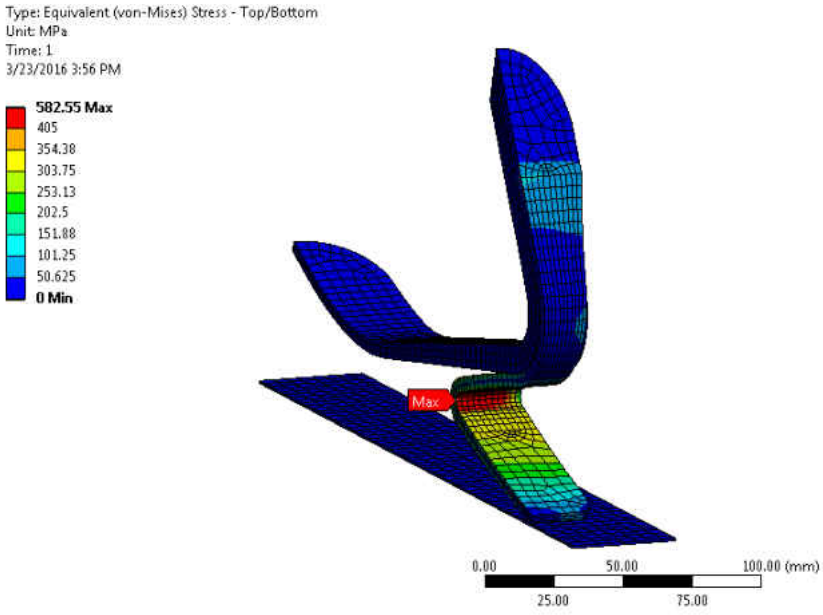


Figure 42: Von Mises stress in isotropic Renegade foot at -15° loading

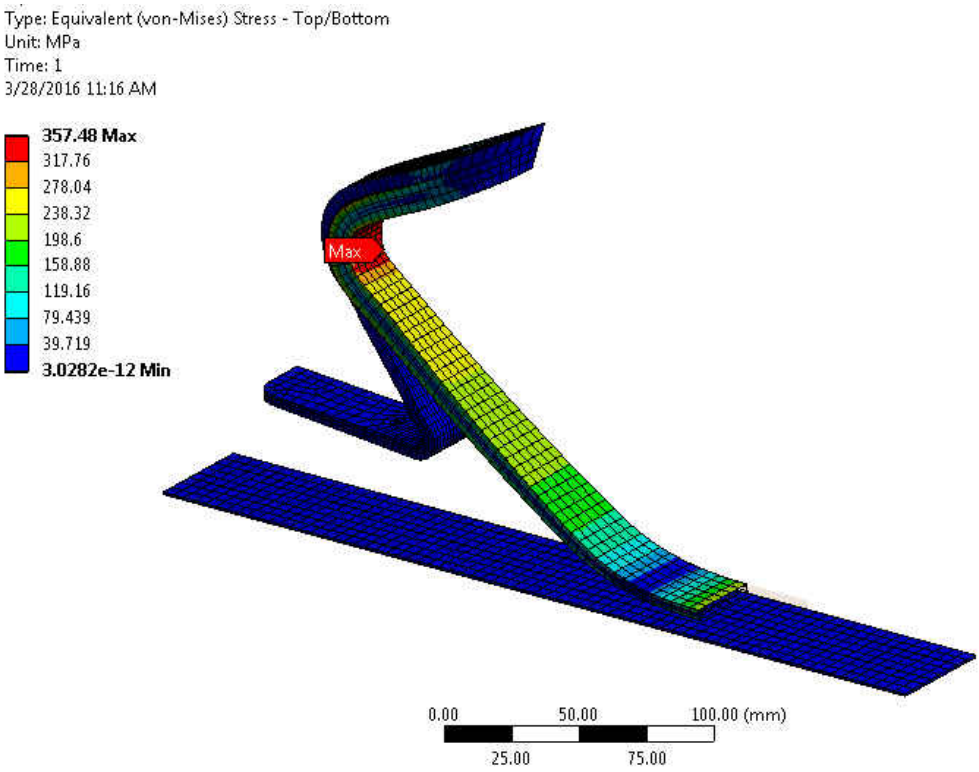


Figure 43: Von Mises stress in isotropic Renegade foot at 20° loading

It was also observed that the during loading the curvatures in the Renegade foot behave similar to a curved beam, with the stress on the maximum principle (tensile) on the outer radius and the minimum principle (compressive) stress on the inner surface as shown in Figure 44 and Figure 45 respectively.

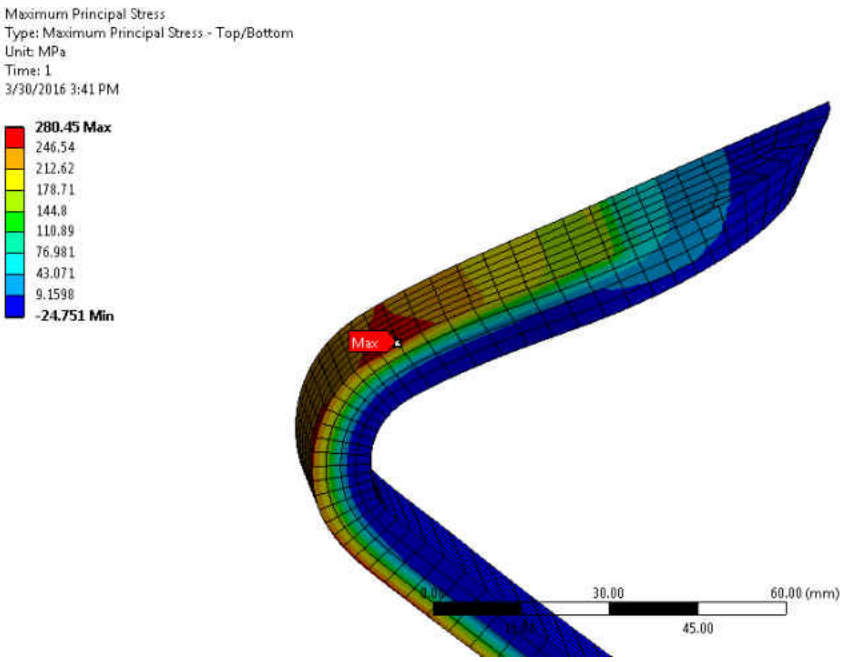


Figure 44: Maximum principle (tensile) stresses during loading of toe of the Renegade model

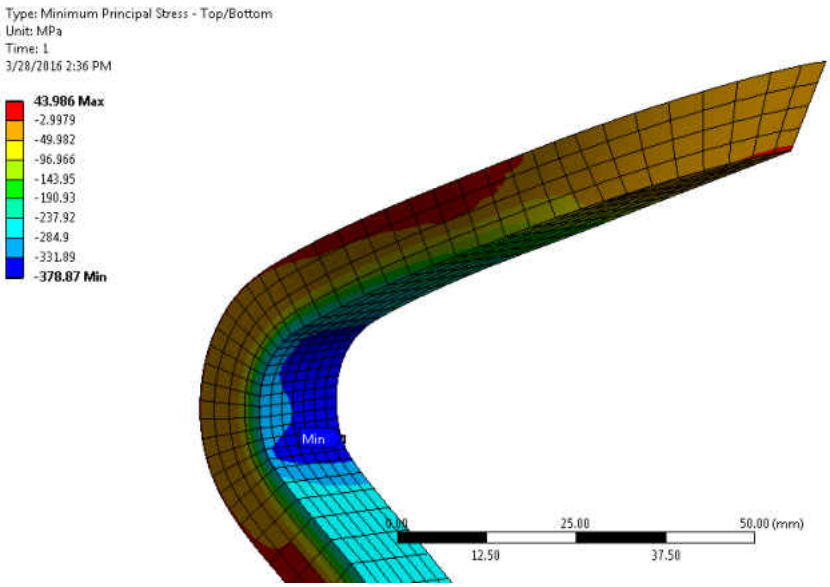


Figure 45: Minimum principle (compressive) stresses during loading of toe of the Renegade model

To verify the combined loading experienced by the FEA model, the curved beam formulas for bending stress on the inner radius ($\sigma_{B_i}$) and outer radius ($\sigma_{B_o}$), shown in Eq.(5.1.1) and Eq.(5.1.2), and the normal stress equation Eq.(5.1.3), were applied to the neck of the keel and heel during their respective peak loads (Ugural et al., 2011).

$$\sigma_{B_i} = -\frac{M\left(R - r_i\right)}{A\left(\bar{r} - R\right) r_i} \tag{5.1.1}$$

$$\sigma_{B_o} = -\frac{M\left(R - r_o\right)}{A\left(\bar{r} - R\right) r_o} \tag{5.1.2}$$

$$\sigma_N = F / A \tag{5.1.3}$$

Where $r_i$, $r_o$, $\bar{r}$ are respectively the inner, outer, and average radius of the smallest cross-section in the foot, $F_y$ represents the vertical compressive force, $M_z$ is the moment during bending, $h$ represents the thickness of the foot cross section, $b$ represents the width of the foot, $A$ is the cross-section area, and $R$ is the radius of the neutral axis in a curved beam which is calculated by Eq.(5.1.4).

$$R = \frac{h}{\ln\left(r_o / r_i\right)} \tag{5.1.4}$$

The analytical stress was calculated using the superposition principle, shown in Eq.(5.1.5), to combine the normal and bending stress.

$$\sigma_C = \sigma_N + \sigma_B \tag{5.1.5}$$

The dimensions used in these calculations were measured from the CAD model shown in Table 5. Additionally, the $M_z$ experienced during the loads was estimated by multiplying the vertical load $F_y$ by the distance from the fillet in the CAD to the contact point.

Table 5: Dimensions of toe and heel neck in bending calculations

| | **Toe (20° load)** | **Heel (-15° load)** |
|---|---|---|
| Outer radius, $r_o$ (cm) | 3.74 | 0.87 |
| Inner radius, $r_i$ (cm) | 1.40 | 0.37 |
| Thickness, $h$ (cm) | 1.00 | 0.50 |
| Width, $b$ (cm) | 3.80 | 5.00 |
| Vertical load, $F_y$ (N) | -1273 | -1271 |
| Moment, $M$ (N·m) | 426.46 | 197.0 |

A comparison of the analytical and numerical stress values, shown in Table 6, suggest that the FEA model is accurate, however, it is noted that the principle stresses experienced by the heel exceeds the maximum compressive strength of most composites.

Table 6: Analytical and numerical stress calculations

| | **Toe (20° load)** | **Heel (-15° load)** |
|---|---|---|
| FEA $\sigma_i$ (MPa) | -378.87 | -654.31 |
| FEA $\sigma_o$(MPa) | 280.45 | 391.77 |
| Analytical $\sigma_i$ (MPa) | -415.20 | -654.96 |
| Analytical $\sigma_o$ (MPa) | 282.30 | 361.87 |

This would suggest that a CAD error was during the modeling of the dimensions of the heel in the Renegade foot. To further validate the approximation of the elastic modulus of the material

used by the toe, the Von Mises strain of the foot during loading at 20 degrees, shown in Figure 46, was compared to the previously observed strain the DIC shown in Figure 38.

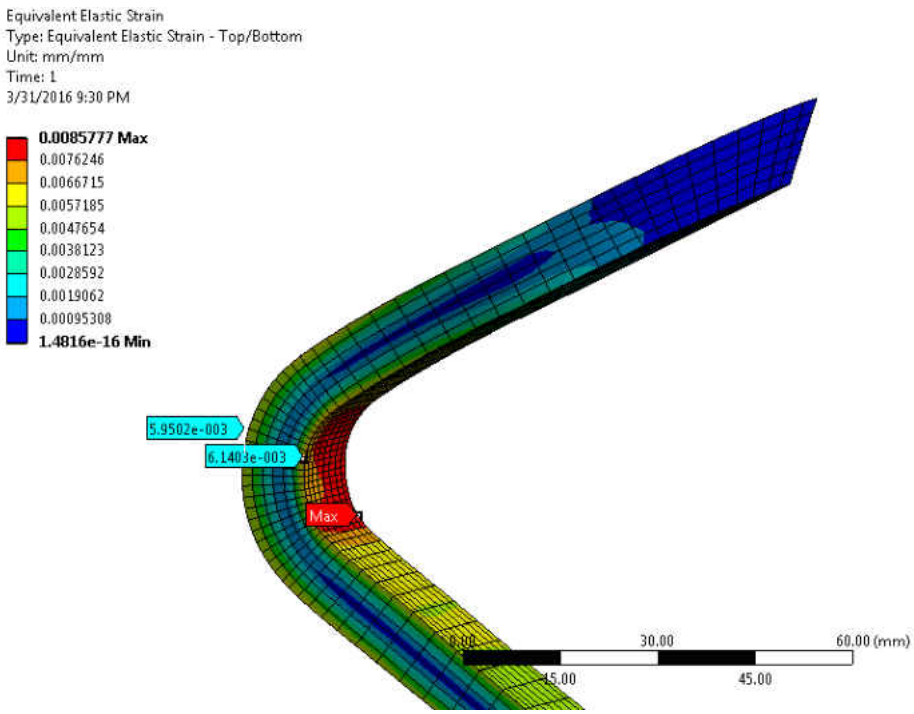


Figure 46: Von Mises strain in toe of Renegade isotropic model at 20°

Here it is observed that the maximum strain in the model occurs at the symmetric boundary condition in the middle of the foot at a value of 0.0086, and that the free surface of the foot has strain value of 0.0059 and 0.0061 respectively along the outer and inner radius of the toe. These values are similar to the maximum strain of 0.0045 recorded by the DIC. This would suggest that these initial simulations have provided a reasonable an approximation of the Renegade foot geometry and its' material properties.

To prepare a more realistic FEA model for parametric analysis, a transversely isotropic material model was developed from based on materials values found in literature for simulation of both the heel and the toe. The in plane properties of this constitutive model were developed

from Corum's material data for 0/90° woven Thronel T300 carbon fibers in Baydur 420 IMR urethane matrix. The out of plane elastic the elastic modulus ($E_{epoxy}$) and Poisson's ratio ($\nu_{epoxy}$) were developed using the properties of Baydur 426 IMR which bears a similar rating as Baydur 420 IMR (Covestro, 2015; EpoTek, 2015). These values were additionally used with Eq.(5.1.6) to approximate the out of plane shear modulus, $G_{XZ}$ and $G_{YZ}$ as summarized in Table 7 and Table 8.

$$G_{ij} = \frac{E_{epoxy}}{2(1+\nu_{epoxy})} \tag{5.1.6}$$

Table 7: Orthotropic Young's Modulus

| **Direction** | **Young's Modulus, E (GPa)** |
|---|---|
| X | 44.9 |
| Y | 44.9 |
| Z | 10.5 |

Table 8: Orthotropic Shear Modulus and Poisson's ratio

| **Direction** | **Poisson's Ratio, ν** | **Shear Modulus, *G* (GPa)** |
|---|---|---|
| XY | 0.05 | 2.96 |
| YZ | 0.30 | 4.04 |
| XZ | 0.30 | 4.04 |

The FEA model with transversely orthotropic properties produced a similar stresses distribution and vertical deflection as the isotropic model as shown in Table 9. These similarities between the transversely isotropic and the isotropic FEA model suggest that the 0/90° woven carbon fiber is a reasonable estimate of the material the prosthetic foot.

Table 9: Comparison of stress and deflection

| | **Transversely Isotropic** | **Isotropic** | **Experimental** |
|---|---|---|---|
| *UY* (mm) at -15° | -10.65 | -14.80 | -15.88 |
| *UY* (mm) at 20° | -36.48 | -38.53 | -39.6 |
| Stress $\sigma_{VM}$ (mm) at -15° | 596.8 | 582.6 | - |
| Stress $\sigma_{VM}$ (mm) at 20° | 365.8 | 357.48 | - |

Additionally, it is inferred that an isotropic model may be acceptable for modeling the bending behavior of a curved beam when additional information is unavailable.

## 5.2 Parametric 2D Model

In the process of developing a parametrically generated design, a two-dimensional model prosthetic foot model with an idealized 10 cm depth was prepared from profile the Renegade CAD. While this model does not accurately reflect a finalized geometry for manufacturing, the use of a two-dimensional model allows for reduced computational solve time and rapid design exploration of the planar geometry. The initial thickness of the keel ($T_{k1}$), the tapered thickness of the keel ($T_{k2}$), and thickness in the heel ($T_H$) were selected as parametric input variables. Additionally, to eliminate rebuild errors in the Solidworks CAD, it was necessary to fully constrain the profile with the length parameters used in the Section 5.1 model as shown in Figure 47; the parametric variables are shown in red, and the constrained dimensions are shown in black. A transition point from the tapering of the keel thickness from $T_{K1}$ to $T_{K2}$ is also shown below the keel radius in the toe.

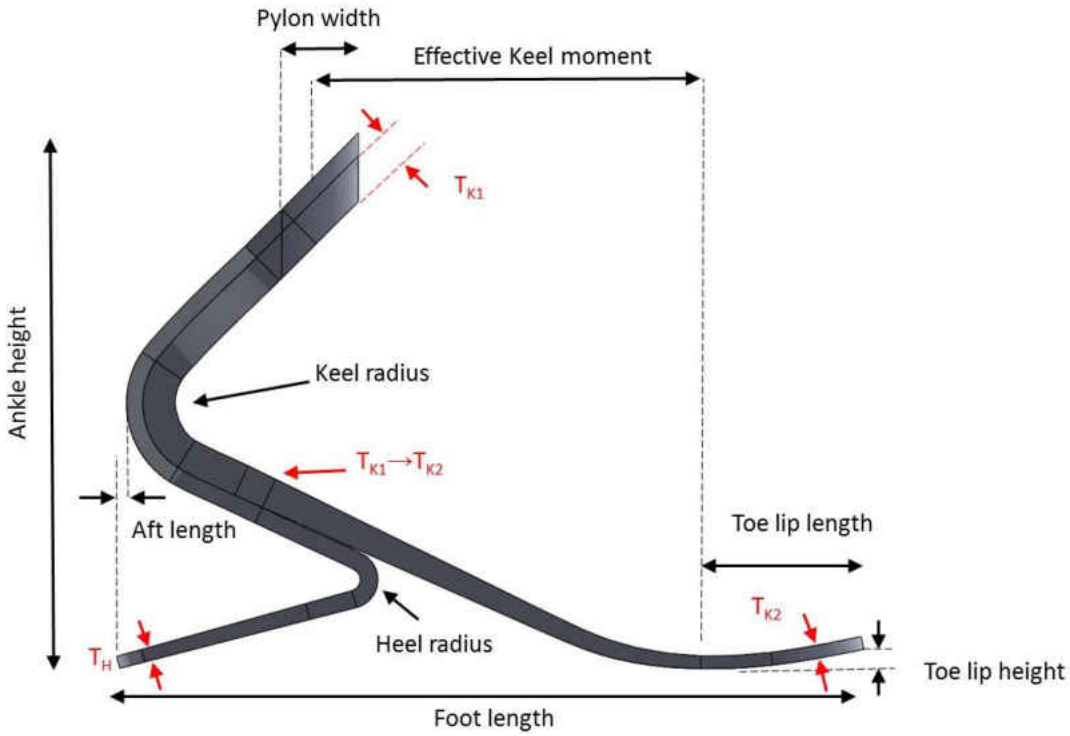


Figure 47: Parametric foot 2D profile

During the design exploration of the possible geometries, it was decided that the $T_H$ and $T_{K2}$ dimensions would be constrained between the values of 0.4 and 0.6 cm, and that the $T_{K1}$ dimensions would be constrained between 0.75 and 1.25 cm.

The parametric simulation of this 2D profile was conducted using plane strain element formulation with a refined quadrilateral mesh along the bends in the foot geometry as shown in Figure 48. Similar to the FEA model presented in Section 5.1, this 2D simulation examined the response of the parametric design at several critical angles during static loading. To properly align the contact surfaces in the simulation, an APDL command snippet was inserted into the ANSYS Workench model. This code repositioned the model such that the foot nodes come into contact with the rigid plate elements at any load angle. Additionally, weak spring elements were attached to each body to prevent rigid body movement; these springs apply a negligible force

that does impact the results of the simulation, however, they are used to fully define the model for a static simulation.

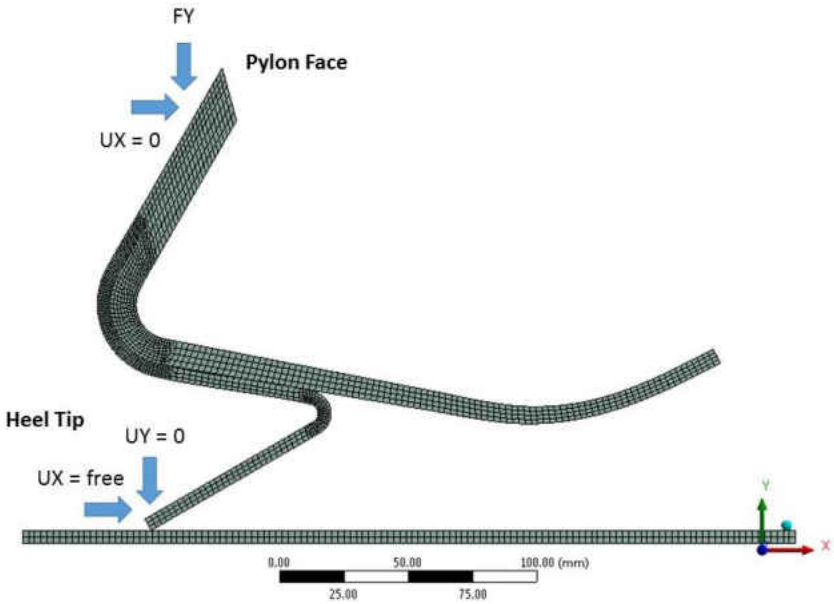


Figure 48: Parametric foot 2D mesh and boundary conditions

Because the orthotropic model was not supported in this 2D solver, an isotropic assumption of the previously developed constitutive model in Section 5.1 was utilized; where the Poisson's ratio was set 0.3 and the Young's modulus was set to 44.9 GPa.

A central composite method was used to generate fifteen variations of the 2D model, each of which were simulated at four angles of the roll-over. Several goal driven constraints were applied to parametric results to develop a feasibility plot of the data. These included minimizing the peak Von Mises stress in the model at -15° ($\sigma_{VM_{-15}}$) and 20° ($\sigma_{VM_{20}}$), minimizing the mass ($m$) of the prosthetic design, and maximizing the elastic strain energy ($W_{20}$) during push off at 20°, and achieving a targeted roll-over radius; which was calculated by transforming the center of pressure center during roll-over in the global axis ($COP_{XY}$) into the shank or tibial axis ($COP_S$). To find the $COP_{XY}$ in the FEA model, the weighted average position ($X_{avg}$) of the contact nodes ($N$) was calculated with Eq.(5.2.1),

$$X_{avg} = \frac{\sum_{i=1}^{N} F_{y_i} \cdot X_i}{\sum_{i=1}^{N} F_{y_i i}} \tag{5.2.1}$$

Where $F_{Y_i}$ represents the vertical forces on each node ($i$) and $X_i$ represents their position in the global X-axis. Because the center of pressure always occurs at the global Y-axis location of the contact plate ($Y_{plate}$), the $COP_{XY}$ can be determined as follows,

$$COP_{XY} = \left( X_{avg}, Y_{plate} \right) \tag{5.2.2}$$

To transform the $COP_S$ into the shank coordinate system, a key-point was generated in the global coordinate system at the $COP_{XY}$ location. The position of the key-point was then exported in a local coordinate system aligned with the tibia. To perform these calculations in the FEA model, an APDL command snippet was inserted into the ANSYS Workbench model. This code is

shown in Appendix A. Following a similar approach as Hansen, the radius (*R*) of this roll-over shape was determined by performing a regression of the $COP_S$ position over the loading angles with the equation of the lower half of a circle(Hansen et al., 2000).

$$COP_{S_Y} = y_0 - \sqrt{R^2 - \left(COP_{S_X} - x_0\right)^2} \tag{5.2.3}$$

This is shown by Eq.(5.2.3) where the $COP_{S_X}$ and $COP_{S_Y}$ respectively represent the center of pressure, and $x_0$ and $y_0$ represent the center of the circle in the local X and Y-axis. A plot of the roll-over shape over fifteen angles is shown in Figure 49. In comparison to the roll-over profiles from literature, shown in Figure 5, it was noted that there was a gap in the distribution of $COP_S$ data points. This caused by the split geometry of the toe and heel in the FEA model. The position of the $COP_S$ data points, and the curvature of the roll-over shape are directly influenced by the compliance of the heel and the toe.

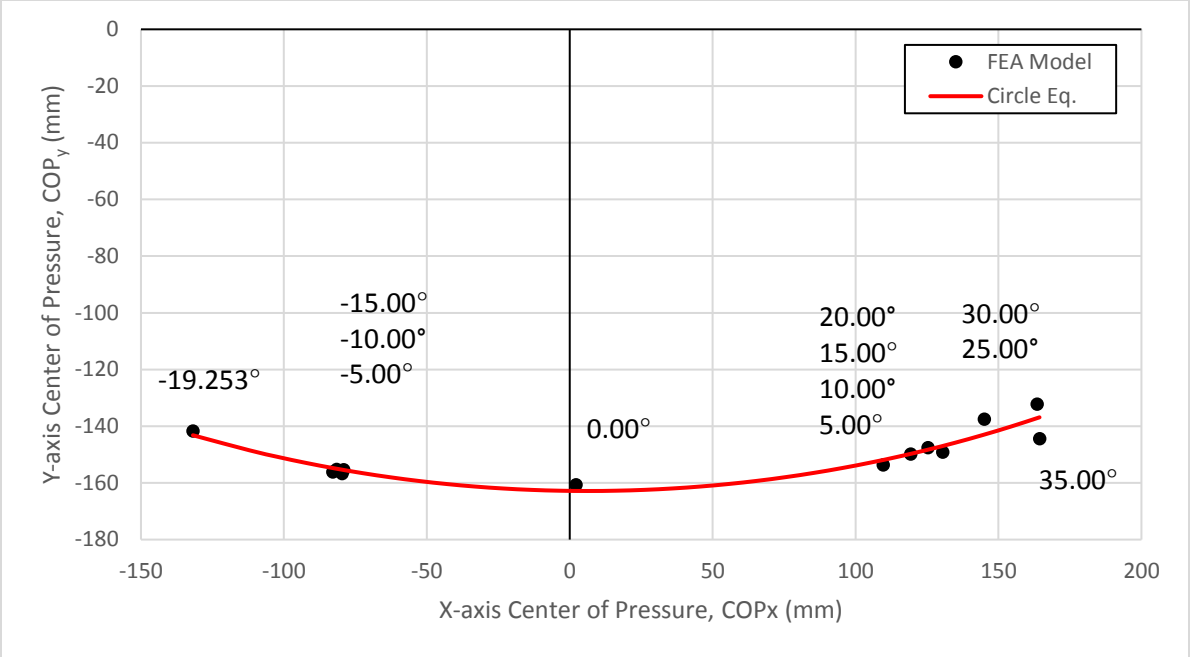


Figure 49: FEA Roll over shape

To reduce computational time in the parametric design, it was determined that only four angles, -15°, 0°, 10° and 20°, would be sufficient to determining approximate roll-over shape in the parametric design. It was assumed that the goal driven roll-over radius of the parametric model should be 30% of the leg length. Using Drillis' anthropomorphic model of the human body shown in Figure 50, the roll-over radius of the model foot was approximated 26.52 cm (Drillis et al., 1966).

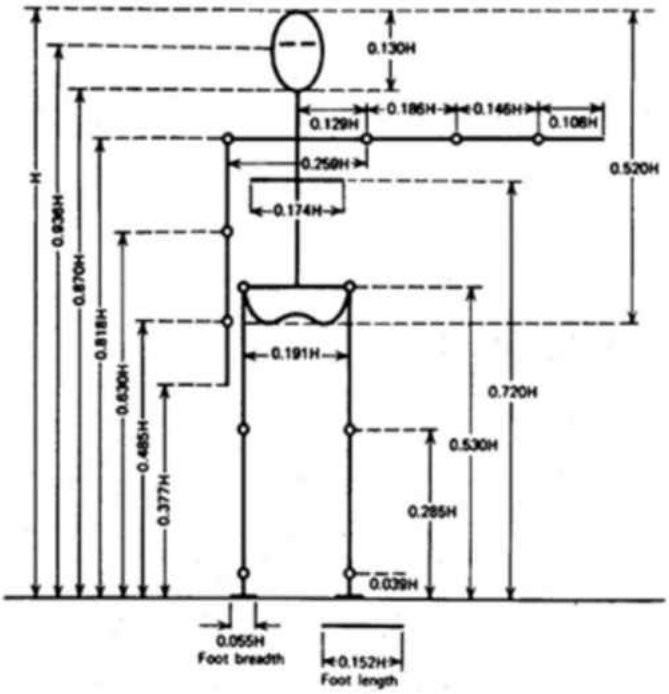


Figure 50: Anthropomorphic diagram (Drillis et al., 1966)

Additionally, following Adamczyk's study it was decided that the center of roll-over shape ($X_0$) should be anteriorly located 7.6 cm from the tibia (Adamczyk et al., 2006). However, a trade-off plot shown in Figure 51, revealed that with the current dimensional constraints on this 2D design model it is unfeasible to achieve the desired radius and center position of the roll-over shape.

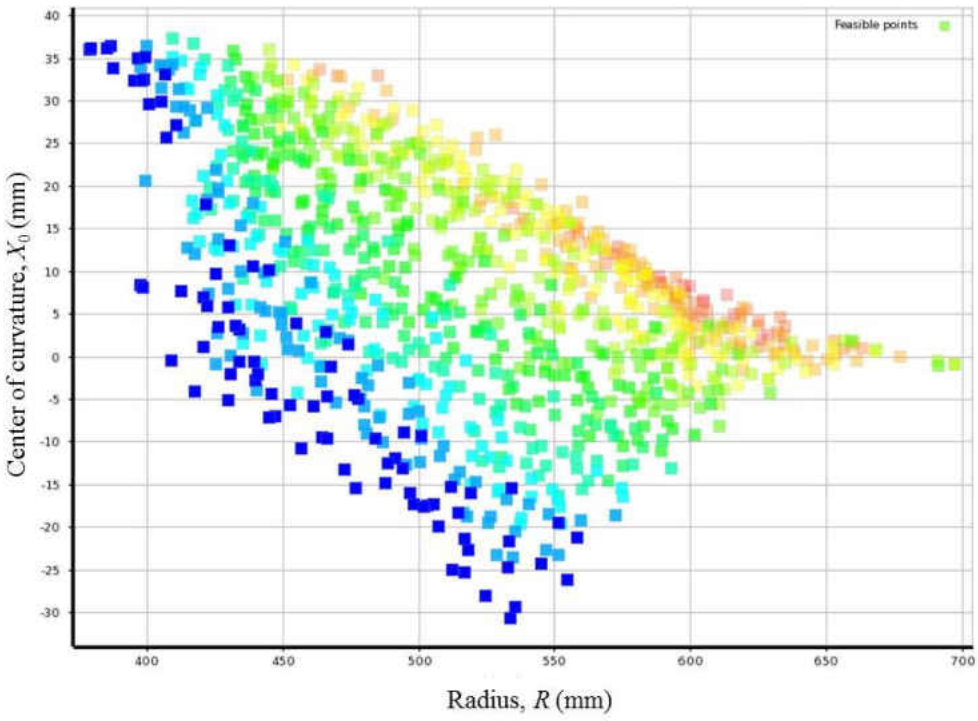


Figure 51: Roll-over trade-off plot of center position ($X_0$) and radius ($R$) for 2D model

Nevertheless, it is observed that there are a number of candidate design points that are better performing under the design criteria of minimizing the weight and peak stress in the design, and maximizing the elastic energy in the toe. These design points are shown in Figure 51 by the blue colored Pareto frontier. This is additionally demonstrated in a plot of the maximum Von Mises stress over the four angles versus the design mass shown in Figure 52. Here the density of the carbon fiber was assumed to be 1.6 g/cm$^3$.

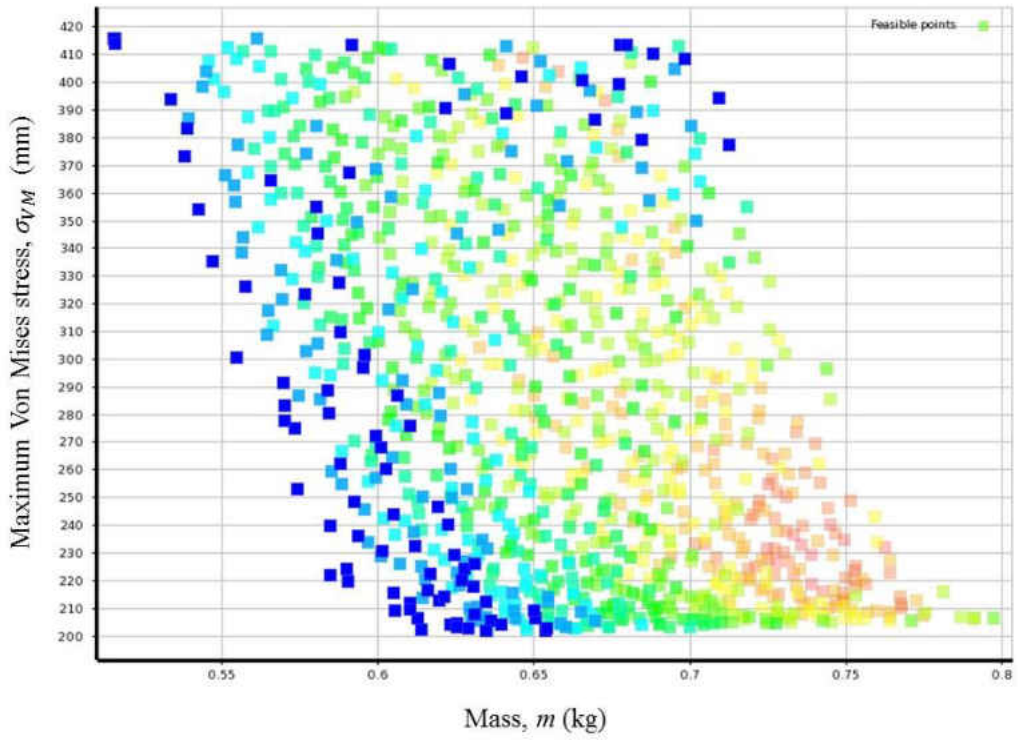


Figure 52: Trade off plot of maximum Von Mises stress versus mass in 2D parametric analysis

Here it is observed that the design point with the lowest mass and minimal stress appears in the lower left-hand corner. Interestingly, it is noted that many successful marketed carbon fiber prosthetic feet, such as the Renegade AT, are also designed with a weight of 0.515 kg (Freedom-Innovations, 2014).

## 5.3 Parametric 3D Model

A 3D parametric model of the transversely isotropic foot was generated in order to evaluate the response of the Renegade foot during experimental testing and to examine the effect of the foot alignment during compressive loading. This was accomplished by selecting the three thickness variables from in the 2D parametric model and shown in Figure 47, as well as three

dimensions of the foot's profile depth ($D$) along the toe and keel of the foot shown in red in Figure 53 where the pylon width is considered to be constant.

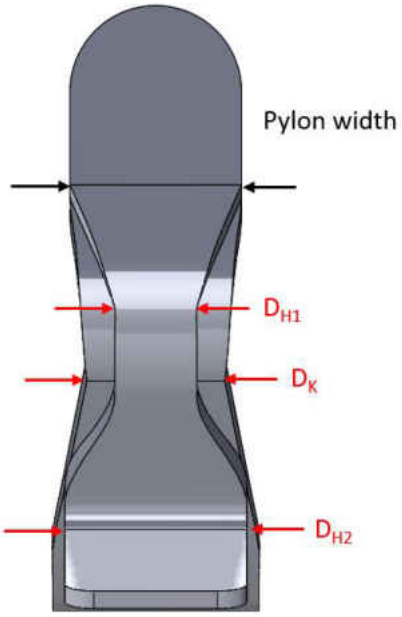


Figure 53: Depth ($D$) dimensions of the foot that were selected for parametric analysis

Using a central composite design of experiments in the Ansys FEA software at total of 45 geometries were generated to examine the response at three levels for each parametric dimension. The thickness of the heel ($T_H$) was varied between 0.40-0.60 cm. The thickness of the keel component was varied between 0.75-1.25 cm at the pylon face ($T_{K_1}$) and between 0.40-0.60 cm at the toe ($T_{K_2}$). Similarly, the profile depth in the two components was also varied at the two major inflection points in the design. At the keel joint the profile depth of the heel ($D_{H1}$) was varied between 2.0-3.6 cm and the depth of the keel ($D_K$) was varied between 3.5-4.72 cm, and at the heel joint the profile depth of the heel component ($D_{H1}$) was varied between 4.5-5.5 cm. To prevent rendering errors from occurring during the geometry update, several constrained

dimensions (Figure 53**Error! Reference source not found.**) were added to the CAD drawing to ensure that the model was fully define. This consisted of restricting foot height to 16 cm, the length to 23 cm, and placing several additional constraints along the foot profile.

Similar to the 2D parametric analysis, the foot geometry was subjected to static loading at the angles of -15, 0, 10 and 20 degrees over the ISO 22675 loading curve. By selecting these four angles, it was possible to develop a response plot of the foot from the heel strike to the push-off. This was accomplished by writing an APDL script in Ansys to output the $COP_{S_X}$ and $COP_{S_Y}$ of the foot, and to ensure that each geometry was placed in contact with the compression plate at each of the roll-over angles. To prevent meshing errors, 10-node tetrahedral elements with automated meshing used to examine the parametric geometries with an average of 16919 total elements in each geometry. Additionally, boundary conditions were applied to enforce sliding contact between the heel and toe with the load plate, and the plyon face was constrained to allow motion only in the Y-axis, as shown in Figure 54.

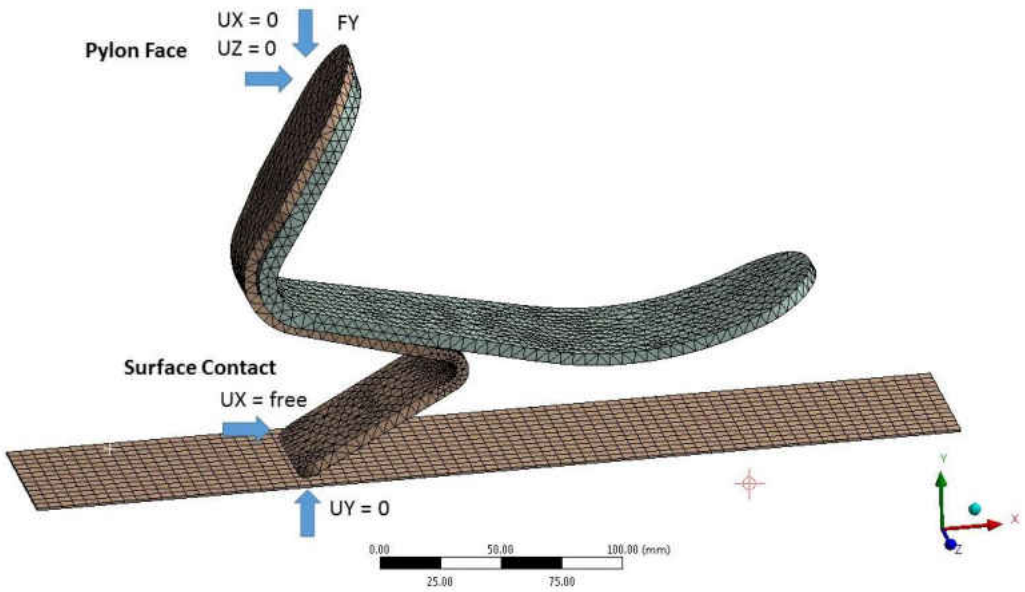


Figure 54: Boundary conditions used on 3D parametric model with 0° toe out

While the ISO 22675 standard recommends a 7° lateral rotation ($\tau$) of the prosthetic foot to simulate the toe-out during cyclic loading, many experimental studies do not include this rotation during their investigation (Geil, 2002; Haberman, 2008; Unnthorsson et al., 2008). To examine the effect of a lateral rotation on the prosthetic foot during loading, the parametric model was rotated counterclockwise about the tibial axis. This is shown during the heel-strike in Figure 55a and push-off in Figure 55b.As a result an additional torque was placed on the toe and heel components during the rollover.

a) b)

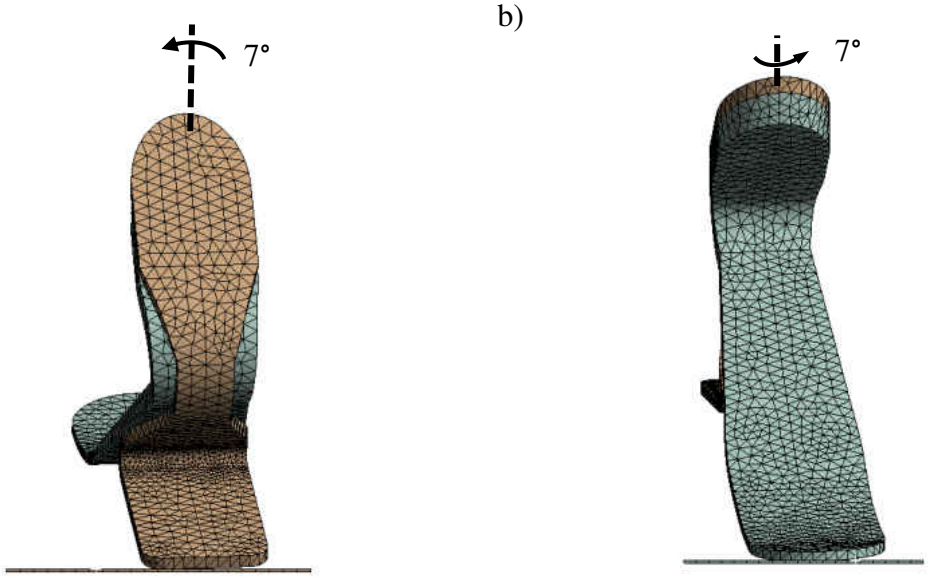


Figure 55: FE model of prosthetic foot with 7° lateral rotation about pylon axis

It was observed that the prosthetic foot with the 7° toe out experienced a greater stress concentration on along the inner and outer surface during compressive loads. A comparison of the principle stresses on the original geometry is shown in the updated Table 10.

Table 10: Maximum principle stresses due to lateral rotation in original geometry

| | **Transversely Isotropic $\tau = 0°$** | **Transversely Isotropic $\tau = 7°$** |
|---|---|---|
| Stress $\sigma_i$ (MPa) at -15° | -620.23 | -614.76 |
| Stress $\sigma_o$ (MPa) at -15° | 413.82 | 395.84 |
| Stress $\sigma_i$ (MPa) at 20° | -372.29 | -388.23 |
| Stress $\sigma_o$ (MPa) at 20° | 312.99 | 287.45 |

Here it can be seen that the foot with $\tau = 7°$ on average experienced an 18% greater stress magnitude during the loading of the heel and a 10% greater stress magnitude during the

compressive loading of the toe. This suggests that the alignment of the prosthetic foot must be considered during the design phase of the device.

A parametric analysis was conducted on the prosthetic foot with $\tau = 0°$ and $\tau = 7°$. The response plot of each parametric analysis was constructed using a genetic aggregation method in the Ansys Design Explorer to examine the output response variables in each FEA model. These variables included the maximum tensile stress, compressive stress, and Von Mises stress, the maximum moment on the ankle joint during roll-over, the strain energy at -15° and 20° loads, the mass of the foot, and the center of pressure location at each angle. This allowed for a tradeoff plot to be generated showing the response of the potential design geometries. The tradeoff response of the principle stresses in the prosthetic foot versus the mass of each design with $\tau = 0°$ is shown in Figure 56a-b, and the tradeoff response of the foot with $\tau = 7°$ is shown in Figure 59a-b.

a)

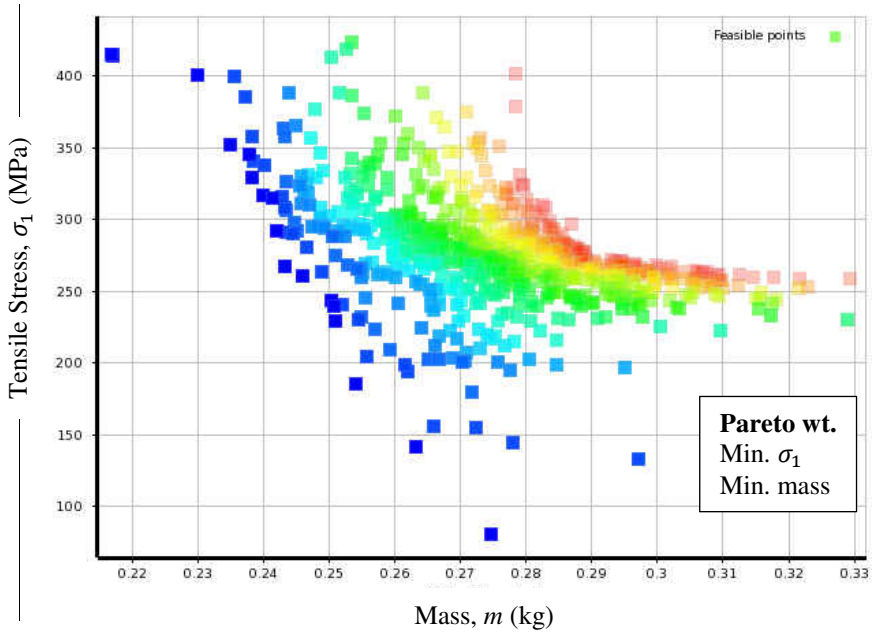


b)

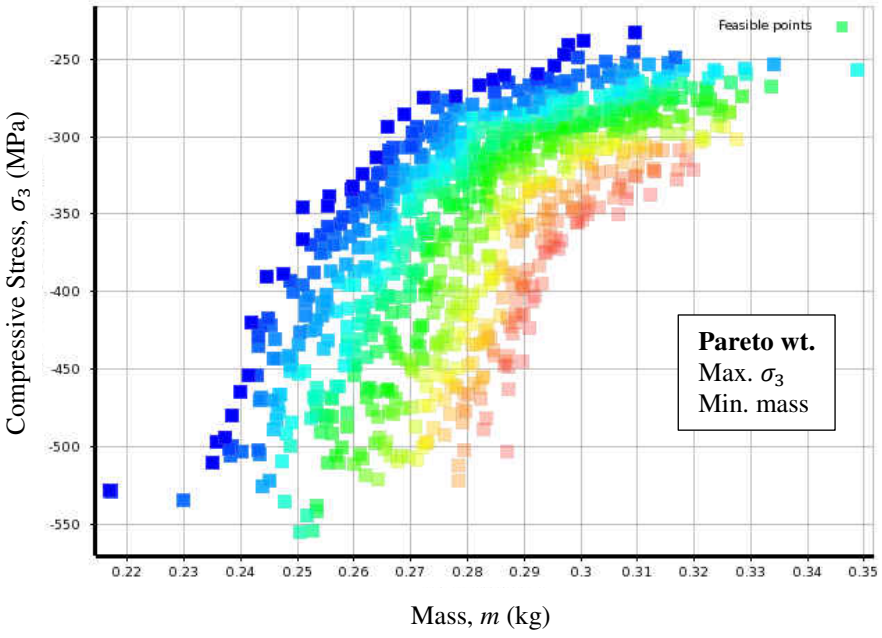


Figure 56: Trade off plot of tensile a) and compressive stress b) versus mass in 3D parametric analysis with 0° toe-out

a)

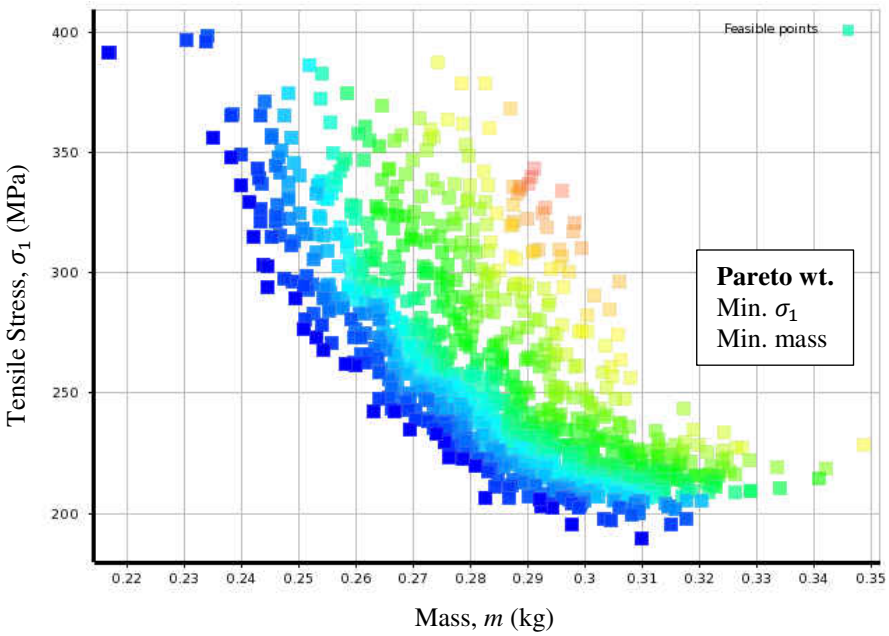


b)

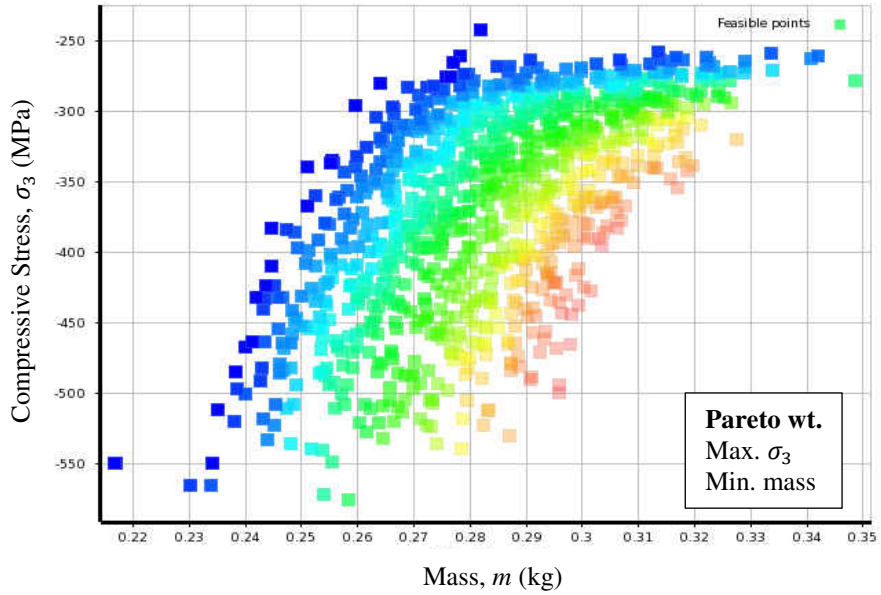


Figure 57: Trade off plot of tensile a) and compressive stress b) versus mass in 3D parametric analysis with 7° toe-out

In principle stress response plots shown in Figure 56 and Figure 57, Pareto weights were added to the feasibility plot such that the mass was minimized and the stress magnitude in compression and tension were also minimized. As expected, a trend is apparent in the tradeoff plots for both the principle tensile stress and compressive stress showing that the stress magnitude can be reduced as the mass of each design is increased. A direct comparison cannot be made to the Renegade foot with a mass of 0.337 kg because several components including the metal pylon and overload spring were not included in this FE model. However, an approximation of the service life can be estimated using Corum's (Corum, 2001) fatigue model (R=0.1) for 0/90 woven carbon fiber shown in Eq.,

$$\sigma_{\mathrm{T}} = \exp\left(\frac{\ln\left(N_f \times 7.162 \times 10^{-209}\right)}{-77.47}\right) \tag{1}$$

Where the maximum tensile stress ($\sigma_T$) in the design can be estimated by substituting in a target number of cycles to failure ($N_f$). Hence, for a design to withstand a minimum of $10^6$ cycles the geometry should experience a maximum of 427.96 MPa, which is well within the feasible design shown in design Figure 56. The compressive fatigue limit $10^6$ cycles for was also approximated as 85% of the static compressive strength or approximately -406.30 MPa [28]. It can be seen in Figure 59 that there are also a number of acceptable designs at or below this stress magnitude. It is also apparent that the most favorable designs along the Pareto front shown in blue.

A response plot of the roll-over shape of the foot under with $\tau = 0°$ and $\tau = 7°$ was generated from the parametric analysis, respectively shown in Figure 58 and Figure 59.

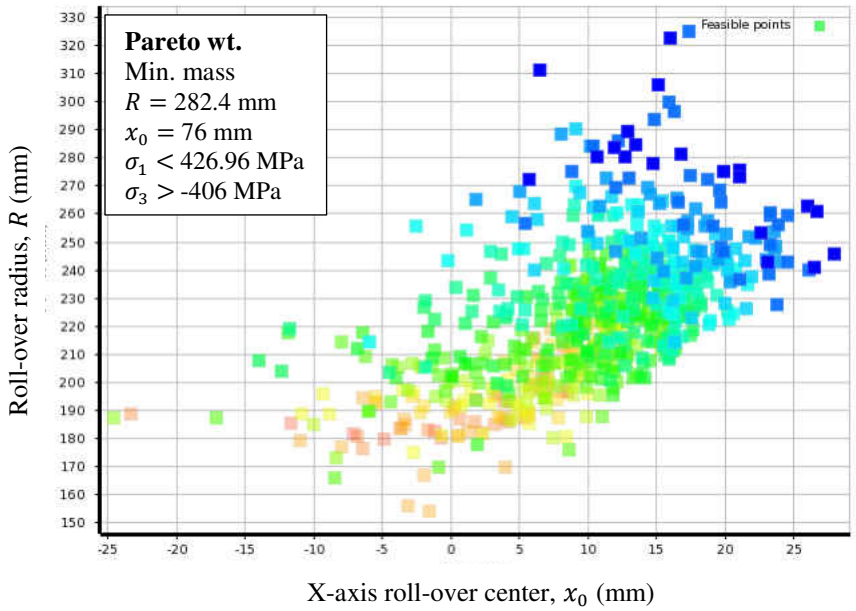


Figure 58: Roll-over tradeoff plot of center position ($x_0$) and radius ($R$) for 3D model at 0° toe-out

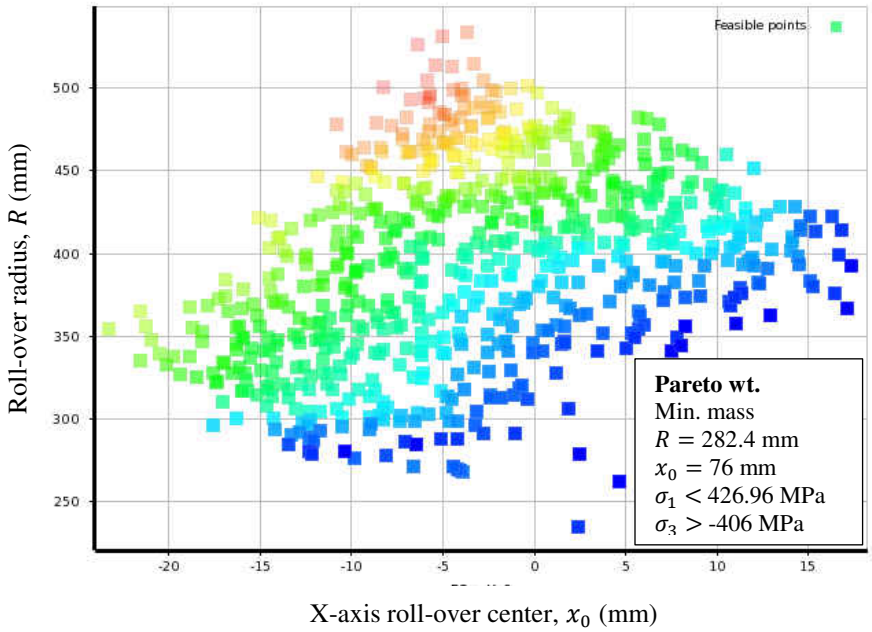


Figure 59: Roll-over tradeoff plot of center position ($x_0$) and radius ($R$) for 3D model at 7° toe-out

Pareto weight were added to Figure 58 and Figure 59 such that the $x_0$ was set equal to 7.6 cm and $R$ equals 28.24 cm. Additionally, a constraint was added to limit the design points to those with a stress less 427.96 MPa in tension and 406.30 MPa in compression. It was observed that the desired roll-over radius was well within the scope of the parametric design, however, the changes to the foot geometry did not allow for the target $x_0$ value to be reached, suggesting that further design exploration may be needed to achieve this idealized offset value.

A comparison of the work from the vertical force-displacement of the Renegade design at during heel-strike and push-off with $\tau = 0°$ and $\tau = 7°$ is presented in Figure 60 and Figure 61. Pareto weights were added to each plot in order to maximize the energy storage capacity, minimize the mass, limit the compressive and tensile stress, and to attempt to reach the idealized roll-over shape. There is an apparent tradeoff in the potential designs that are capable of maximizing the amount of energy that is returned during both the heel-strike and the push-off. The response of the prosthetic foot at these two critical angles suggest that the toe of the Renegade foot may be designed to elastically store about three times the energy of its heel.

It was also observed that when the foot is subjected to a compressive load with $\tau = 7°$, the foot may be able to store a slightly greater amount of energy than the direct loading ($\tau = 0°$) of the foot. This is likely due to the additional torque that the pronated foot experiences during pronated loading shown in Figure 55.

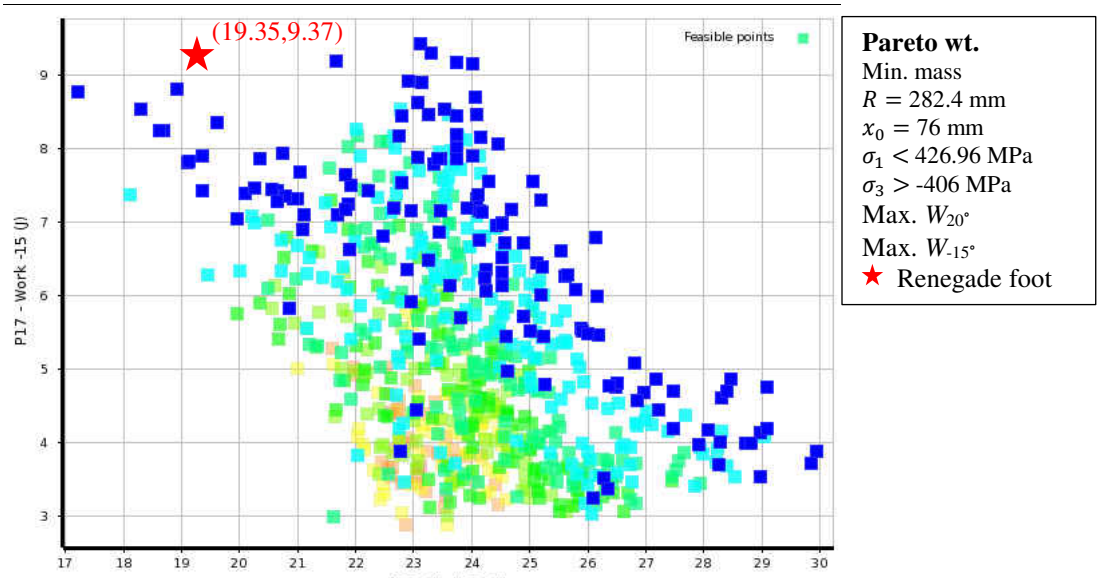


Figure 60: Work done by vertical-displacement during heel-strike and push-off at 0° toe-out

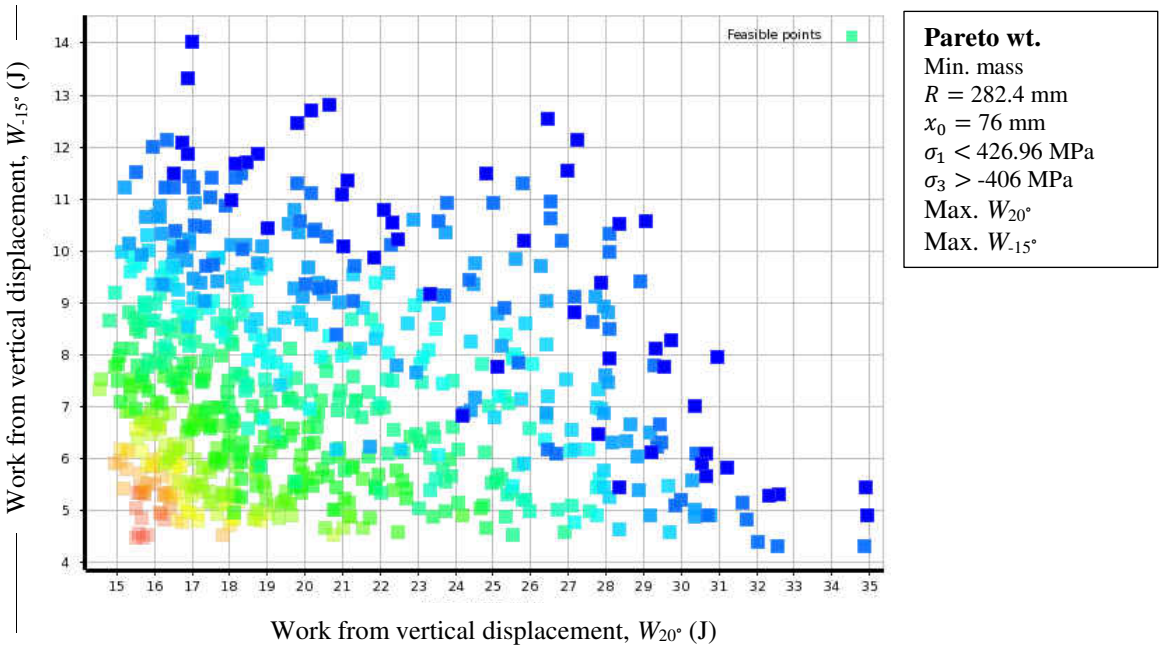


Figure 61: Work done by vertical-displacement during heel-strike and push-off at 7° toe-out

The experimental results of the Renegade foot are also shown with the parametric data in Figure 60; indicated by the red star. During the mechanical loading of the Renegade foot in Chapter 4, it was observed that the Renegade foot was able to elastically store 9.37 joules of energy at -15 degrees and 19.35 joules at 20 degrees. It is observed that the heel of the Renegade provides a greater amount of energy return than many of candidate design points. However, the parametric analysis suggests that there may be other designs that provide a greater amount of energy return during push-off.

The parametric feasibility analysis presented in this section had demonstrated that relatively minor changes in the thickness of a prosthetic design can significantly influence the roll-over characteristics and the mechanical behavior in the design. These results also suggest that prosthetic design optimization may lead to the production of more robust devices that can be developed for the gait pattern of a specific gait pattern.

# CHAPTER 6: CONCLUSIONS

The development and prescription of a prosthetic foot for a specific amputee is a time consuming process that is driven by iterative feedback and clinical experience rather than parametric design. The need to improve this production process has led to the identification of the essential design parameters that influence the gait pattern of amputee, namely, the component stiffness, the roll-over shape, the weight, the energy return capacity, and the weight of the device. However, mechanical testing of these properties and the development process has not yet been standardized, subsequently their influence on an amputees' gait remains poorly understood. To help fill this gap in knowledge, this investigation has conducted a case study on Freedom Innovations' Renegade foot and TLM Prosthetics' TaiLor Made foot to demonstrate that mechanics of materials approaches can be utilized to evaluate the mechanical response of prosthetic feet. Additionally, this paper has provided a framework for design optimization process by conducting a parametric finite element analysis on a representative foot model. A brief summary of these accomplishments and recommendations for future work are presented in the following sections.

## 6.1 Concluding Statements

In order to evaluate the mechanical response of the Renegade and TaiLor Made prosthetic feet a series of compressive tests involving monotonic loading and force relaxation were conducted with a universal test machine using a customized loading platform at fifteen different angles. The compressive loads and angles used during these tests were adapted from the ISO 22675 standard for the fatigue testing of foot-ankle devices in order to simulate the vertical

forces experienced by prosthetic foot during regular walking. In Chapter 4, it was shown that the both the Renegade and TaiLor Made have an excellent energy return efficiency and storage capacity during push off at 20 degrees. The Renegade foot which was designed for a 100kg individual showed energy capacity of 19.50 joules and an energy return efficiency of 92.03%, whereas the TaiLor Made, which was designed for a 60 kg individual, demonstrated an energy capacity of 13.54 joules with an energy return efficiency of 83.26% without their foam covers. It was also observed that the foam cover caused a decrease in the overall efficiency by 3.2 – 5.47% during the push off phase. Interestingly, the TaiLor Made behaved with greater energy return efficiency at 0 degrees during loading with its cosmetic cover foam cover. It was also noted that due the tibial springs in the TaiLor Made design allowed for a greater compliance during the mid-stance phase when both the heel and toe contacted the load plate.

During the force relaxation testing each foot was compressively loaded and held at a fixed displacement for a period of 180 seconds in order to capture the viscous behavior of the component. A regression model using the Norton-Bailey power law for constitutive creep models was generated for this data. It was shown that the cosmetic foam cover predominated the viscous behavior of both feet and had a much greater influence on the heel of the TaiLor Made foot. The experimental results from this work are to be presented in journal publication entitled the "Mechanical Characterization of Prosthetic Feet and Shell Covers Using a Force Loading Apparatus".

In Chapter 5, finite element analyses (FEA) were conducted to approximate the material properties and stress in the Renegade foot during loading based on the force deflection response and digital image correlation in Chapter 3. This material approximation was then used in a series of parametric models to generate a feasibility plot for the mechanical response of potential

designs. The use of the parametric optimization and mechanical testing approaches presented in this thesis could allow for the production of prosthetics devices with a well understood mechanical response and potentially lead to improved understanding of the influence a prosthetic device has on the gait pattern of a lower limb amputee. The findings and parametric outline in this study are to be presented in a publication entitled "Parametric design of mechanical response in prosthetic feet".

## 6.2 Recommendations for future work

While this work has successfully applied mechanics of materials and numerical optimization techniques to development of lower limb prosthetics, many of these approaches require further validation through the testing of additional new quality existing prosthetic feet, the production of a parametrically optimized design, and ultimately biomechanical gait analysis. To further address the limitations of this methodologies presented in this study, the following recommendations are for future investigations are provided.

- **Conduct digital image correlation (DIC) tests as a validation tool in the prosthetic design process in conjunction with finite element analysis (FEA)**. The digital image correlation technique was shown that it can be successfully used to measure the surface strain along the cross-section of a prosthetic device. However, as the FEA analysis showed the maximum strain in the design did not occur at the speckle painted surface. Thus, it is recommended that DIC be used to validate the stress in a FEA model when the material properties are known.
- **Development of a frictionless surface for the prosthetic loading plate.** During the course of the compressive testing slippage of the foot without the cosmetic cover was

occasionally noticed in the first one to two loading cycle of the five cycle preload. While these frictional forces were considered to be negligible,

- **Conduct transient dynamic finite element analysis for walking gait pattern.** To further extend the design optimization methods presented in this paper, it is also recommended that an explicit dynamic simulation be incorporated in the parametric analysis. A transient model could provide additional insight into the role a prosthetic device has on the gait pattern of an amputee and the reaction forces acting on a patients joints.

# APPENDIX A: CODES

List of ANSYS APDL CODES

**Code 1: Offset APDL Command Snippet**

```
!=============================================================
3/27/2016
!
!MOMRG-UCF-MAE
!FOOT RE-POSITION & BOUNDARY CONDITIONS
!KEVIN C. SMITH

!FUNCTIONS:
! - Code offsets foot to touch plate if gap is greater than tolerance
! - Calcualtes the angle theta based on  Ankle and Ankle2
! - Fixes lowest point on heel and toe at selecct angles to single node to surfacce contact errors

! Required named Selections in Workbench:
!                Ankle
!                Ankle2
!                TOE_NODES
!                HEEL_NODES
!                SURF_NODES

/prep7
CMSEL,S,Toe_NODES,NODE
CMSEL,A,HEEL_NODES,NODE
CM, Foot_NODE, NODE
CMSEL, S, Foot_NODE, NODE
*vget, FN_list,NODE,all,NLIST
*GET, FN_count, NODE, 0, COUNT,
*GET, FN_YMIN, NODE, , MNLOC, Y


CMSEL,S,SURF_NODES,NODE
!*GET, PLATE_NODE_NUM, NODE, 0, NUM, MAX
!*GET, Y_SURF, NODE, PLATE_NODE_NUM, LOC, Y
*GET, Y_SURF, NODE, , MXLOC, Y
NSEL, R, LOC, Y, Y_SURF
esln

*get, plate_ELM_num, elem, , num, min
*GET, plate_ELE_TYPE,ELEM,plate_ELM_num ,attr,type

CM, SURF_NODES, NODE
D,All,UX,0
D,All,UY,0
D,All,UZ,0
allsel
```

```
Offset = Y_SURF - FN_YMIN
AbsOffset = abs(offset)
Tolerance = 1E-6

!offset nodes & elements if not near surface
*IF,AbsOffset,GT,Tolerance,THEN
CMSEL, S, Foot_NODE, NODE
ESLN
NSLE                              ! grabs the weak spring nodes attached to foot
NGEN,2,0,ALL,,,0,offset,0
allsel
*ENDIF


CMSEL, S, Ankle, NODE
*GET, Ankle_NUM, NODE, 0, NUM, MAX
*GET, AY, NODE, Ankle_NUM, LOC, Y,
*GET, AX, NODE, Ankle_NUM, LOC, X,

CMSEL, S, Ankle2, NODE
*GET, Ankle_NUM2, NODE, 0, NUM, MAX
*GET, AY2, NODE, Ankle_NUM2, LOC, Y,
*GET, AX2, NODE, Ankle_NUM2, LOC, X,
allsel


CMSEL,S,TOE_NODES,NODE
*GET, TOE_ND_Y, NODE, , MXLOC, Y
NSEL,R,LOC, Y,TOE_ND_Y
ESLN
*get, TOE_ELM_num, elem, , num, min
*GET, TOE_ELE_TYPE,ELEM,TOE_ELM_num ,attr,type

CMSEL,S,HEEL_NODES,NODE
*GET, HEEL_ND_Y, NODE, , MXLOC, Y
NSEL,R,LOC, Y,HEEL_ND_Y
ESLN
*get, HEEL_ELM_num, elem, , num, min
*GET, HEEL_ELE_TYPE,ELEM,HEEL_ELM_num ,attr,type


pi = acos(-1)
theta = atan( (AX-AX2) / (AY-AY2) )*180/pi                    !CMSEL uses intial positions of
pylon nodes used find theta
```

```
CMSEL,S,HEEL_NODES,NODE
*GET, HEEL_MIN_Y, NODE, , MNLOC, Y

*IF,theta,LT,0,THEN
!CMSEL, S, Heel_pin, NODE
!ESEL,s,type,,HEEL_ELE_TYPE
!nsle
CMSEL,S,HEEL_NODES,NODE
NSEL,r, loc, y, HEEL_MIN_Y
*get,selmin,node,0,num,min,
nsel,s,node,,selmin
D,All,UY,0
allsel
*ENDIF


CMSEL,S,Toe_NODES,NODE
*GET, Toe_MIN_Y, NODE, , MNLOC, Y

*IF,theta,GE,14,THEN
!CMSEL, S, Toe_pin, NODE
!ESEL,s,type,,TOE_ELE_TYPE
!nsle
CMSEL,S,TOE_NODES,NODE
NSEL,r, loc, y, Toe_MIN_Y
*get,selmin,node,0,num,min,
nsel,s,node,,selmin
D,All,UY,0
*ENDIF
allsel
allsel

/solu
```

**Code 2: Output and Calculations APDL Command Snippet**

```
!=================================================================
3/27/2016
!
!MOMRG-UCF-MAE
!Center of Pressure calculations and output
!KEVIN C. SMITH

! FUNCTIONS:
! - calculates the center of pressure (COP) based on the weighted average of the contact forces of
the elements underneath the contact elements
! - COP is calculated in a local coordinate system based on theta and the UY of the foot
! - returns the COPx, COPy, and strain energy to workbench
! - "Rollover" outputs:  theta (deg), COP_sx (mm), COP_sy (mm), strain work (J), UY (mm),
smax (MPa)
! - "RY_SURF" outputs contact forces : Node, X-loc',FY
! - "Press Nodes" outputs list of conta nodes
! Note that adjustments may need to be made for contact element type if mesh order is changed

ALLSEL
/post1
SET, first, , , , , , ,



*GET,LSTSET, ACTIVE, 0, SET, NSET                                    ! NUMBER OF SETS


*dim,RY_FSUM_FIXED,array,LSTSET




t=LSTSET                                ! comment this line for static solvers
!*DO,t,1,LSTSET,1              ! loop for transient
        SET,,,,,,,t                                                                    !Defines the
data set to be read from the results file.
        FSUM, ,                                                                        ! SUM
COMMAND OPTIONS

        allsel

!       FIXED NODES reaction force
```

```
        ALLSEL
        esel, s, type, ,plate_ELE_TYPE,                                          !
SELECT CONTACT ELEMENT TYPE 3,4
        NSLE                                                                     !
SELECT NODES ATTACHED TO SELECTED ELEMENTS
        *GET, LOAD_SUM, FSUM, 0, ITEM, FY,                  ! SUM NODAL FORCES
        RY_FSUM_FIXED(t) = LOAD_SUM                                              !
PLACES LOAD_SUM INTO 'force' ARRAY

!------------------


CMSEL,S,SURF_NODES,NODE
*GET, PLATE_NODE_NUM, NODE, 0, NUM, MAX
*GET, Y_SURF, NODE, PLATE_NODE_NUM, LOC, Y



ESEL,S,TYPE,,4,9,1              ! Element type 4-9 represents contact type
NSLE,S
ESel, S, type, ,plate_ELE_TYPE
NSLE, U
ESLN
ESEL, U, Type,,4,9,1
ESEL, U, Type,,11
!Nforce,

*GET, PRESS_COUNT, NODE, 0, COUNT,
*GET, PLATE_SUM, FSUM, 0, ITEM, FY,
*dim,PRESS_LIST,array,PRESS_COUNT,3
*dim,nnum,array,PRESS_COUNT,
*vget, nnum,NODE,all,NLIST      !get a list of the selected nodes

RY_MAX = 0
RY_MAX_X = 0
SUM = 0
WT_SUM = 0

! Cycles through all the surface nodes
! places node num, x-location, and force into an array
! determines location of max force, and the weighted average of the force
! Note that max force is less realistic than the weighted average of the location


        *DO,i,1,PRESS_COUNT,1
                allsel
```

```
                *GET, X_i, NODE, nnum(i), LOC, X,
                *GET,X_f, NODE, nnum(i), U, X,                  !*GET,X_f, NODE, 180, U,
X,
                Press_X = X_i + X_f
                !*GET, Press_load, NODE, nnum(i), RF, FY,


                nsel,s,node, , nnum(i)
                ESLN
                !FSUM,cont
                FSUM,
                *GET, signed_load, FSUM, 0, ITEM, FY,           ! returns total forces, not
nodal

                !Press_load = abs(signed_load)
                Press_load = signed_load
                PRESS_LIST(i,1) = nnum(i)
                PRESS_LIST(i,2) = Press_X
                PRESS_LIST(i,3) = Press_load

                ! used to determine weighted average of x-location
                SUM = SUM + Press_load
                WT_SUM = WT_SUM + Press_load*Press_X

                ! max force location and value
                *IF,RY_MAX,LT,Press_load,THEN
                        RY_MAX = Press_load
                        RY_MAX_X = Press_X
                *ENDIF



        *ENDDO

!*ENDDO                          ! loop for transient

!-----------------------------------------------------
! Determine COP location from new coordinate system at pylon


CMSEL, S, Ankle, NODE
*GET, Ankle_NUM, NODE, 0, NUM, MAX
*GET, AY, NODE, Ankle_NUM, LOC, Y,
*GET, AX, NODE, Ankle_NUM, LOC, X,
*get, A_UY, node, Ankle_NUM, U, Y
```

```
X_AVG1 = WT_SUM/SUM                    !nodal reaction forces
/PREP7
k, 101, X_AVG1, Y_Surf
Local, 11, 0, AX, AY+A_UY, ,  -theta,              ! local coordinate system at ankle node on
pylon
CSYS, 11
k,102,0,1,
k,103,0,10,
L,102,103
CSYS, 0

/POST1
SET,,,,,,,t
CSYS, 11

*get, COP_sx_k, KP, 101, LOC,X
*get, COP_sy_k, KP, 101, LOC,y
CSYS, 0

!-----------------------------------------------------
! Total Strain energy
allsel
etab, Work, SENE
ssum
*get, total_W, ssum,,item, Work


nsort,s,eqv                            ! Nodal stress maximum von mises
*get,smax,sort,,max

!*get, runtime, ACTIVE, 0, TIME, WALL          ! clock

allsel
!-------- WORKBENCH PARAMETRIC VARIABLES -----------
my_COP_sx = COP_sx_K
my_COP_sy = COP_sy_K
my_total_W = total_W/1000  ! converts mJ to J

!-------------  OPTIONAL FILE OUTPUTS  -----------------
!PRRSOL, FY

! *CFOPEN, RY_SURF,txt    ! DEFAULT OUTPUT IS IN RESULTS FOLDER
! *VWRITE,'Node', 'X-loc','FY'
! %8c   %8C%8C
```

```
! *VWRITE , PRESS_LIST(1,1),PRESS_LIST(1,2),PRESS_LIST(1,3)                ! WRITES
ARRAY
! %14.6G%14.6G%14.6G
! ! node number, X_location, RY
! *CFCLOS

! *CFOPEN, Press Nodes,txt  ! DEFAULT OUTPUT IS IN RESULTS FOLDER
! *VWRITE , nnum(1)                    ! WRITES ARRAY
! %14.6G
! ! node number, X_location, RY
! *CFCLOS


! *CFOPEN, Ankle_UY,txt    ! DEFAULT OUTPUT IS IN RESULTS FOLDER
! *VWRITE,'UY', A_UY
! %11C          %14.6G
! *CFCLOS

! !Variables output for troubleshooting
! *CFOPEN, COP_info,txt     ! DEFAULT OUTPUT IS IN RESULTS FOLDER
! *VWRITE,'X_AVG1', X_AVG1
! %11C          %14.6G

! *VWRITE,'PRESS_SUM', PLATE_SUM
! %11C          %14.6G
! *VWRITE,'SUM', SUM
! %11C          %14.6G

! *VWRITE,'COP_sx_K', COP_sx_K
! %11C          %14.6G
! *VWRITE,'COP_sy_K', COP_sy_K
! %11C          %14.6G
! *CFCLOS



! *CFOPEN, C:\Users\Kevin\Desktop\Output\RollOver,txt,,append
! ! theta (deg), COP_sx (mm), COP_sy (mm), strain work (J), UY (mm), smax (MPa)
! *VWRITE, Theta, my_COP_sx, my_COP_sy, X_AVG1, Y_Surf, my_total_W, A_UY, smax
! %14.6G,%14.6G,%14.6G,%14.6G,%14.6G,%14.6G,%14.6G,%14.6G
! *CFCLOS
```

# APPENDIX B: EXPERIMENTAL DATA

List of Experimental Data

**Experimental Data for Renegade Foot with Cosmetic Cover**

| Time (ms) | Angle, θ (deg) | Peak Load (N) | Load Rate (N/s) | Stiffness (N/mm) | Displacement (mm) | Energy (J) | Efficiency, η (%) |
|---|---|---|---|---|---|---|---|
| 0.00 | -20.00 | - | - | - | - | - | - |
| 53.56 | -19.25 | 634.22 | 147.33 | 82.45 | 15.01 | 2.84 | 90.24 |
| 101.22 | -17.50 | 1109.04 | 127.66 | 102.30 | 18.97 | 6.87 | 93.20 |
| 144.43 | -15.00 | 1274.63 | 122.35 | 114.58 | 19.20 | 8.17 | 93.35 |
| 206.49 | -10.00 | 1121.25 | 119.94 | 126.76 | 15.04 | 5.84 | 93.35 |
| 255.81 | -5.00 | 920.30 | 129.07 | 133.05 | 11.15 | 3.70 | 93.54 |
| 299.16 | 0.00 | 845.19 | 130.80 | 174.06 | 9.93 | 2.40 | 85.24 |
| 339.17 | 5.00 | 906.39 | 120.07 | 68.71 | 21.08 | 6.68 | 86.66 |
| 377.22 | 10.00 | 1052.51 | 120.33 | 65.60 | 25.07 | 9.94 | 88.54 |
| 414.20 | 15.00 | 1208.33 | 124.91 | 59.94 | 33.05 | 14.76 | 90.61 |
| 450.73 | 20.00 | 1277.33 | 123.45 | 51.75 | 41.81 | 19.42 | 92.03 |
| 487.32 | 25.00 | 1176.87 | 125.33 | 42.71 | 47.60 | 20.27 | 93.62 |
| 524.38 | 30.00 | 875.97 | 125.35 | 29.81 | 46.25 | 15.62 | 95.17 |
| 562.06 | 35.00 | 427.76 | 104.11 | 18.94 | 32.56 | 5.23 | 95.80 |
| 601.32 | 40.00 | - | - | - | - | - | - |

**Experimental Data for Renegade Foot without Cosmetic Cover**

| Time (ms) | Angle, θ (deg) | Peak Load (N) | Load Rate (N/s) | Stiffness (N/mm) | Displacement (mm) | Energy (J) | Efficiency, η (%) |
|---|---|---|---|---|---|---|---|
| 144.43 | -15.00 | 1276.96 | 111.77 | 100.48 | 15.88 | 9.37 | 98.96 |
| 299.16 | 0.00 | 845.90 | 132.78 | 169.46 | 8.71 | 2.50 | 88.17 |
| 450.73 | 20.00 | 1276.64 | 115.83 | 50.36 | 39.60 | 19.35 | 97.50 |

**Experimental Data for TaiLor Made Foot with Cosmetic Cover**

| Time (ms) | Angle, θ (deg) | Peak Load (N) | Load Rate (N/s) | Stiffness (N/mm) | Displacement (mm) | Energy (J) | Efficiency, η |
|---|---|---|---|---|---|---|---|
| 0.00 | -20.00 | 0.00 | - | - | - | - | - |
| 53.56 | -19.25 | 455.68 | 113.76 | 27.55 | 34.19 | 4.99 | 74.77 |
| 101.22 | -17.50 | 802.89 | 248.75 | 45.61 | 42.52 | 9.60 | 73.61 |
| 144.43 | -15.00 | 922.05 | 214.65 | 53.56 | 44.48 | 10.89 | 73.79 |
| 206.49 | -10.00 | 811.03 | 181.42 | 47.73 | 42.21 | 9.51 | 74.52 |
| 255.81 | -5.00 | 664.27 | 169.81 | 40.24 | 39.19 | 7.44 | 74.43 |
| 299.16 | 0.00 | 610.02 | 114.15 | 48.36 | 32.79 | 5.25 | 70.99 |
| 339.17 | 5.00 | 650.11 | 151.17 | 52.06 | 24.64 | 4.96 | 71.05 |
| 377.22 | 10.00 | 758.17 | 158.34 | 48.28 | 31.42 | 7.34 | 73.94 |
| 414.20 | 15.00 | 871.02 | 161.06 | 45.61 | 37.97 | 10.20 | 74.80 |
| 450.73 | 20.00 | 921.00 | 170.01 | 44.96 | 43.87 | 12.60 | 80.02 |
| 487.32 | 25.00 | 849.12 | 170.82 | 34.45 | 49.81 | 13.88 | 84.25 |
| 524.38 | 30.00 | 631.59 | 113.08 | 22.99 | 50.57 | 11.10 | 87.53 |
| 562.06 | 35.00 | 310.72 | 102.85 | 12.66 | 39.42 | 4.28 | 88.62 |
| 601.32 | 40.00 | 0.00 | - | - | - | - | - |

**Experimental Data for TaiLor Made foot without Cosmetic Cover**

| Time (ms) | Angle, θ (deg) | Peak Load (N) | Load Rate (N/s) | Stiffness (N/mm) | Displacement (mm) | Energy (J) | Efficiency, η (%) |
|---|---|---|---|---|---|---|---|
| 144.43 | -15.00 | 936.45 | 272.70 | 85.37 | 15.77 | 6.12 | 88.46 |
| 299.16 | 0.00 | 597.47 | 80.37 | 43.71 | 19.71 | 4.21 | 59.40 |
| 450.73 | 20.00 | 919.96 | 148.17 | 40.42 | 44.15 | 13.54 | 83.26 |

# APPENDIX C: SCHEMATICS OF COMPONENTS

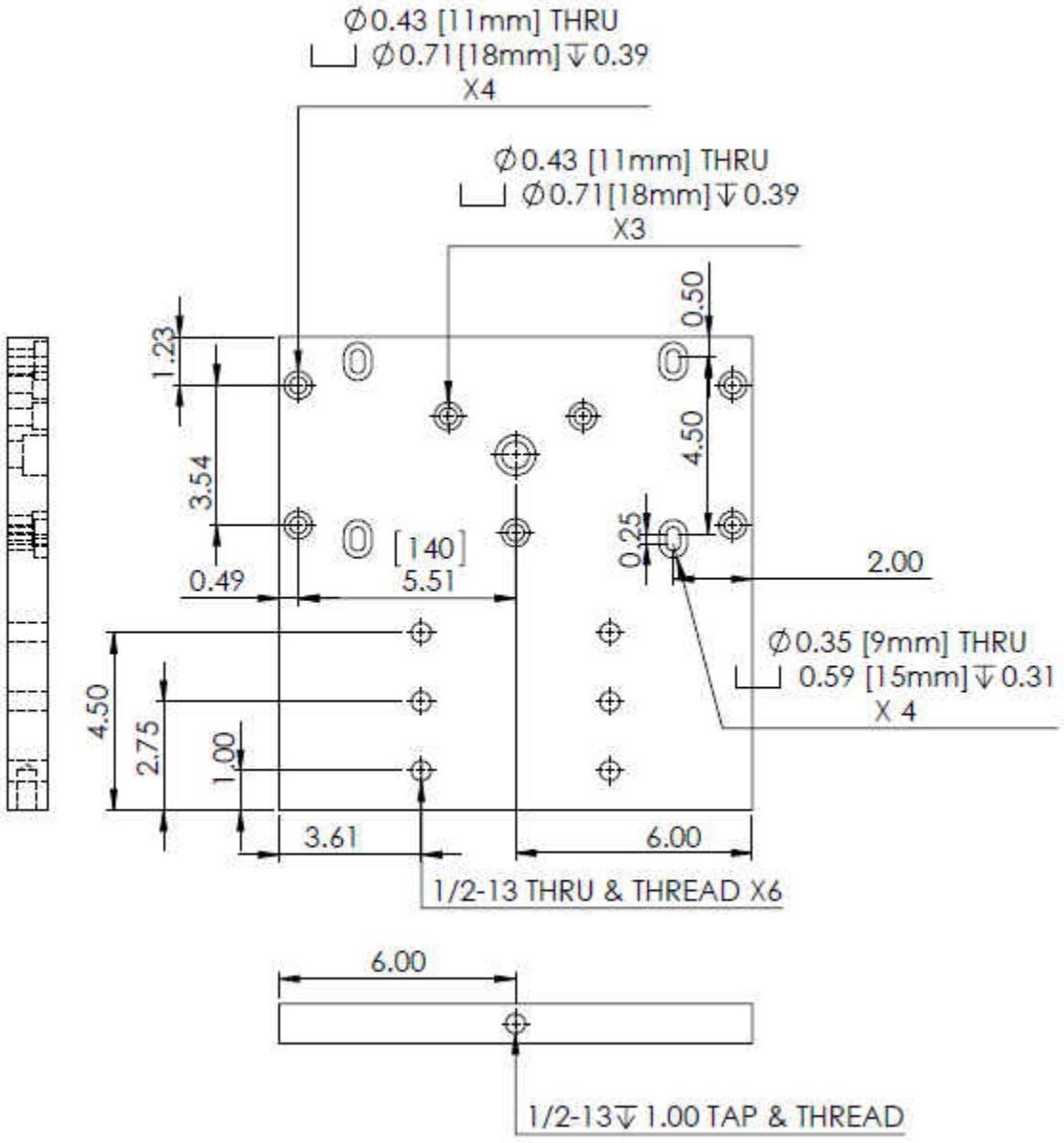


Figure 62: Drawing of baseplate to interface with load frames

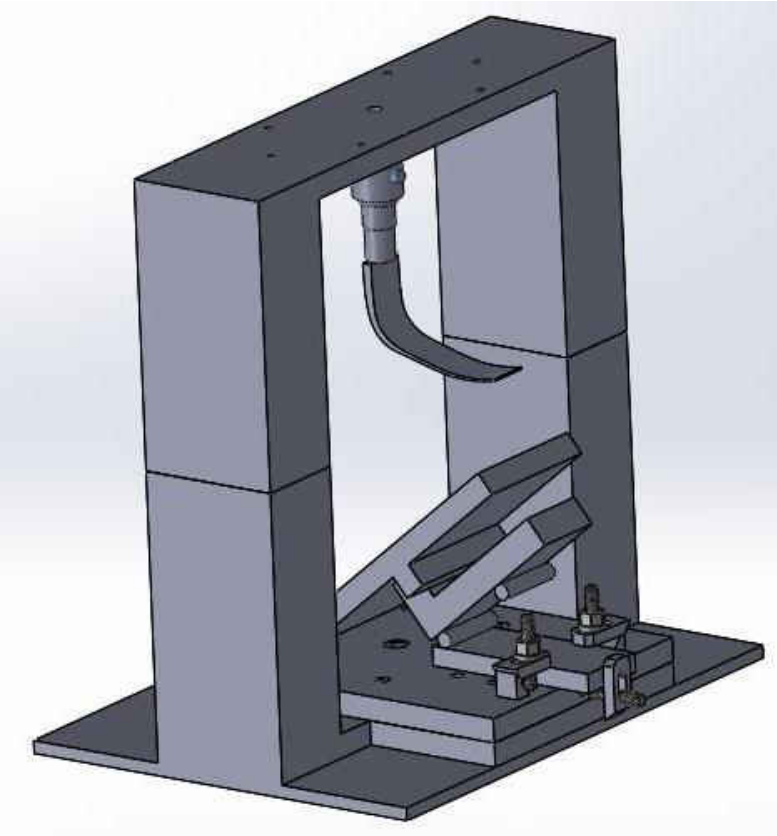

Figure 63: CAD of experimental set-up in MTS 5kN Insight load frame

# APPENDIX D: TEST MATRIX

List of Test Matrices

**Renegade Test Matrix**

| Angle | Time (ms) | P3 Loads (N) | Displacement Rate (mm/s) |
|---|---|---|---|
| -20.00 | 0.00 | 0 | 0.0 |
| -19.25 | 53.56 | 630 | 1.70 |
| -17.50 | 101.22 | 1106 | 1.20 |
| -15.00 | 144.43 | 1271 | 1.00 |
| -10.00 | 206.49 | 1118 | 0.90 |
| -5.00 | 255.81 | 916 | 0.90 |
| 0.00 | 299.16 | 842 | 0.70 |
| 5.00 | 339.17 | 903 | 1.70 |
| 10.00 | 377.22 | 1049 | 1.80 |
| 15.00 | 414.20 | 1204 | 2.00 |
| 20.00 | 450.73 | 1273 | 2.25 |
| 25.00 | 487.32 | 1172 | 2.70 |
| 30.00 | 524.38 | 872 | 4.00 |
| 34.97 | 562.06 | 422 | 5.94 |
| 40.00 | 601.32 | 0 | 0.0 |

**TaiLor Made Test Matrix**

| Angle | Time (ms) | P3 Loads (N) | Displacement Rate (mm/s) |
|---|---|---|---|
| -20.00 | 0.00 | 0 | 0 |
| -19.25 | 53.56 | 453 | 4.0 |
| -17.50 | 101.22 | 795 | 4.0 |
| -15.00 | 144.43 | 914 | 3.0 |
| -10.00 | 206.49 | 803 | 3.0 |
| -5.00 | 255.81 | 658 | 3.0 |
| 0.00 | 299.16 | 606 | 2.0 |
| 5.00 | 339.17 | 649 | 3.0 |
| 10.00 | 377.22 | 754 | 3.0 |
| 15.00 | 414.20 | 866 | 3.0 |
| 20.00 | 450.73 | 915 | 3.0 |
| 25.00 | 487.32 | 843 | 4.0 |
| 30.00 | 524.38 | 627 | 4.0 |
| 34.97 | 562.06 | 304 | 8.3 |
| 40.00 | 601.32 | 0 | 0.0 |

# REFERENCES


ACP Composites. (2014). Mechanical Properties of Carbon Fiber Composite Materials, Fiber / Epoxy resin (120°C Cure).

Adamczyk, P. G., Collins, S. H., & Kuo, A. D. (2006). The advantages of a rolling foot in human walking. *Journal of Experimental Biology, 209*(20), 3953-3963. doi:10.1242/jeb.02455

American Orthotic Prosthetic Association. (2010). AOPA'S Prosthetic Foot Project: What It Is, What It Is Not, and What Patient Care Facility Providers/Practitioners Need to Know….

Barr, A. E., Lohmann Siegel, K., Danoff, J. V., McGarvey, C. L., Tomasko, A., Sable, I., & Stanhope, S. J. (1992). Biomechanical Comparison of the Energy-Storing Capabilities of SACH and Carbon Copy II Prosthetic Feet During the Stance Phase of Gait in a Person with Below-Knee Amputation. *Physical Therapy, 72*(5), 344-354.

Betten, J. (2008). *Creep mechanics*: Springer Science & Business Media.

Chen, N.-Z., Lee, W. C., & Zhang, M. (2006). A numerical approach to evaluate the fatigue life of monolimb. *Medical engineering & physics, 28*(3), 290-296.

Corum, J. (2001). *Basic properties of reference crossply carbon-fiber composite*. Retrieved from

Covestro. (2015). *Baydur 426 IMR*. Retrieved from: http://www.polyurethanes.covestro.com/Handler/GenericForceDownload.ashx?itemID=BFE4EE5E3F0640459CDAF4005C8E18C7&lang=en

Daher, R. L. (1975). Physical response of SACH feet under laboratory testing. *Bulletin of prosthetics research*, 4-50.

Dally, J. W., & Riley, W. F. (2005). Digital Image Correlation *Experimental Stress Analysis* (4th ed., pp. 581-601): College House Enterprises, LLC.

De Koster, K. (2004). Gait Cycle.

Dillingham, T. R., Pezzin, L. E., & MacKenzie, E. J. (2002). Limb amputation and limb deficiency: epidemiology and recent trends in the United States. *Southern medical journal, 95*(8), 875-884.

Dorsiflexion and Plantarflexion.

Drillis, R., Contini, R., & Maurice Bluestein, M. (1966). Body segment parameters1. *Artificial limbs*, 44.

EpoTek. (2015). Understanding Mechanical Properties of Epoxies For Modeling, Finite Element Analysis (FEA).

Fey, N. P., Klute, G. K., & Neptune, R. R. (2011). The influence of energy storage and return foot stiffness on walking mechanics and muscle activity in below-knee amputees. *Clinical Biomechanics, 26*(10), 1025-1032.

Fey, N. P., Klute, G. K., & Neptune, R. R. (2013). Altering prosthetic foot stiffness influences foot and muscle function during below-knee amputee walking: A modeling and simulation analysis. *Journal of Biomechanics, 46*(4), 637-644.

Freedom-Innovations. (2014). Renegade AT Brochure.

Freedom-Innovations. (2015). Renegade & Renegade LP *Freedom-Innovations product catalog* (pp. 10-11).

Geil, M. D. (2001). Energy loss and stiffness properties of dynamic elastic response prosthetic feet. *JPO: Journal of Prosthetics and Orthotics, 13*(3), 70-73.

Geil, M. D. (2002). An iterative method for viscoelastic modeling of prosthetic feet. *Journal of Biomechanics, 35*(10), 1405-1410.

Haberman, A. (2008). Mechanical Properties of Dynamic Energy Return Prosthetic Feet.

Hafner, B. J., Sanders, J. E., Czerniecki, J., & Fergason, J. (2002a). Energy storage and return prostheses: does patient perception correlate with biomechanical analysis? *Clinical Biomechanics, 17*(5), 325-344.

Hafner, B. J., Sanders, J. E., Czerniecki, J. M., & Fergason, J. (2002b). Transtibial energy-storage-and-return prosthetic devices: a review of energy concepts and a proposed nomenclature. *Journal of Rehabilitation Research & Development, 39*(1), 1-11.

Hansen, A., Gard, S., & Childress, D. (2000). *The determination of foot/ankle roll-over shape: clinical and research applications.* Paper presented at the Pediatric Gait, 2000. A new Millennium in Clinical Care and Motion Analysis Technology.

Hansen, A., Nickel, E., Medvec, J., Brielmaier, S., Pike, A., & Weber, M. (2014). Effects of a flat prosthetic foot rocker section on balance and mobility. *Journal of Rehabilitation Research & Development*(1), 137.

Hansen, A. H., Childress, D. S., & Knox, E. H. (2004). Roll-over shapes of human locomotor systems: effects of walking speed. *Clinical Biomechanics, 19*(4), 407-414.

Hansen, A. H., & Dudley, C., S. (2004). Effects of shoe heel height on biologic rollover characteristics during walking. *Journal of Rehablitation Research and Development, 41*(4), 547-554.

Hansen, A. H., Meier, M. R., Sessoms, P. H., & Childress, D. S. (2006). The effects of prosthetic foot roll-over shape arc length on the gait of trans-tibial prosthesis users. *Prosthetics and Orthotics International, 30*(3), 286-299.

Highsmith, J. (2009). *Prosthetic Feet Classification and Overview*. College of Medicine School of Physical Therapy & Rehabilitation Sciences. University of South Florida. Retrieved from http://oandp.health.usf.edu/Pros/pros_feet/prosthetic_feet.pdf

Hoffman, M. D., Sheldahl, L. M., Buley, K. J., & Sandford, P. R. (1997). Physiological comparison of walking among bilateral above-knee amputee and able-bodied subjects, and a model to account for the differences in metabolic cost. *Archives of physical medicine and rehabilitation, 78*(4), 385-392.

Innovations, F. Silhouette®.

International Organization for Standardization. (2006a). Prosthetics -- Structural testing of lower-limb prostheses -- Requirements and test methods.

International Organization for Standardization. (2006b). Prosthetisc – Testing of ankle-foot devices and foot units – Requirements and test methods.

Jensen, J. S., & Heim, S. (2000). Evaluation of polypropylene prostheses designed by the International Committee of the Red Cross for trans-tibial amputees. *Prosthetics and Orthotics International, 24*(1), 47-54.

Jensen, J. S., & Treichl, H. B. (2007). Mechanical testing of prosthetic feet utilized in low-income countries according to ISO-10328 standard. *Prosthetics and Orthotics International, 31*(2), 177-206. doi:10.1080/03093640701210986

Kadaba MP, Ramakrishnan HK, Wootten ME, Gainey J, Gorton G, & Cochran GV. (1989). Repeatability of kinematic, kinetic, and electromyographic data in normal adult gait. *Journal of Orthopaedic Research, 7*(6), 849-860.

Kapp, S., & Cummings, D. (1992). *Atlas of Limb Prosthetics: Surgical, Prosthetic, and Rehabilitation Principles* (2nd Ed.). Rosemont, IL: American Academy of Orthopedic Surgeons.

Klodd, E., Hansen, A., Fatone, S., & Edwards, M. (2010). Effects of prosthetic foot forefoot flexibility on gait of unilateral transtibial prosthesis users. *Journal of Rehabiltation Research & Development, 47*(9), 899-910.

Klute, G. K., Berge, J. S., & Segal, A. D. (2004). Heel-region properties of prosthetic feet and shoes. *Journal of rehabilitation research and development, 41*(4), 535-546.

Larson, R. G. (1985). Constitutive relationships for polymeric materials with power-law distributions of relaxation times. *Rheologica Acta, 24*(4), 327-334. doi:10.1007/bf01333961

Lehmann, J. F., Price, R., Boswell-Bessette, S., Dralle, A., & Questad, K. (1993). Comprehensive analysis of dynamic elastic response feet: Seattle Ankle/Lite Foot versus SACH foot. *Archives of physical medicine and rehabilitation, 74*(8), 853-861. doi:10.1016/0003-9993(93)90013-z

Lehmann, J. F., Price, R., Boswell-Bessette, S., Dralle, A., Questad, K., & deLateur, B. J. (1993). Comprehensive analysis of energy storing prosthetic feet: Flex Foot and Seattle Foot Versus Standard SACH foot. *Archives of physical medicine and rehabilitation, 74*(11), 1225-1231.

Limmer, L., Weissenbach, G., Brown, D., McIlhagger, R., & Wallace, E. (1996). The potential of 3-D woven composites exemplified in a composite component for a lower-leg prosthesis. *Composites Part A: Applied Science and Manufacturing, 27*(4), 271-277.

Logan, S. J. (2007). Ground reaction force differences between running shoes, racing flats, and distance spikes in runners.

Loudon, J., Swift, M., & Bell, S. (2008). *The clinical orthopedic assessment guide* (2nd ed.). Champaign, IL: Human Kinetics.

Macfarlane, P. A., Nielsen, D. H., Shurr, D. G., & Meier, K. (1991). Gait Comparisons for Below-Knee Amputees Using a Flex-FootTM] Versus a Conventional Prosthetic Foot. *JPO: Journal of Prosthetics and Orthotics, 3*(4), 150-161.

McGeer, T. (1990). Passive dynamic walking. *The international journal of robotics research, 9*(2), 62-82.

Menard, M. R., & Murray, D. D. (1989). Subjective and Objective Analysis of an Energy-Storing Prosthetic Foot. *JPO: Journal of Prosthetics and Orthotics, 1*(4), 220-230.

National Research Center for Rehabilitation Technology and Aids. (2013). Prosthetic detection chamber dynamic tests: Ministry of Civil Affairs of the People's Republic of China.

Nielsen, D. H., Shurr, D. G., Golden, J. C., & Meier, K. (1988). Comparison of Energy Cost and Gait Efficiency During Ambulation in Below-Knee Amputees Using Different Prosthetic Feet-A Preliminary Report. *JPO: Journal of Prosthetics and Orthotics, 1*(1), 24-31.

Nobbe Orthopedics, I.). Best Feet Forward. *Prosthetic & Orthotic Update*.

Pan, B., Yu, L. P., & Wu, D. F. (2014). *High-accuracy 2D digital image correlation measurements using low-cost imaging lenses: implementation of a generalized compensation method*.

Parnell, T. K. (2014). Prosthetic Feet using Carbon Fiber Composites: Design, Simulation and Testing. Retrieved from http://www.mscsoftware.com/events_assets/Webcasts/2014_Nonlinear/Prosthetic_Feet_Carbon_Fiber_Composites_Design_Simulation_Testing.html

Pekaje. (2007). Generalized Maxwell model.

Perry, J. (1992). Gait Analysis: Normal and Pathological Function: Slack Incorporated.

Postoperative SACH foot (cutaway). American Academy of Orthotists & Prosthetists.

Powers, C. M., Torburn, L., Perry, J., & Ayyappa, E. (1994). Influence of prosthetic foot design on sound limb loading in adults with unilateral below-knee amputations. *Archives of physical medicine and rehabilitation, 75*(7), 825-829.

Prosthetics, T. (2015). TaiLor Made.

Reddy, J. N. (2013). *An Introduction to Continuum Mechanics* (2 ed.): Cambridge University Press.

Rihs, D., & Polizzi, I. (2001). *Prosthetic Foot Design*. The Monash Rehabilitation Technology Research Unit. Monash University. Retrieved from http://monash.edu.au/rehabtech/research/reports/FEETMAST.PDF

Romo, H. D. (1999). Specialized Prostheses for Activities: An Update. *Clinical Orthopaedics and Related Research, 361*, 63-70.

Snyder, R. D., Powers, C. M., Fontaine, C., & Perry, J. (1995). The effect of five prosthetic feet on the gait and loading of the sound limb in dysvascular below-knee amputees. *Journal of rehabilitation research and development, 32*(4), 309-315.

South, B. J., Fey, N. P., Bosker, G., & Neptune, R. R. (2009). Manufacture of Energy Storage and Return Prosthetic Feet Using Selective Laser Sintering. *Journal of Biomechanical Engineering, 132*(1), 015001-015001. doi:10.1115/1.4000166

Thompson, D. (2006). Dynamic Response Feet: University of Oklahoma Health Center.

Toh, S. L., Goh, J. C. H., Tan, P. H., & Tay, T. E. (1993). Fatigue testing of energy storing prosthetic feet. *Prosthetics and Orthotics International, 17*(3), 180-188. doi:10.3109/03093649309164379

Torburn, L., Perry, J., Ayyappa, E., & Shanfield, S. L. (1990). Below-knee amputee gait with dynamic elastic response prosthetic feet: a pilot study. *J Rehabil Res Dev, 27*(4), 369-384.

Truper. (2012). College Park.

Ugural, A. C., & Fenster, S. K. (2011). *Advanced mechanics of materials and applied elasticity*: Pearson Education.

Unnthorsson, R., Runarsson, T. P., & Jonsson, M. T. (2008). Acoustic emission based fatigue failure criterion for CFRP. *International Journal of Fatigue, 30*(1), 11-20.

Waters, R. L., & Mulroy, S. (1999). The energy expenditure of normal and pathologic gait. *Gait & Posture, 9*(3), 207-231.

Western, S. Ankle/Foot Wear Simulator.

Wevers, H. W., & Durance, J. P. (1987). Dynamic testing of below-knee prosthesis: Assembly and components. *Prosthetics and Orthotics International, 11*(3), 117-123. doi:10.3109/03093648709078193

Winter, D. A. (2009). *Biomechanics and motor control of human movement*: John Wiley & Sons.

Ziegler-Graham, K., MacKenzie, E. J., Ephraim, P. L., Travison, T. G., & Brookmeyer, R. (2008). Estimating the prevalence of limb loss in the United States: 2005 to 2050. *Archives of physical medicine and rehabilitation, 89*(3), 422-429.